On The Wave Activity within Vortex Cores

Jian Wang

A Thesis in The Department of

Mechanical Engineering

Presented in Partial Fulfillment of the Requirements
for the degree of Doctor of Philosophy at
Concordia University
Montréal, Québec, Canada

ISBN 0-612-18468-4

Canada

ABSTRACT

On The Wave Activity Within Vortex Cores

Jian Wang, Ph. D.
Concordia University, 1995

The present thesis is concerned with the instability of liquid vortices generated in a cylindrical container, using a flat disk rotating at the bottom. For relatively low viscosity fluid, several stationary states of the core were found to reside within a certain range of disk speeds. This range becomes narrow as the wave number grows. Between the stationary states, mixed, time dependent states were found to exist. Their intervals of perseverance decrease with the wave number. The disk speed at which the static state first appears and ends increases linearly with the original liquid height. The phase velocity of the stationary waves rises with the angular velocity of the disk.

The linearized stability analysis is employed to investigate the wave behavior in a water vortex. Two flow cases are considered herein. The first case deals with waves developed on the free surface of a hollow vortex, while the second deals with waves generated in the flooded core of a Rankine vortex. It is evident from the analysis that the experimental dispersion velocity approaches the calculated one when the wave amplitude becomes smaller. The latter is consistent with the small perturbation assumption that is inherent in the theory. For the case where the core is flooded, the presence of a cylindrical wall is shown to enhance the wave speed. A hypothesis as to how the core develops in the mixed state regions, is proposed. The graphical simulations appear to predict reasonably well the main features of the observations.

For a liquid of intermediate viscosity, abrupt transitions from one equilibrium state to the other are taking place. Steady vortex core patterns with wave numbers from one to eleven are observed. States where the basic

pattern is subharmonically modulated and states where a wave packet periodically encircles the core are also encountered. Hysteresis is also clearly evident during transitions of states. Artificial disturbance has triggered mutations of stable equilibria at identical determing boundary conditions, also demonstrated the existence of S-bifurcation. Co-grade and retrograde waves are observed, which is not possible in water. Bifurcations between steady flow, single frequency periodic flow and two frequency quasi-periodic flow are witnessed. As an initial value problem, the flow development history impacts the final flow state, experimentally the driving disk's acceleration is found to be a determing factor of the flow.

The core of a highly viscous liquid is stable. Turbulent and macroscopic equilibrium waves appear at very large liquid heights and disk speeds.

Water wave sloshing is present under certain prevailing flow conditions, wave activity changes dramatically during and after a sloshing. Numerical simulation furnishes one possible solution.

Acknowledgments

The author wishes to express his sincere gratitude to his advisers Drs. G. H. Vatistas and S. Lin for their valuable guidance. I owe a lot to Dr. Vatistas, who has provided many ideas and reviewed extensively the script. Dr. Lin's suggestions and encouragement were essential for my studies at Concordia The care and kindness from my supervisors are unforgettable.

The technical support from laboratories in the mechanical engineering department, particularly by Mr. J Elliot is greatly appreciated.

I also want to thank my wife Mengxuan for her constant support.

The financial support from Concordia University, FCAR and NSERC are indispensable for the completion of the thesis

TABLE OF CONTENTS

LIST OF FIGURES

List of tables

Nomenclature

$f(r)$	perturbation amplitude
g	gravitational constant
h_0	initial liquid level
n	circumferential wave number
p	pressure in the flow
q	total velocity of liquid particles
r	radial coordinate
r_c	radial core size of a Rankine vortex
r_e	core radius of a free vortex
r_t	radius of tank inner wall
$\hat{r}(z)$	radial profile of the free surface
t	time
u	tangential component of velocity
$V(r)$	velocity without perturbation
v	velocity, radial component
x_c	ratio of a core radius and tank inner radius
z	vertically axial coordinate
$z(r)$	free surface elevation

ϕ	stream function
σ	wave angular frequency
θ	azimuthal coordinate
λ	radial amplitude of the wave boundary in Rankine vortex core
Ψ	stream function for flow free of perturbation
$\hat{\psi}$	stream function of perturbed flow
$\hat{u}$	velocity, tangential perturbed term
$\hat{v}$	velocity, radial perturbed term
$\hat{\pi}$	pressure perturbation due to wave
ρ	density of the liquid
$\Pi(r)$	pressure without perturbation
$\hat{\psi}$	stream function, perturbation component
ω	angular velocity of the solid rotation core
ω_d	disk rotation
κ	vortex strength

CHAPTER 1

INTRODUCTION

1.1 General

The term vortex is used to characterize the general rotary motion of an ensemble of material particles moving around an imaginary axis. Consequently, vortices may be generated in fluids, plasma or in a collection of solid bodies (particles). Vortices with a wide range of sizes can be found in nature (see Table 1-1 for example). Disk-like vortices are those whose "height" to diameter ratio is small, while the columnar type are those whose ratio is large. If most of the vorticity is confined to a small region within the core, the type is often referred to as a concentrated vortex.

In the natural world, vortices can be found in planetary atmospheres, oceans, the flow of rivers, movement of the earth's mantle, in the motion and biological process of living organisms, human physiology, and the motion of galaxies. Besides their common occurrence in the natural world, vortices can also be found in the majority of industrial applications. Among a large number of examples that one can cite are: the vortex separator, the cyclone combustion, the vortex valve, the swirl atomizer, intakes and draft tubes of turbines, turbine and compressor blades, wing tips, and many others.

Table 1-1. Ranges of Vortex Size*

	Diameter
Quantized vortices in liquid Helium	10^{-8} cm
Smallest turbulent eddies	0.1 cm
Vortices generated by insects Vortices behind leafs Vortex rings of squids	0.1-10 cm
Dust whirs on the street Whirlpools in tidal currents Dust devils	1.0-10 cm
Vortex rings in volcanic eruptions Whirlwinds and waterspouts Con /ection clouds	100-1000 m
Vortices shed from the Gulf Stream Hurricanes High- and low-pressure stems	100-2000 km
Ocean circulations General circulation of the atmosphere Convection cells inside the earth	2000-5000 km
Great Red Spot of Jupiter Rings of the planet Saturn Sun Spots	5000-10^5 km
Galaxies	order of light years

* Adopted from : Lugt H, J. "Vortex Flow in Nature and Technology" John Wiley and Sons, New York 1983.

To explain and predict motions of a fluid under the influence of various forces is the mission of fluid mechanics as a science. For small Reynolds numbers, the viscous effects overweight the inertia and the incompressible Navier-Stokes equations, together with mass and energy conservation equations, yield unique solutions to the fluid motion given the boundary conditions and extraneous forcing functions. These unique and symmetric solutions are independent of initial conditions. For larger Reynolds numbers, the uniqueness of the flow is lost, giving rise to multiple solutions.

Flows with more complex structures in space and time might appear. This flow behavior is consistent with the second law of thermodynamics, as the latter suggests in an axiomatic manner that everything in nature advances from an orderly state towards disorder. Therefore, as far as fluid flow is concerned, one can distinguish two asymptotic conditions; the laminar physical state where the fluid motion possesses the highest order, and the turbulent state where total disorder exists. In between, as one proceeds from the first towards the second condition (by increasing the Reynolds number), flow fields with a decreasing degree of order exist. The overwhelming interest in turbulent flows arises from the fact that most of the artificially generated industrial or naturally occurring flows are of this type. Consequently, the origin and the process, from which turbulence evolves, has attracted the curiosity of scientists for generations since Orsborne Reynolds.

There are two experimentally known ways for a flow to change from the laminar to "turbulent" conditions. The first is realized through a spontaneous (catastrophic) transition to turbulence. Examples are the Hagen-Poiseuille flows in a pipe and the Coutte flows within two concentric cylinders, spheres with the outer one rotating while the inner one is stationary. At low Reynolds numbers, the flow is laminar, therefore having a maximum symmetry. As a critical Reynolds number is passed, the flow changes to the turbulent condition through an interval where the flow field is segregated to laminar and turbulent packets (Wygnanski & Champagne, 1973). The second is characterized by repeated finite bifurcations. As the Reynolds number is increased, the maximum flow symmetry splits, giving rise to another laminar type of flow having a different pattern of symmetry. Finally, as the Reynolds number is increased further, a continuous magnification of dynamical noise (turbulence) consumes the flow. Classical examples of flow transformation through spectral development are the Coutte flows within two concentric cylinders, spheres with the inner rotating while the outer is stationary and the Bénard-Maragony convection between two plates. Flow instability manifested due to the temperature stratification in a cylindrical annular space was also investigated by Hide(1966). These systems, where the onset of turbulence is characterized by gradual flow structure transformations from flow patterns of high degree of order towards "chaos", are of special interest to both experimentalists and theoreticians. The latter

affinity emanates from the view that such systems furnish researchers with details of flow transition. Many believe that if a good understanding of the underlying mechanism is acquired, then a better turbulent model might be developed. In addition to the classical examples mentioned above, details about the flow behavior during "slow" transition can also been realized using a spinning disk immersed in liquids (Vatistas, 1990). Although the latter case might be, from the mathematical modeling point of view (complex boundary conditions), more involved than the classical problems, it is simple in construction. Furthermore, as will be shown, it can provide the researchers with a wide window into the study of flow transition.

1.2 Problem definition

The flow generated by a spinning disk immersed in a fluid was successfully explained by Stuart (1955). Lord Kelvin (1880), more than a century ago, postulated that the core of columnar vortices is able to accommodate perturbations with different wave numbers. Vatistas (1990) was the first to report the existence of these equilibria under laboratory conditions. The experimental set-up used was comprised of a cylindrical container filled with water with a flat disk rotating at the bottom. Several interesting phenomena with respect to slow transition were discovered. The present work is the continuation of Vatistas' original discovery.

The study concentrates on the structures of vortex flow and their instabilities, the evolution of liquid vortex flow with respect to the change of driving force – the disk rotation, generated in a cylindrical container with a flat disk rotating at the bottom. Experimental and analytical investigations are performed, with emphasis on experiments due to the enormous difficulty encountered with the mathematical approach.

The experimental study is conducted with water and two types of oil (Shell 10W, 40W). Observations show that the flow undergoes a sequence of structural transformations as the driving disk spins up quasi-statically. In each stage of the sequence, the flow is a laminar with an equilibrium wave

present in the flow until eventually reaching turbulence. When quasi-statically reducing the driving disk's rotation from certain rpm (at which the flow is not yet turbulent), the sequence of flow states is not the same as the spin-up's one, which implies the existence of hysteresis and bifurcation.

High viscous vortex possesses considerably more complexities than water's. In the case of water, the order in which the equilibria come up one after another with changing disk rotation is the same during ascending and descending sequences. The difference between the two lies in the hysteresis during transition from one flow structure into another. In the case of high viscous oil vortices, not only the order of flow patterns in spin-up and spin-down sequences can be different; also, three or more flow states could exist at the same boundary conditions and same disk rotation speed. Two general characteristics of bifurcations have been observed in the present study. The acceleration process is found to have effects on the flow state at the terminal disk rpm.

Wave phase speeds in the core of hollow and flooded bell-shaped vortices of water have been calculated by a model of inviscid, small amplitude, harmonic perturbation analysis. The comparison of the theory with experimental measurements show a reasonable agreement, provided the conditions remain within the realm of the assumptions.

The characteristics of the flow vary with geometric arrangements, such as the size of the disk, the initial level of liquid, etc..

Sloshing was found for certain combinations of parameters (the disk rotation, liquid level and disk size), which shows the simultaneous presence of two waves with comparable amplitudes, close or approximate multiple frequencies. Qualitative simulations are performed to demonstrate the main characteristics of several phenomena involved.

In 1880, Lord Kelvin mathematically investigated the perturbed columnar vortices formations. One of the three cases considered is that of the perturbations in a potential vortex base flow with a hollow core in a stationary cylindrical tank. The perturbations are three dimensional and

harmonic. Kelvin's study shows that a core disturbed in the form of symmetric polygons can exist in an inviscid flow field. Recently, Vatistas (1990) did, for the first time, observe these equilibria core in a water vortex experiment produced in a cylindrical container using a rotating flat disk at the bottom (included in Photo plate 1).

For the cases where a relatively low viscous fluid (such as water) is used, several stationary polygon cores are found to exist within certain limits of disk speeds. These speeds intervals decrease as the circumferential wave number increases. Between the stationary states, mixed, time-varying core shapes are present. Their range of disk speeds shrinks with the increasing order of neighboring equilibria.

For cases where high viscous liquid oil is employed, abrupt transition from one steady equilibrium to another takes place. Steady vortex patterns with polygon orders from one to eleven are observed. States in which a lower wave number core is harmonically modulated by another with higher wave number and states where a wave packet periodically encircles the base wave core are also visualized. Hysteresis and bifurcation among the equilibria transitions are clearly evident.

The study aims to reveal the flow evolution with gradually increasing and reducing the characteristic number, Reynolds number or Taylor number through disk rotation. Initially, the simplest laminar flow is present, then at a higher Reynolds number a less simple laminar flow with perturbation n=2 wave is superimposed on the base flow, and at still a higher disk rotation an n=3 perturbation happens. When the speed is between n=2 and n=3, the flow presents a combined perturbation of these two; its wave form is time dependent. With continuously quasi-stationary increases of disk rotation, the vortex flow goes through mixed n=3 and n=4, a single stable n=4, mixed n=4 and n=5, single n=5, mixed time dependent n=5 and n=6, single n=6, finally, turbulence develops due to the relatively large Reynolds number.

The above sequence is for water. When high viscous liquid, such as Shell 10W oil, is used, the sequence of flow states is completely different. Generally, during the ascending rotation process, it starts from n=11 or 10,

then goes to 7 or 5 depending on the initial level of oil added. Further on, the wave number augments until at relatively high rotation the turbulence comes up eventually. A distinct new phenomenon with oil is that the rotation descending sequence shows strong hysteresis and multi-mutations. Three stable flow structures could be present at the exact same Taylor number and boundary conditions. At high initial levels of liquid, the base flow is no longer free vortex; instead, a perturbed forced-free one, is observed.

Based on the above mentioned phenomena, the definition of the work in the present study can be summarized as:

1) Transition of low viscous vortex flow from laminar to turbulence, its structural transformations during the process,

2) Analytical approximation of the inviscid vortex flow.

3) Transition of **high** viscous vortex flow from laminar to turbulence during quasi-static rotation ascending process,

4) The hysteresis and bifurcation between the ascending and descending sequence for high viscous oil,

5) The hysteresis and bifurcation between the quasi-static variation of Taylor number and its accelerating variations,

6) Exploration of sloshing and its simulation.

These phenomena will be explored in the following chapters of the present thesis.

1.3. LITERATURE SURVEY

The flow instability problem has been a hot topic since Taylor's pioneering work in 1923. A book edited by Swinney and Gallub gives much information on the subject. In the rotatory flow regimes, Rayleigh (1916) gave the first analytical stability criterion for inviscid rotation flow. Then, the elegant analysis by Taylor and the corresponding convincing experiments have encouraged and led to many fruitful results in stability theories. Chandrasekhar (1961) made many valuable analyses on hydrodynamic and hydro-magnetic flow transformations. Geogory, Stuart and Walker (1955) explained analytically the experimental results of 3 D n=6 disturbance vortices in the flow above a rotating disk, motivated by the transition on a swept wing. Weske (1963) studied secondary vortex flow, and obtained n=7 polygon pattern. Hide (1966) showed the effects of radial body force on rotation flows, he observed disturbances with wave number n=3, 4, 5, 6. Kou (1973) gave the flow patterns in shallow ocean and atmosphere resulting from quasi-geotropic instability due to the earth's rotation. Cambell and Ziff (1978) suggested equilibrium configurations for n<31, n=37, 50. Aref (1983) indicated that at least one stable equilibrium must exist for every n polygon arrangements. Rabaud, Couder (1983), Chomaz, Rabaud and Couder (1988) found circular shear layer instability in the form of n= 3, 4, 5, 6 elliptic cat eye patterns. Dritschel (1985, 1986, 1989) did a lot of 2D inviscid uniform voracity evolutions, found n=2, 3, 4, 5, 6, 7, 9 lobes vortices. Abrahamson et al (1989) showed flow between two co-rotating shrouded disks, obtained n=5 case. Griffiths and Linden (1981) studied viscoelastic liquid stick to a rotating rod, the radial shapes are n=2, 3.

The general flow characteristics of atmosphere in the earth's polar regions are similar to the present experimental arrangement. Having in mind that other effects such as temperature variations are also present in the natural settings, the similarity in the trajectories traced by a balloon around the south pole released in New Zealand, see Mason (1971), with the flow patterns observed (Vatistas 1990) is worth noting. Similar vortex core modal shapes have also been found during vibrations of cylindrical thin shells and evaporating liquid drops, respectively. Alike equilibrium and mixed state mode shapes of vibrating conical shells have been reported by Schneider et al. Luminosity

waves of interstellar gas are also evident in the core of galaxies. Recently, Lauer and his associates (1993), with the help of the Hubble Space Telescope, have shown that Andromeda (M31) galaxy has two cores. One of the explanations as to why M31 has two cores is based on the idea that the present double core is the result of the collision of two venerable galaxies. Yet another, equally possible cause might be due to the unstable nature of the vortex center (Vatistas, New Scientist, 1993), similar to the vortex sloshing phenomenon to be reported in this thesis.

Bifurcation and hysteresis are common properties in nonlinear systems. They have been found in fluid flows around spheres, airfoils, in the gap between concentric rotating cylinders, etc.. The last case was the first experimental evidence of bifurcation in fluids (Pai, 1943). Recently, Benjaming and Mullin (1982) reported many bifurcation cases in the circular Couette flow. Zierep (1970) and Wimmer (1980) disclosed the bifurcation and hysteresis in the spherical shell flow. The present study reveals the existence of bifurcations in high viscous hollow vortex flow; two common characteristics of bifurcations were observed.

CHAPTER 2

Experiments of water vortex

This chapter reports the experimental findings with respect to wave activity in the core of disk-shaped vortices generated in a cylindrical container with a flat disk rotating at the bottom.

The process which leads an orderly laminar flow to a complex, random turbulent state is very intuitive and interesting. The study of such a process can be beneficial in two respects, one in that it may shed light on what provokes chaos in a system of simple order, another in that it may be helpful in establishing certain models of the turbulence.

Water, a low viscosity fluid, probably the easiest liquid to manage in a lab is chosen in the flow phenomena exploration. It has delivered quite revealing information despite its simplicity. Experiments have shown the existence of laminar stationary states of the vortex core within a certain range of disk speeds, before the driving rotation is high enough to bring the flow to turbulence. This range becomes narrower as the equilibrium circumferential wave number grows. Between the stationary states, mixed time dependent states were found to occur. Their intervals of endurance decrease with the

wave number. The disk speeds at which the stationary state first appears and ends increase linearly with the original height of the water before rotation. The phase velocity of the stationary waves rises with the angular velocity of the disk.

Meticulous care in the tests has revealed the presence of a weak hysteresis. This demonstrates the non linearity of the flow structure in a wider Reynolds number spectrum. The last part of this chapter examines the impact of the driving disk's diameter on the equilibria in terms of the flow parameters.

A Laser Doppler Anemometer is used to quantify the flow field behavior. It helps to depict the periodical feature when equilibrium is developed. The measurements also give quantitative descriptions of the order of perturbations incurred by the presence of equilibria and the flow mean parameters

2.1 Experimental facility for liquid vortex flows

The experiments have been conducted in Concordia's liquid vortex agitator, which is schematically illustrated in Figure 2-1. The agitator consists of a stationary plexiglass cylindrical container, with a flat aluminum disk rotating in the counter-clockwise direction, mounted on a shaft at the bottom of the container. The shaft is driven, through a belt pulley assembly, by a Direct Current (DC) speed variable motor. There is a relatively large metal flywheel attached to the shaft to assure the constancy of the rotation. The DC motor has a power of three-quarters hp, and a speed range from 0 to 1500 rpm, adjustable by a rotatory variac.

Liquid can be introduced into the container from the top opening and drained from a 90 degree small hole in the bottom plate, or by a siphon through the top.

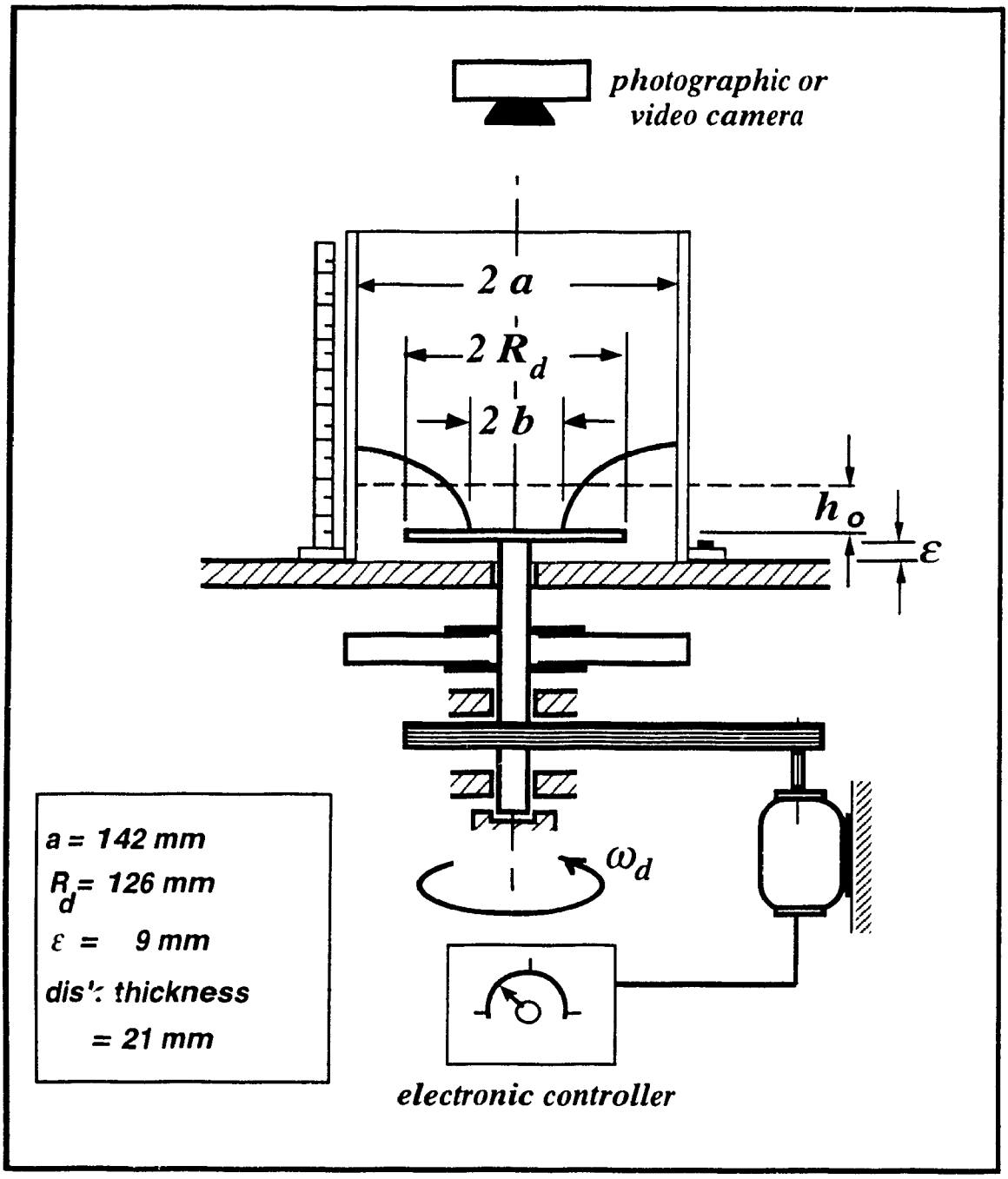

Figure 2-1 The experimental set-up

Different disk diameters are used in the experiments. The liquid initial level above the disk's upper surface before rotation is measured by a ruler placed on the side of the container.

2.2 Instrumentation

The tangential velocity in the liquid is measured by an air cooled Laser Doppler Anemometer (LDA) from Dantec. The Ion-Argon laser beam is of 300 mW, a beam separator of 60 mm, a bragg cell of 40 Mhz frequency shift (in order to get a shifted beam; so a reverse, negative velocity is detectable by the equipment), a beam diameter of 0.82 mm and also a transverse mechanism controlled by a micro computer through IEEE-488 bus. The frequency signal indicating the tiny particles' speed from the photo detector is fed to a flow velocity analyzer box, then to a special circuit card in the personal computer. There the sampling data is processed, and time series of velocity, spectrum analysis, histograms, various correlations, etc. can be performed. The whole LDA system, including the data conversion, is managed by a powerful software package from Dantec called FLOWARE.

The disk angular velocity is determined by a photo reflective digital meter from Ametek. The equilibria wave phase speeds are obtained by visual counting and a digital timer.

Video and photo cameras are mounted right at the top of the container, centered to get the flow equilibria patterns and their transition dynamics.

The liquid free surface elevation profile is mapped by a transverse mechanism with a sharp pointer. The three dimensional transverse arms are all scaled.

The Cannon-Fenske routine viscometer, tested according to ASTM D445-61 for transparent liquids, is used to get the viscosity values of the working media.

To quantitatively obtain the equilibria geometry, one of the disks is gridded with concentric circles, hence, from a photo, its geometry can be evaluated and compared with mathematical approximations.

A water soluble dye is employed to mix with otherwise transparent water in order to bring into contrast the various equilibria patterns from the intersection between the free surface and the exposed aluminum disk's upper surface.

2.3 Evolutions of waves

It takes many steps of evolution for a water vortex to start from a static state (relative to the ground), pass through a few of structurally different laminar states, and finally reach the turbulent state at a high Reynolds number. Hence, let us first have a look at the process of development of the equilibria.

Before setting the disk into rotation, the tank is filled with shallow water, initial height h_0 (10 - 60% of the tank diameter) above the disk's upper surface. Then the rotatory motion imparted to the liquid by the disk generates a centrifugal force field, which compels the water towards the circumferential tank wall. The receding water can expose the central part of the disk surface to air, then the contact line between water and the solid metal disk surface will outline Kelvin's stable rotating shapes of the core. A blue dye helps to bring into relief the various patterns for photography. The disk is set to rotate at a slow, constant speed, and is subsequently sped up in small increments.

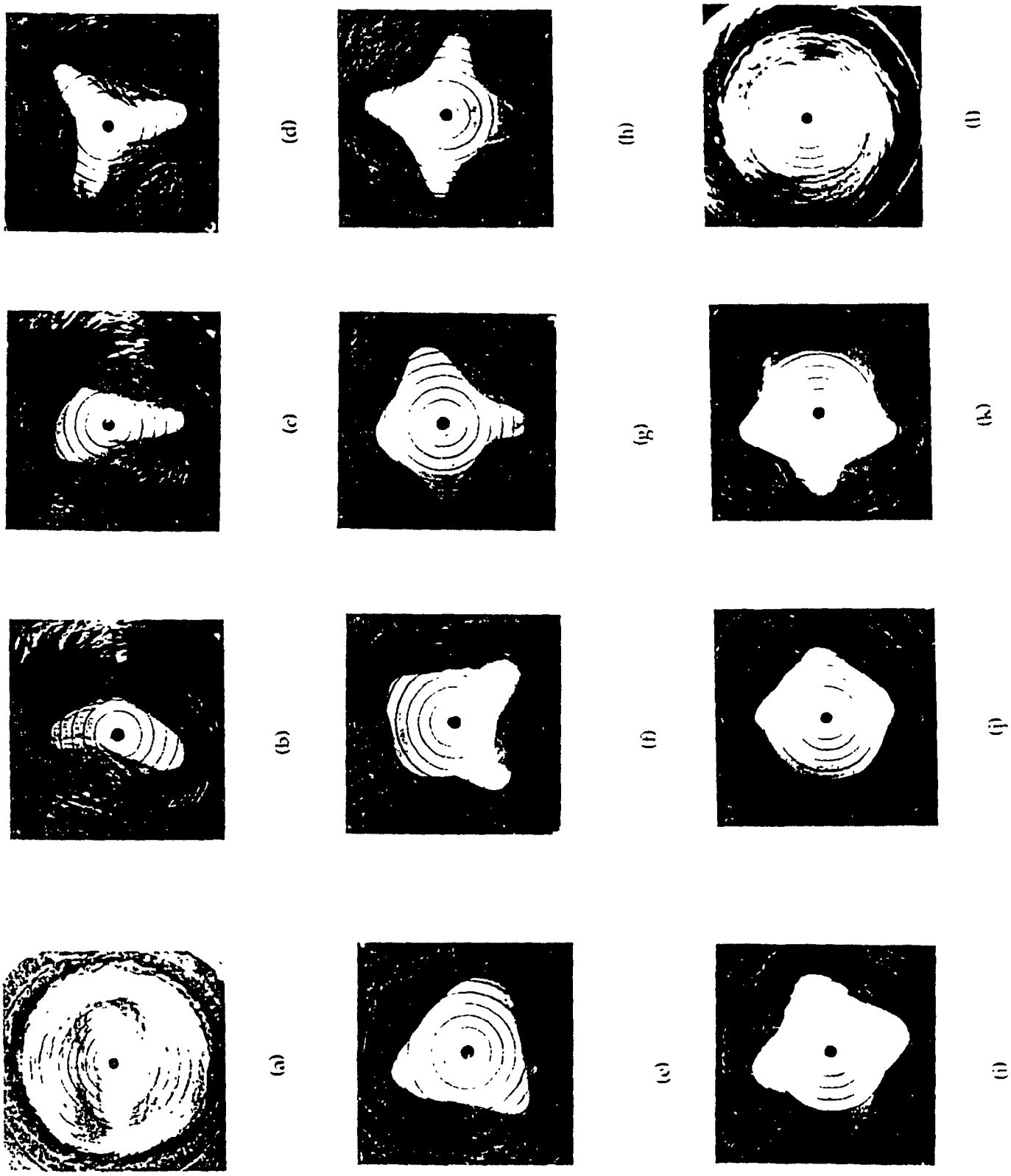

Photo plate 1 : a whole spectra of equilibria

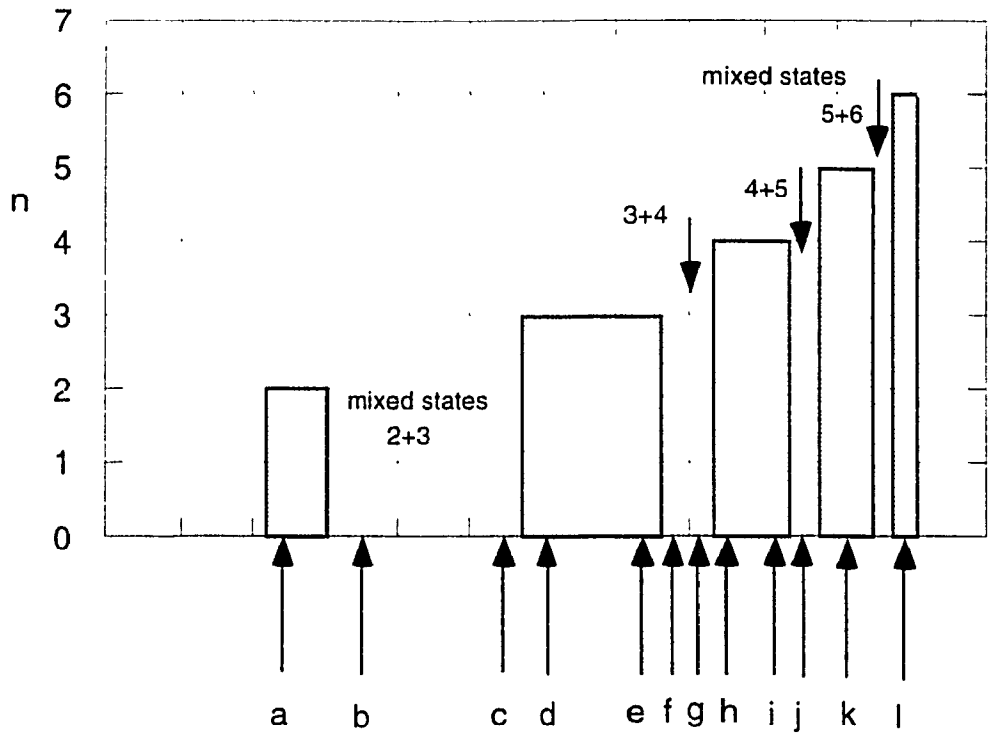

Figure 2-2 A typical spectrum of Kelvin's equilibrium transformations corresponding to the last photo assembly.

In the very beginning, a smooth forced-free (Rankine) vortex free surface appears, then the central portion of the liquid free surface touches the disk and a circular contact line shows up. When the speed is slowly increased, a wave of n=2 moving around in the same direction as the flow is formed, see Figure 2-2(a). Its phase speed is much lower than the disk's. As the rotation is increased incrementally, the symmetry disappears. In its place, a shape as in Figure 2-2(b) appears. While the small increments of rpm continues, a squeezed triangular shaped equilibrium core rotating at a slower speed than that of the disk appears, see Figure 2-2(d); the n=3 wave becomes gradually fuller at higher speeds, see Figure 2-2(e). Increasing the disk rotation further, the full triangular shaped core becomes unstable and flow shows unsteadiness. During this time, one of the three vertices is bigger than the other two, which is termed a "mixed mode" between triangle and square waves. At even higher ω_d, a squeezed square pattern appears, see Figure 2-

2(h), then it transforms into a fuller-rounded-corner square shape, see Figure 2-2(i). Subsequently an unstable mixed mode of square and pentagon shaped core develops. By continuously augmenting the disk speed, stable pentagon, Figure 2-2(k), unstable state, then stable hexagon, Figure 2-2(l) , unsteadiness in the flow, was observed in turn. At slower phase speeds, the rotation of each stable equilibrium is co-grade, and have been recorded by stop watch and verified by Laser Doppler Anemometer. Eventually the flow is turbulent, a circular but rough contact line resulting.

The equilibrium wave number n versus disk speed is measured for h_0 = 24 and 27 mm, see Figure 2-3.

The above experimentally observed symmetric air core shape is astonishingly similar to the contours conjectured by Kelvin. Detailed geometry mapping from photo and Fourier analysis have substantiated such a conclusion. Each vortex equilibrium (n=3, 4, 5, 6) persists within a certain range of disk rotation $\{\omega_{ni}, \omega_{nf}\}$ as indicated in Figures 2-3. Inside each range, the shape is squeezed toward ω_{ni+}, fuller towards ω_{nf-}. The pattern wave phase speed ω_p is a linear function of the disks' in that speed segment. The higher the ω_d, the faster the ω_p. For example, at its initial height ho = 92 mm, ω_d = 420 rpm, the n=3 wave rotates at ω_3=103 rpm, while at ω_d = 540 rpm, ω_3 = 130 rpm. The wave phase speed for n=3 versus the disk speed is plotted in Figure 2-4 for three different initial heights. The n=4 wave speeds for two different initial heights are presented in Figure 2-5. The graphic characteristics of the equilibria vs ω_d for different h_0 are almost parallel to each other. It is clear from the figure that the higher the h_0, the higher the phase speed. When h_0 is low, more equilibrium states are visible (n=3 up to 6); for relatively high h_0, only n=3, 4 or 2, 3 even only 3 could be observed. Since at high liquid level, the free surface does not touch the disk at low rotation, usually only 2, 3 are possible, while at high rotation the flow easily goes to turbulence.

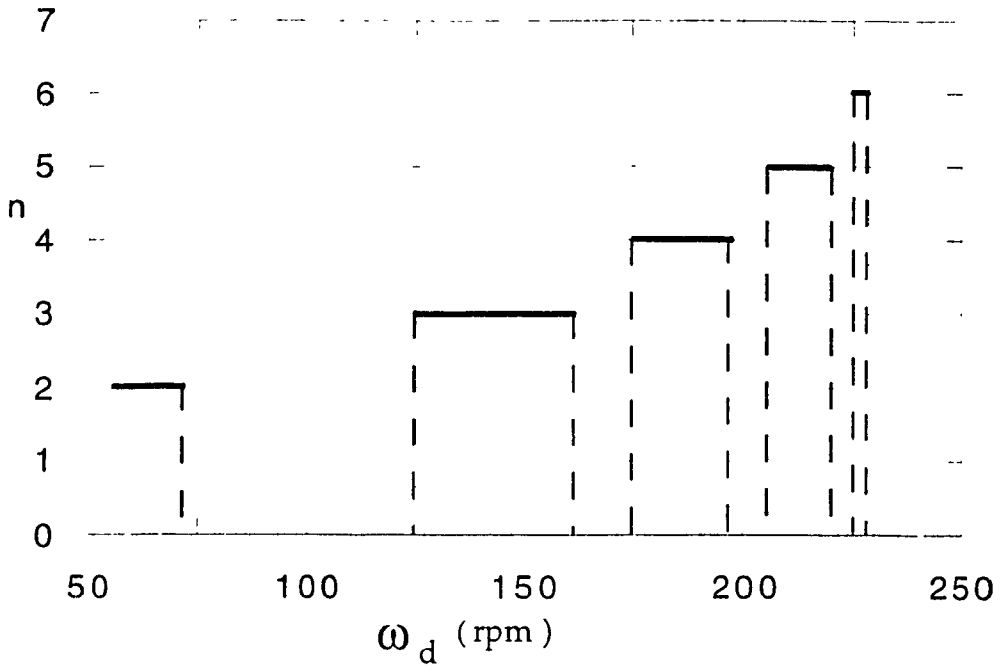

(a)

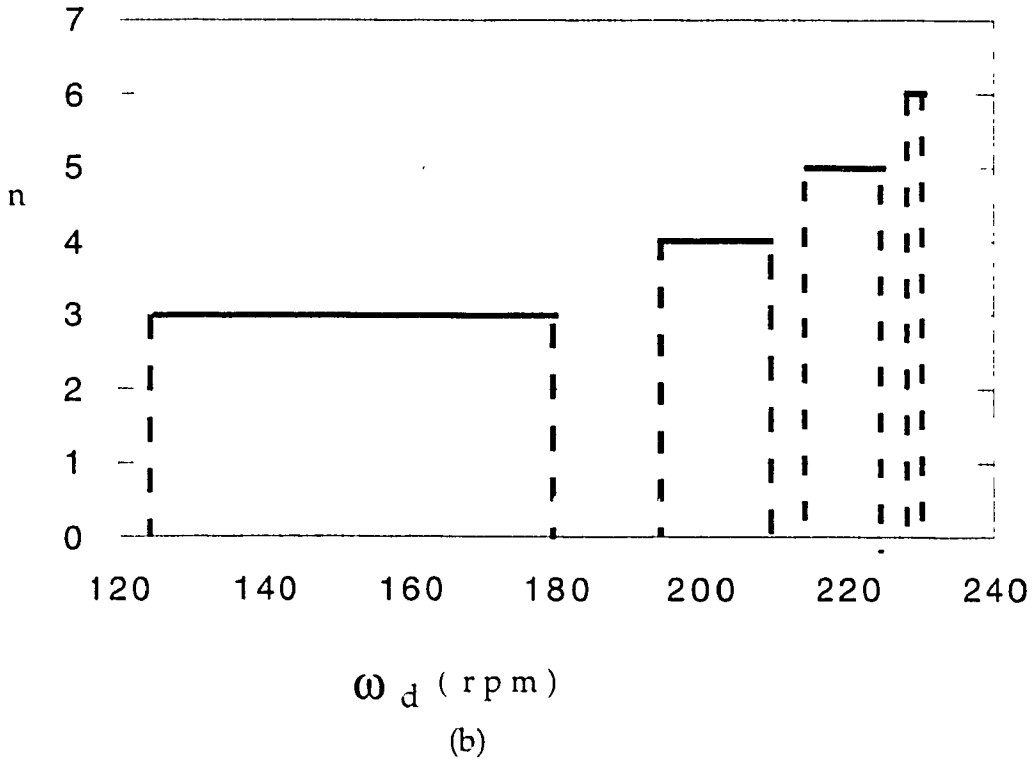

(b)

Figure 2-3 Spectra of water equilibria for (a) h_O = 24 and (b)27 mm

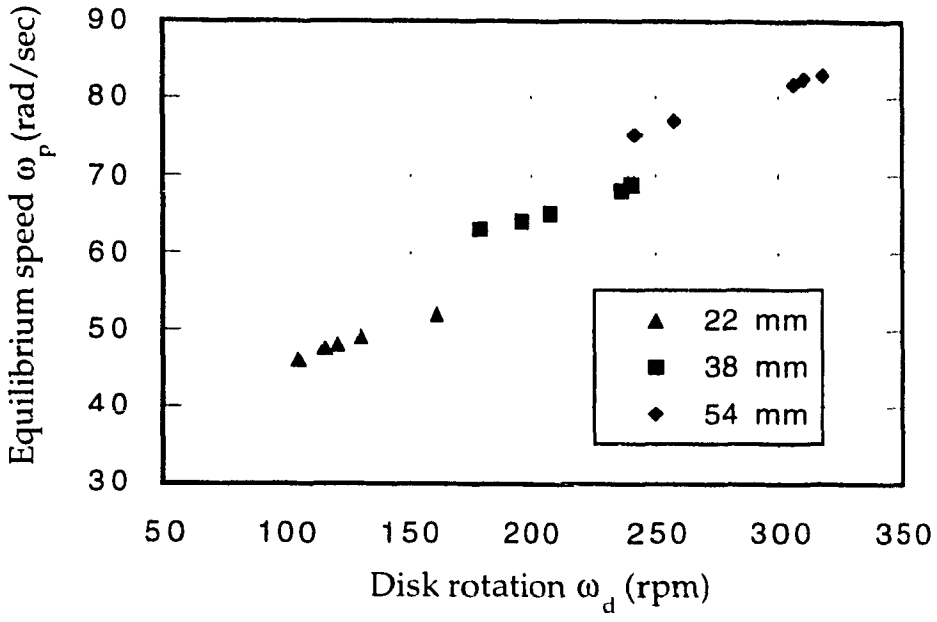

Figure 2-4 Equilibrium speeds from measurements for n=3, h_0 = 22, 38 and 54 mm.

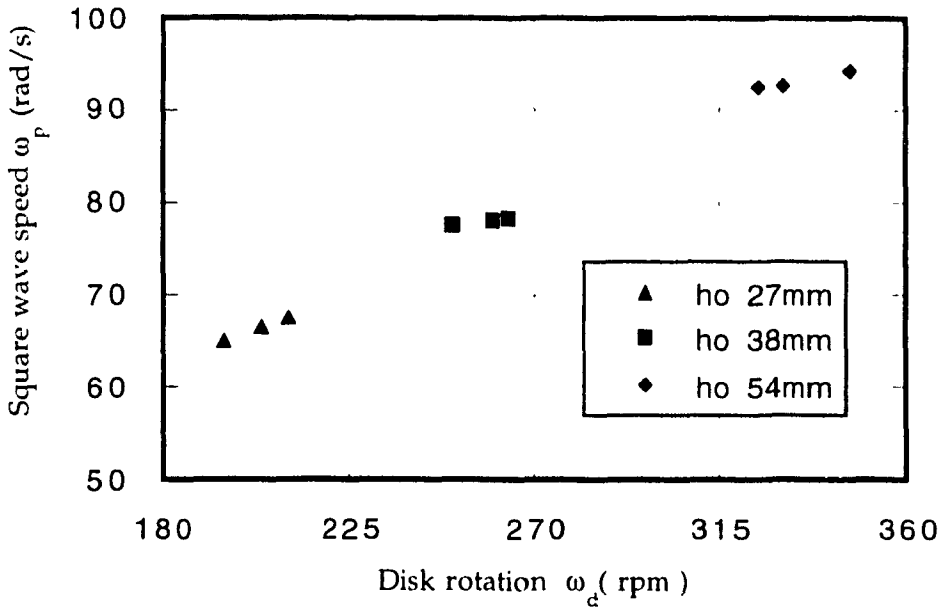

Figure 2-5 Equilibria phase speeds from experiments for n=4 and initial levels of h_0 = 27, 38, 54 mm.

The two speed limits, the initial speed ω_i and the final speed ω_f of the disk for a specific equilibrium to exist are also linear functions of the initial liquid level h_O. The higher the h_O, the higher the two values for the corresponding wave form. For example at h_O =45 mm, ω_{3i} = 126 rpm, ω_{3f} = 180 rpm, while at h_O = 55 mm, the two limits are 175 rpm and 232 rpm respectively. The lines of ω_i and ω_f vs h_O are also almost parallel, see Figure 2-5 (a) and (b) for triangle and square waves.

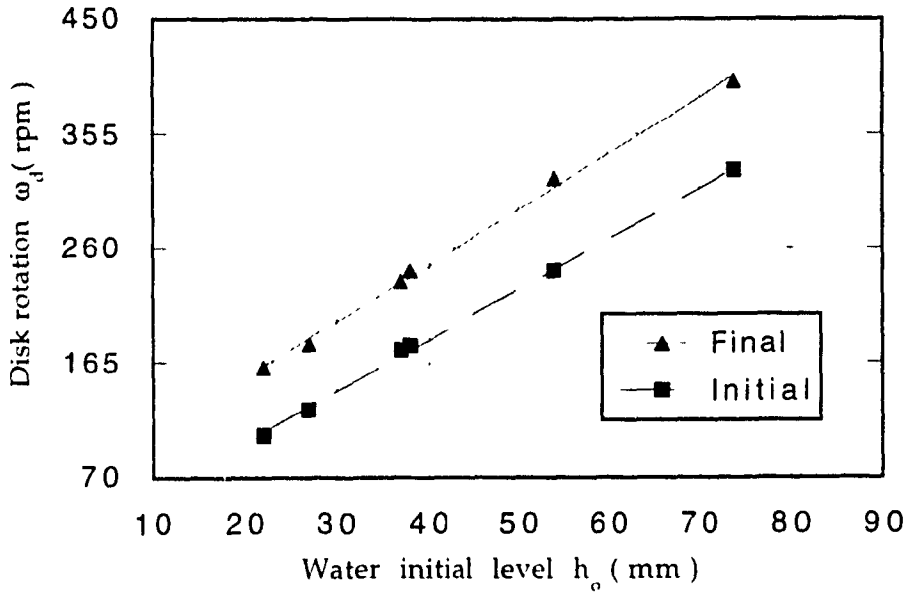

Figure 2-6 The initial and final disk rotation limits versus ho for n=3.

At some higher h_O, before the central portion of the free surface touches the disk, a disturbance with n = 2 can be easily seen before the triangular core shape appears. A careful examination of the flow by viewing the videotapes in slow motion reveals the presence of many small amplitude waves on the surface. For disk speed lying between two speed segments of consecutive states, like $\{\omega_{3f}, \omega_{4i}\}$, the contact line is a transitionally distorted, nonsymmetrical mode, that is unstable.

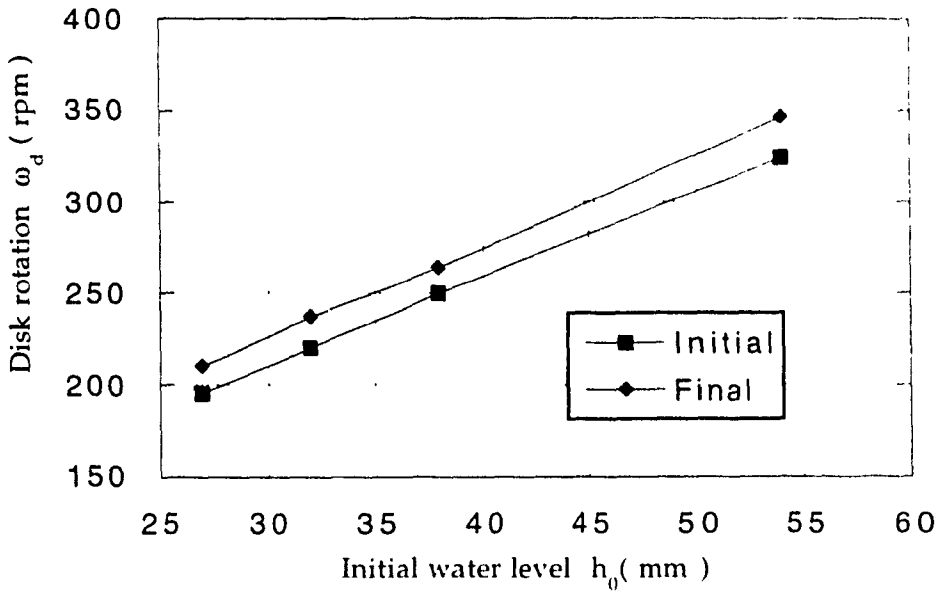

Figure 2-7 The initial and final disk rotation limits versus ho for an n= 4 equilibrium.

At relatively high h_O (approximately two times that of the disk diameter compared with about 50% in previous cases) and at high ω_d, turbulent shapes as n=2, 3, 4, which are quasi-stable, are clearly visible. There must be a defined corresponding set of parameters, including disk rotation, initial height and disk diameter (ω_d, ho, D_d) to have the disturbances behave in a macro stable symmetric fashion. The disk surface roughness and very small waddling do not appear to have significant effects on the phenomena.

2.4 Flow measurements with LDA

The flow field mapping by appropriate methods can give us a most in-depth view of how flow parameters change during transitions. For a problem of instability where the flow states are not far from the thresholds to transitions, even a very small disturbance may contaminate the integrity of measurements. Hence the Laser Doppler Anemometer is the best non-intrusive, if not the only tool to study the phenomena.

The tangential velocity of the flow field for an n=3 equilibrium has been measured, see Figure 2-8, the sampling point is at r = 11.4 cm. The near-harmonic variations of the velocity component for equilibria n= 3 is evident. These data provide the means to perform quantitative analysis. Similar measurements for n=4, 5 have also been obtained.

The measurements of the tangential component velocity of the vortex flow field have made it possible to,

1. Demonstrate the periodic oscillation of the flow parameters when a symmetric equilibrium is present, see Figure 2-8.

2. Establish a correlation for the free vortex circulation (strength) versus the driving disk's rotation, see Figure 2-9.

3. Confirm the small perturbation assumption, see Figure 2-10.

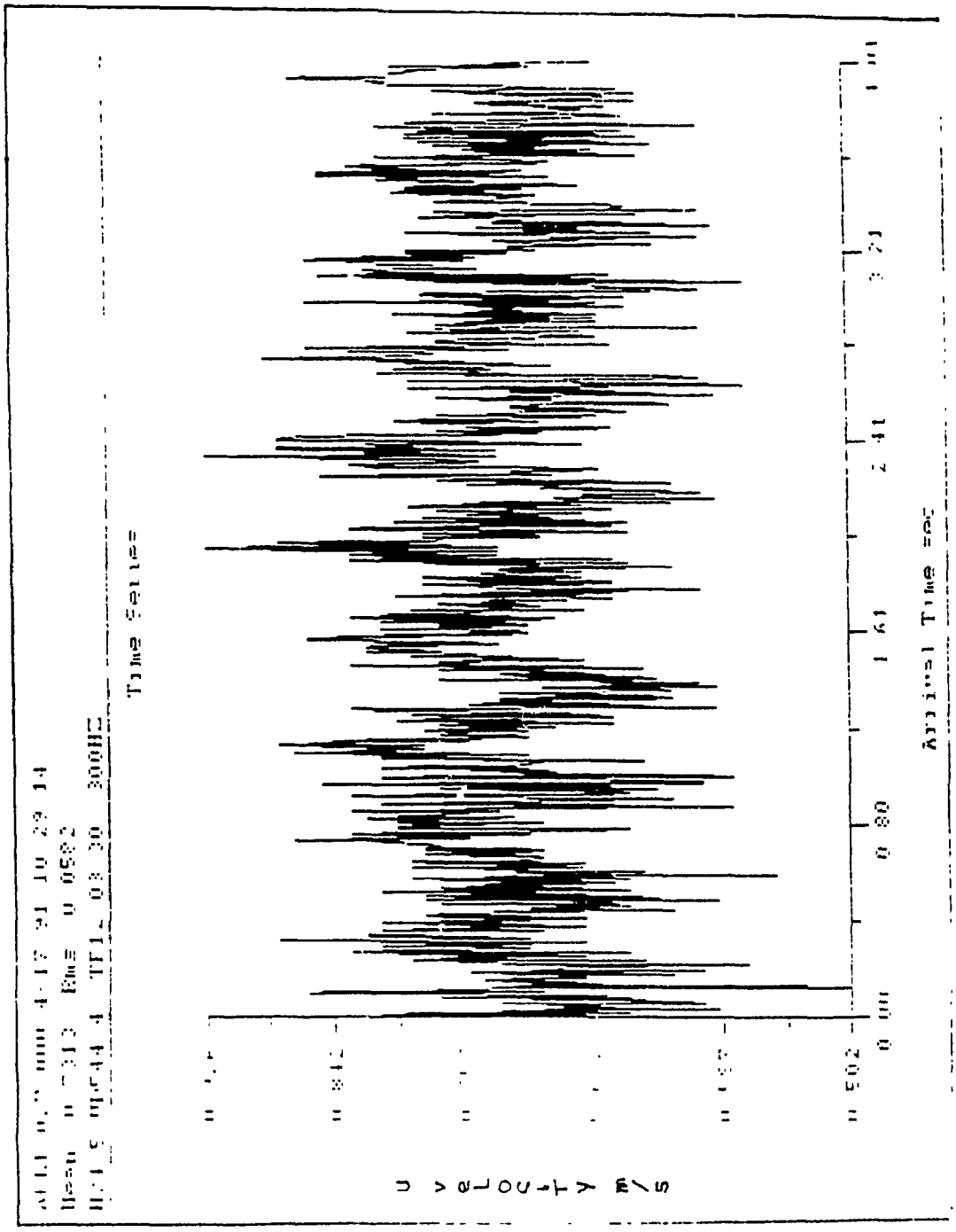

Figure 2-8 Tangential velocity by LDA

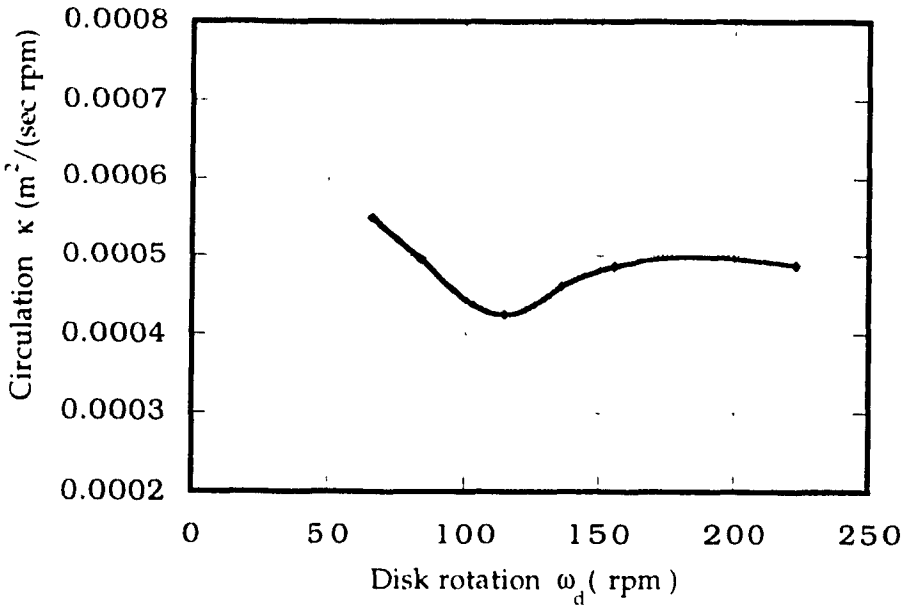

Figure 2-9 Circulation (2π r V_t) in the hollow core vortex by LDA, h_O=46 mm.

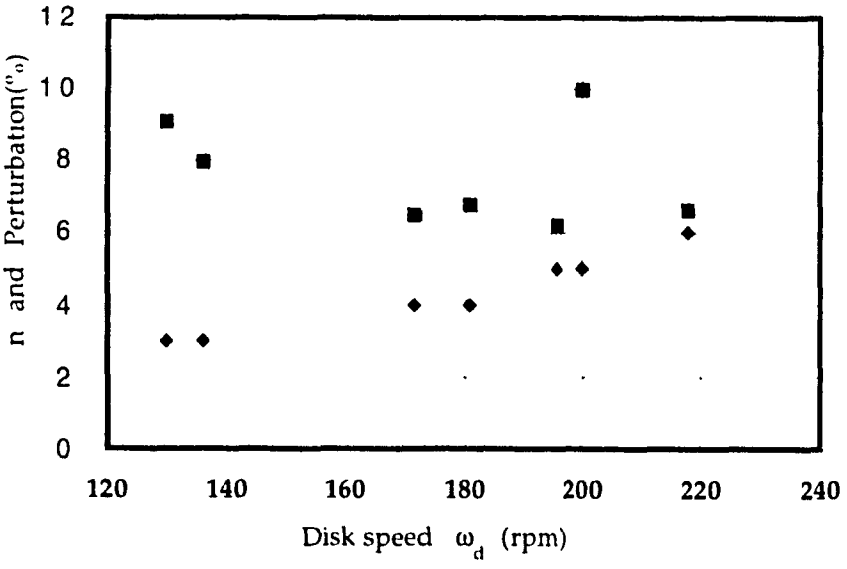

Figure 2-10 Confirmation of small perturbation (rms of the velocity over mean value) in the vortex equilibria, n is the wave number.

2. 5 Hysteresis

Since the flow exhibits a non-linear behavior as it undergoes structural transformations during the stepwise, quasi-static spin-up and spin-down of the disk rotation, it is suspected that hysteresis may be present between the two sequences. In fact, this logical deduction does hold. In order to witness the differences, the flow structural evolution with respect to ascending and descending processes of the disk rotations has been conducted for the same heights of liquid. Table 2-1 lists the two lower limiting disk rotation speeds for n=3 equilibrium. The first column is the initial liquid level. The second column indicates the disk rpm at which a n=3 wave starts to emerge on the ascending sequence from a mixed n=2+3 state. The third column lists the rpm at which a symmetric n=3 wave gives way to a mixed n=2+3 state on the descending sequence. The numerical values in the two columns should be identical if there was no hysteresis. This test is repeated for 12 different initial levels to show the persistence of hysteresis.

Table 2-1. Hysteresis (water), n=3 and d = 252 mm, Initial rpms versus h_o.

h_o (mm)	rpm (asnd)	rpm (desnd)
23.0	105.6	105.0
27.0	122.0	114.6
32.0	139.5	129.4
37.0	162.9	159.1
39.0	173.7	163.5
45.0	198.5	190.2
49.0	211.7	204.2
56.5	239.8	230.5
65.0	268.8	258.4
73.0	298.1	280.6
80.0	332.5	305.0
91.0	360.0	335.5

Table (2-2) shows the two upper limiting disk rotation speeds for triangular equilibrium. The second column indicates the disk angular velocity at which a n=3 wave terminates during the ascending sequence. The third column lists the RPMs at which a symmetric triangle wave begins to show up from a mixed n=3+4 state during the descending sequence. The numerical values in the two columns should be identical if there was no hysteresis. This test is repeated for 13 different initial levels to show its consistency, which are listed in the first column of the table.

Table 2-2. Hysteresis (water), n=3 and disk diameter d = 252 mm, final rpms versus h_0.

h_0 (mm)	rpm (asnd)	rpm (desnd)
20.0	130.5	126.8
23.0	153.9	148.0
27.0	172.4	163.4
32	195.8	186.2
37	227.0	223.9
39	238.0	236.2
45	269.2	267.0
49	288.1	285.9
56	320.8	320.4
65	360.2	358.1
73	394.7	387.8
80	427.0	428.5
91	459.4	456.77

Similarly, Tables (2-3) and (2-4) show the results for n=4 equilibria. As previously, the numerical values in columns 2 and 3 should be identical if there was no hysteresis. This test is repeated for 13 different initial levels to show its consistency.

Table 2-3. Hysteresis (water) Initial disk rpm, n=4 and disk diameter d = 252 mm.

h_o (mm)	rpm (asnd)	rpm (desnd)
20	141.4	140.8
23	157.6	150.1
27	177.0	166.0
32	196.8	188.9
37	238.2	235.0
39	249.5	247.2
45	280.1	278.7
49	297.6	296.6
56.5	332.1	331.0
65	370.3	369.8
73	415.4	409.6
80	457.3	457.3

Table 2-4. Hysteresis (water), final disk rpm for n=4 versus h_o, disk diameter d = 252 mm.

h_o (mm)	rpm (asnd)	rpm (desnd)
20	174.4	170.5
23	189.9	186.5
27	210.6	204.8
32	224.2	226.0
37	254.6	254.6
39	267.5	267.0
45	299.0	299.4
49	319.4	317.8
56.5	358.1	359.0
65	405.3	405.3
73	448.3	448.8
80	491.0	491.0

2. 6 The effect of the disk's diameter

The objective of this section is to examine how the disk's size affects the equilibrium wave at the same initial height of water.

Since the size of the disk in rotation obviously determines the strength of the vortex generated, the base flow for the equilibrium waves, due to the amount of shear force at the rotatory boundary. Hence, it is logical to presume that the wave's occurrence, such as its amplitude and the disk's initial rotation at which equilibrium waves start to emerge, would be influenced by the disk's size.

Three disks of same thickness, same material, and different diameters are made for this purpose. Four initial liquid heights are chosen to perform the comparison tests.

In the following graphs, the horizontal axis is the disk rotational speed, the vertical one is the disk diameter, and the solid horizontal line segment joining two points represents the duration of speed that must be for a wave (triangular or square) to exist.

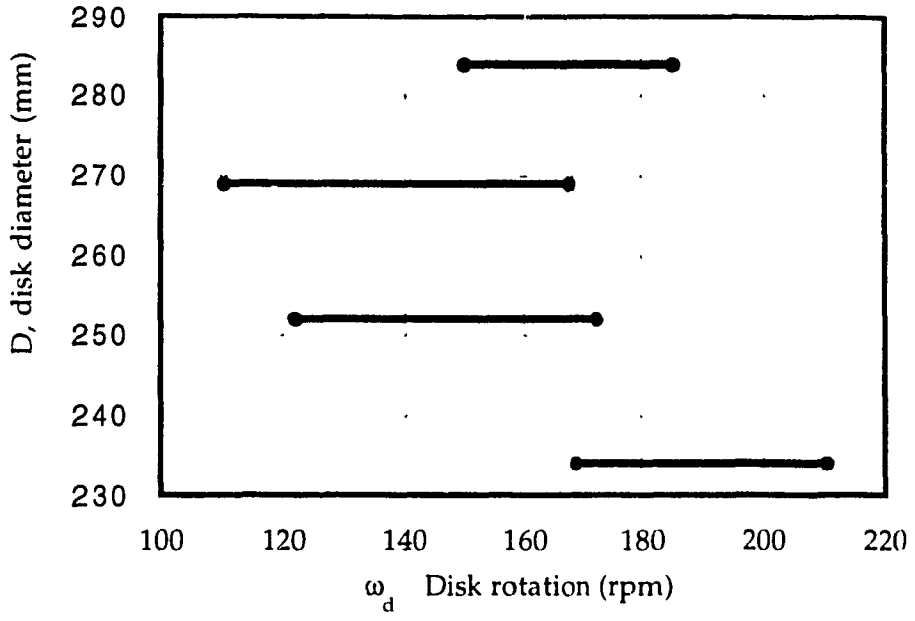

Figure 2-11 Disk speed limits of an n=3 equilibrium for different disk diameters and h_O = 27 mm.

What we can see from this graph is that the disk speed range in which a wave of n=3 persists is shifted toward lower values for disks 234, 252, 268 mm diameter, except for 284 mm, which is almost the size of the tank's inner wall. Another point worth noticing is that the speed segment range generally increases with the diameter of the disks. Regarding the largest disk, which

does not behave as do the other three, the explanation is not obvious. One possible explanation could be that, due to the fact that there is virtually no space between the disk's outer edge and the tank's inner wall, the base flow is no longer a free vortex, but instead a forced vortex.

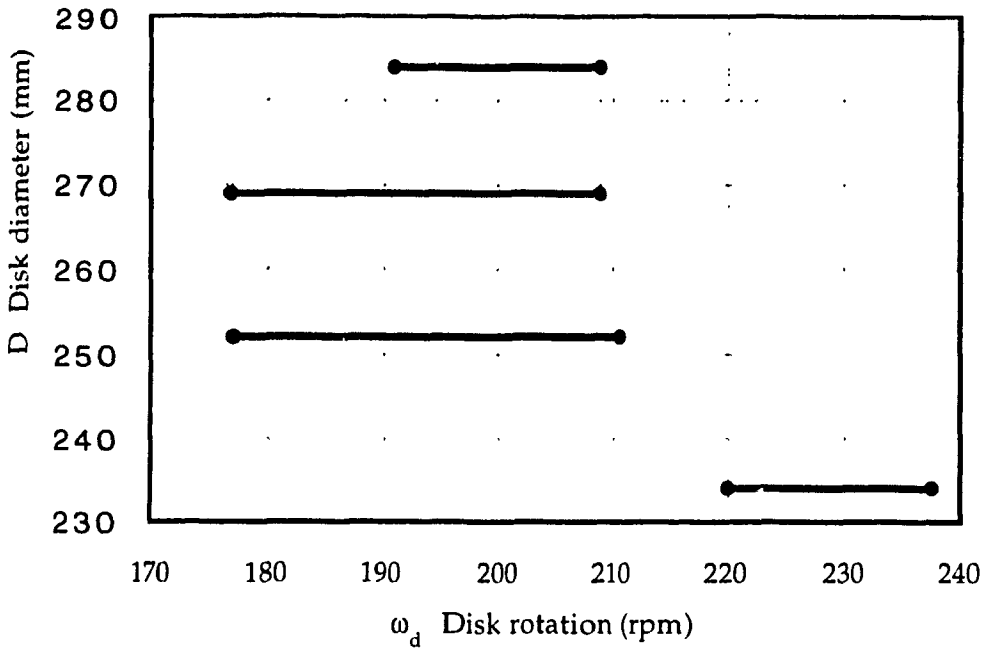

Figure 2-12 The disk speed limits of an n=4 equilibrium for different disk size and initial level of h_O = 27 mm.

This graph shows similar characteristics for an n=4 wave as was for the case an n=3 wave in the last plot.

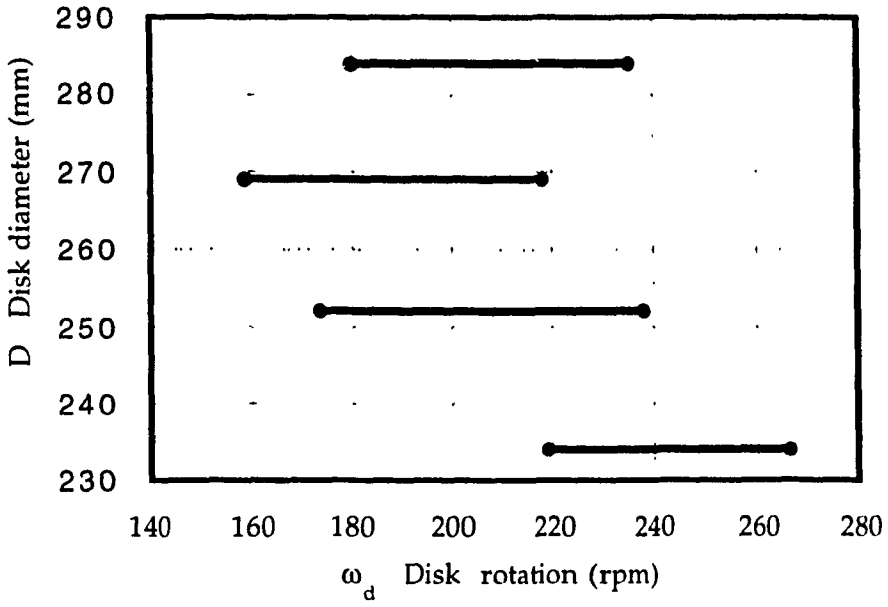

Figure 2-13 Disk speed limits of n=3 equilibria for different disk diameters at h_0 = 39.2 mm.

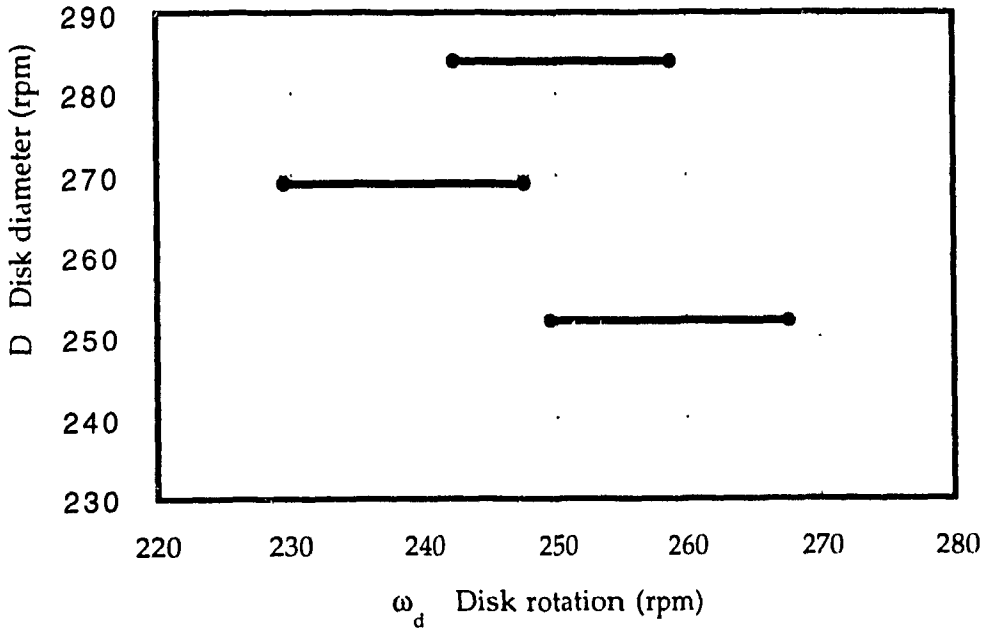

Figure 2-14 Disk speed limits of n=4 equilibria for different disk diameters at h_0 = 39.2 mm.

At the initial height of 39.2 mm, a disk of diameter 234 does not produce a square core. The spectrum shift is also obvious in this case.

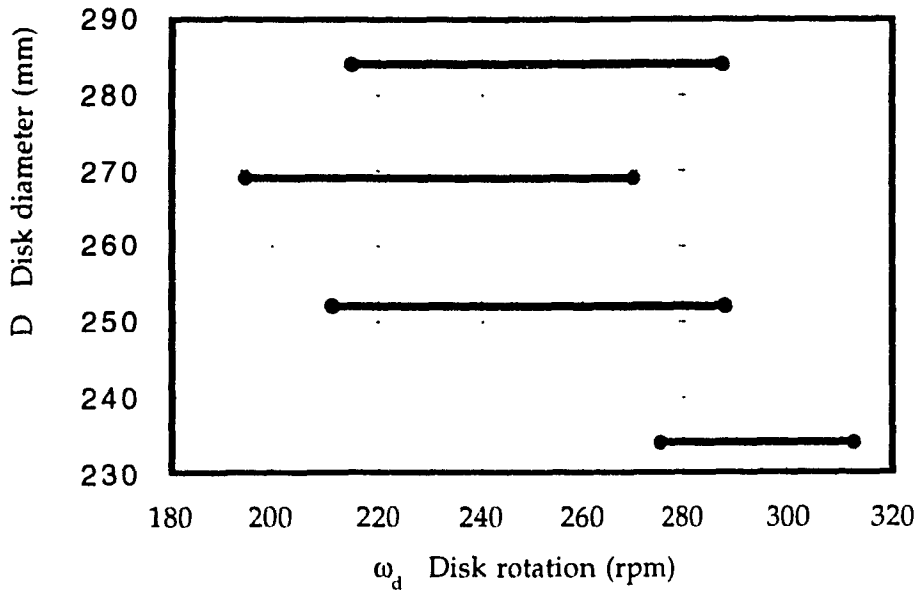

Figure 2-15 Disk speed limits of triangle equilibrium for different disk diameters at h_O = 49 mm.

The general conclusion is that for the four different sizes of disks, except the largest one, the disk range in which a wave pattern is present is shifted to the left (lower) for larger disks.

CHAPTER 3

LINEARIZED ANALYSIS FOR LOW VISCOSITY LIQUIDS

The linearized stability analysis is applied to investigate the wave behavior in a non-viscous liquid vortex. Two flow cases are considered herein. The first case deals with waves developed on the free surface of a hollow liquid vortex, while the second one deals with waves generated in the core of a Rankine vortex. The result of the analysis makes it evident that the equilibrium experimental dispersion velocity approaches the calculated one when the wave amplitude is small. The latter is consistent with the small perturbation assumption that is inherent in the theory. For the case where the core is flooded (*Rankine vortex*), the presence of a cylindrical wall is shown to enhance the wave phase speed. A hypothesis is advanced as to how the core equilibria develop in the mixed state regions. The graphical simulations appear to predict reasonably well the main features of the observations.

In light of Kelvin's derivations, a simplified 2-dimensional version analysis is employed here. Although this approach might be a simplistic address to a complex problem, nonetheless, it does provide a good qualitative picture of several phenomena associated with the present flow situations.

3.1 The base flow is free vortex

For a flow situation depicted as in Figure 3-1, the liquid is compelled to the outer region of the disk, which is taken as the outer part of a Rankine vortex.

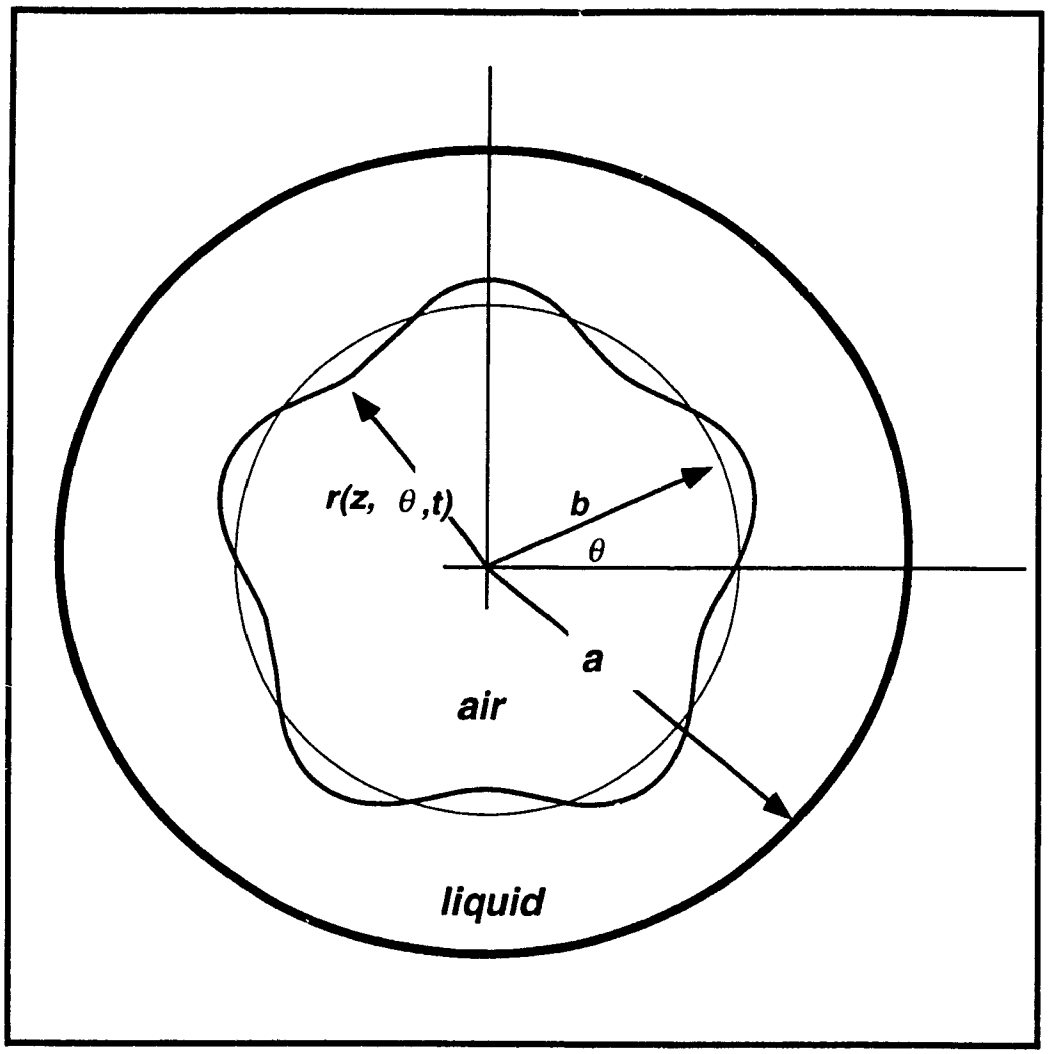

Figure 3-1 Top view of an equilibrium in free vortex.

The continuity equation in the polar coordinate system is,

$$\frac{\partial^2 \Phi}{\partial r^2} + \frac{1}{r}\frac{\partial \Phi}{\partial r} + \frac{1}{r^2}\frac{\partial^2 \Phi}{\partial \theta^2} = 0 \qquad (1)$$

Where Φ is the velocity potential,

Assuming that the equilibrium flow is the sum of base flow and a small harmonic perturbation,

$$\Phi(r, \theta, t) = \kappa\theta + f(r)\, i\, e^{i(n\theta - \sigma t)} \qquad (2)$$

the radial and tangential velocities are,

$$u = \frac{\partial \Phi}{\partial r} = f'\, i\, e^{i(n\theta - \sigma t)} \qquad (3a)$$

$$v = \frac{1}{r}\frac{\partial \Phi}{\partial \theta} = \frac{\kappa}{r} - \frac{n}{r} f e^{i(n\theta - \sigma t)} \qquad (3b)$$

where n is the circumferential wave number, σ is the angular frequency and κ is the strength of the base vortex, and the prime denotes differentiation with respect to the radius.

From continuity requirement,

$$f'' + r^{-1} f' - r^{-2} n^2 f = 0 \qquad (4)$$

together with the non-penetration boundary condition at the solid wall,

$$u(r=a) = 0$$

we have

$$f(r) = C\left(\frac{r^n}{r_e^{2n}} + \frac{1}{r^n}\right) \qquad (4a)$$

where C is a constant.

Referring to Figure 3-1, the radial hollow core shape can be approximated by

$$r(z,\theta,t) = r_e(z) + \hat{r}(z)\, e^{i(n\theta-\sigma t)} \qquad (5)$$

Here, the third dimension z is introduced into the equations due to the fact that the hollow air core is not constant, it expands from the bottom upwards. By involving z in this fashion, one more condition is implied : that all the thin horizontal flow layers are independent of each other.

The boundary condition at the hollow free surface is that the radial velocity matches the shape rotation, or in other words, a liquid particle on the free surface stays there,

$$u = \frac{\partial r}{\partial t} + \frac{v}{r}\frac{\partial r}{\partial \theta} \qquad (6)$$

Neglecting the second order terms, this leads to

$$r(z,\theta,t) = r_e(z) - \frac{f'(r_e)}{\sigma - \frac{\kappa n}{r_e^2}}\, e^{i(n\theta-\sigma t)} \qquad (6a)$$

The time dependent Bernoulli's momentum equation for the inviscid flow is

$$\frac{\partial \Phi}{\partial t} + \frac{1}{2}q^2 + \frac{p}{\rho} = f_n(t) \qquad (7)$$

where q is the total velocity at a fixed point in the flow field, function $fn\ (t)$ on the right hand side is a time dependent integration constant across the flow field.

Applying this condition to the free surface yields

$$\sigma f(r_e)\, e^{i(n\theta-\sigma t)} + \frac{\kappa}{2r_e^2} + \frac{\kappa}{r_e^3}\frac{\dot{f}(r_e)}{\sigma - \frac{\kappa n}{r_e^2}}\, e^{i(n\theta-\sigma t)}$$

$$-\frac{n\kappa}{r_e^2} f(r_e)\, e^{i(n\theta-\sigma t)} + \frac{p}{\rho} + g z = fn(t)$$

Bernoulli's equation applies to both unperturbed free vortex flow and small harmonically perturbed flow. Subtracting the equation for the unperturbed flow from the above, an expression for the disturbance wave phase speed or dispersion relation is obtained as,

$$\frac{c}{\omega} = \frac{\sigma}{\omega n} = 1 \pm \eta \sqrt{\frac{1}{n}} \qquad (8)$$

where,

$$\eta = \sqrt{\frac{1 - k^{2n}}{1 + k^{2n}}} \qquad (9)$$

where k = b/a, the plus and minus signs represent fast and slow waves.

In order for the wave speed to be finally calculated, two parameters remain to be given : the hollow core radius b and the free vortex strength κ. The free vortex strength has to be obtained experimentally from measurements by LDA (see previous chapter). For the present analysis, the following empirical correlation is used,

$$\kappa\ [m^2/s] \approx 0.0005\ \omega_d\ [RPM] \qquad (10)$$

The hollow core radius b can be obtained from conservation of mass, with the base flow as quasi-3D potential. Equating the volumes during steady rotation and before rotation is initiated, we have,

$$\pi a^2 h_o = \int_0^a 2\pi r\, dr\, z\,(r)$$

where

$$z\,(r) = \frac{\Omega^2}{2g}\left[\frac{1}{b^2} - \frac{1}{r^2}\right] \qquad (11)$$

The above condition gives

$$\left(\frac{b}{a}\right)^2 \left\{\gamma - 2\ln\left(\frac{b}{a}\right)\right\} - 1 = 0$$

where

$$\gamma = \frac{2a^2 g h_o}{\kappa^2} + 1$$

The solution of the above equations by any numerical method will provide the value for b.

Up to now, we have all that is required to evaluate the wave phase speed c. In Figures 3-2 to 3-10, comparisons between the calculations and experimentally measured values are plotted, where a slow speed from the Eqn.(8) (negative sign) is chosen. The slow speeds are the ones closer to what is obtained from visual observations. Concerning why the faster wave is not observed, one proposition is that since its amplitude is much less significant than that of its slower partner, its presence is not visible.

Based on the comparison, what is evident here is that the simplified linear small perturbation theory does give encouraging results for the speed of the wave, although it could not give the exact shape or the amplitude of the disturbances, because there is still one integration constant to be determined. The way to complete this constant is to find one additional condition, either from the measured equilibrium shape or from the tangential velocity by LDA for a specified radial location. Matching either of these two variables will provide the supplemental condition in short.

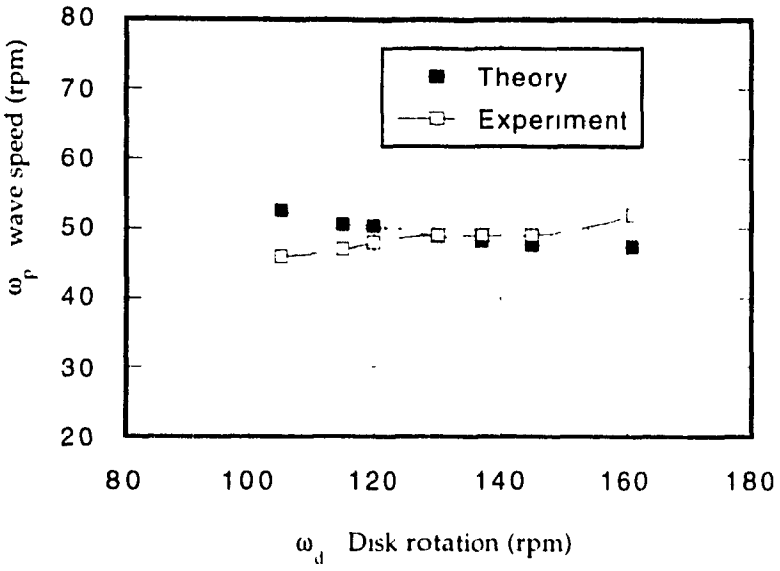

Figure 3-2 Equilibrium wave speed in a free vortex, n=3, h_0 = 22 mm.

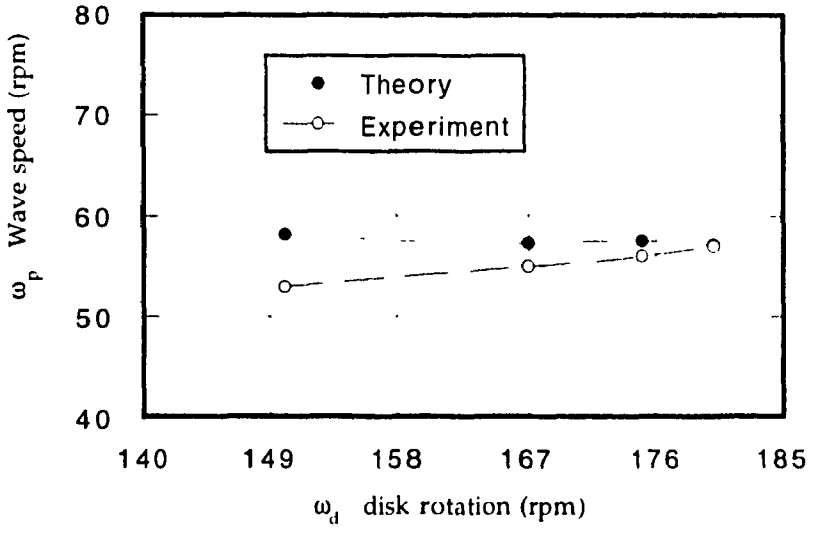

Figure 3-3 Equilibrium wave speed in a free vortex n=3, h_0 = 27 mm

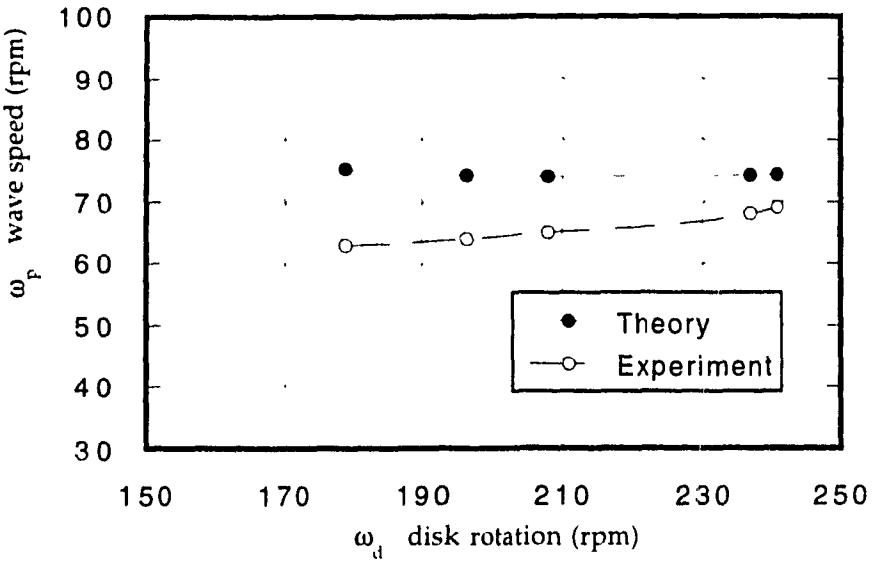

Figure 3-4 Equilibrium wave speed in a free vortex n=3, h_O = 38 mm

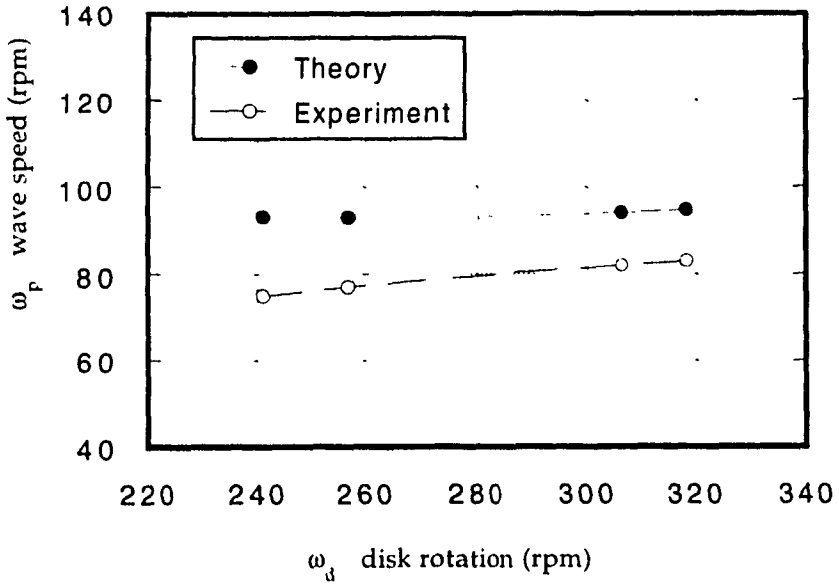

Figure 3-5 Equilibrium wave speed in a free vortex, n=3, h_O = 54 mm

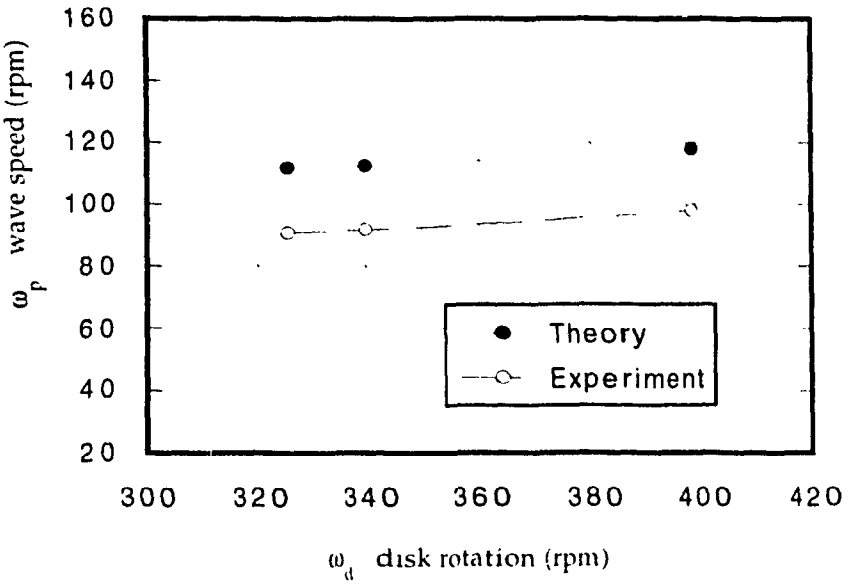

Figure 3-6 Equilibrium wave speed in a free vortex, n = 3, h_0 = 74 mm.

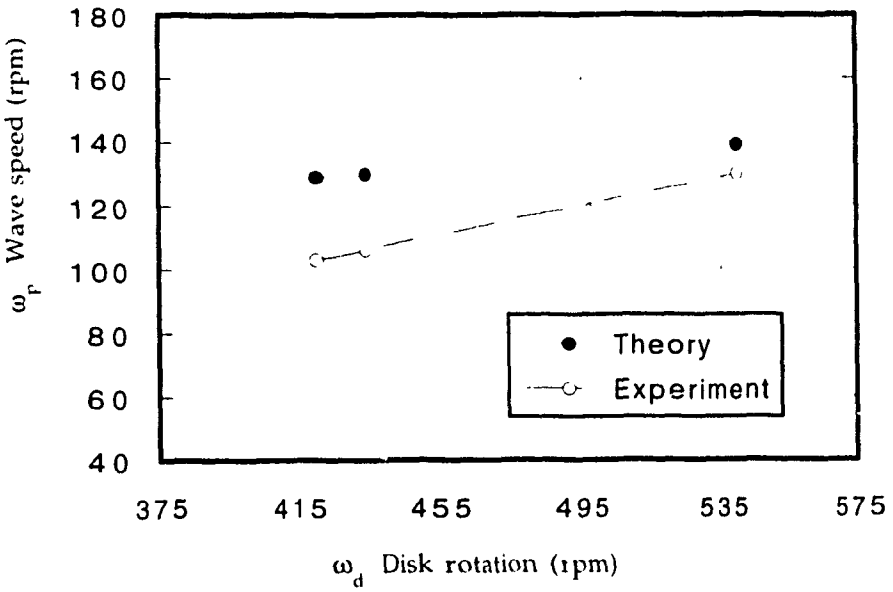

Figure 3-7 Equilibrium wave speed in a free vortex, n = 3, h_0 = 92 mm.

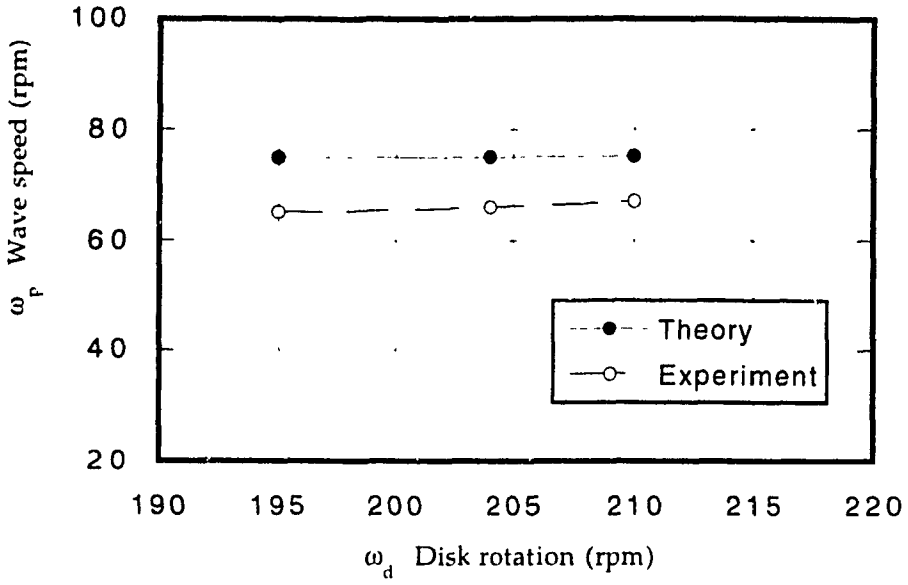

Figure 3-8 Equilibrium wave speed in a free vortex, n = 4. h_O=27 mm

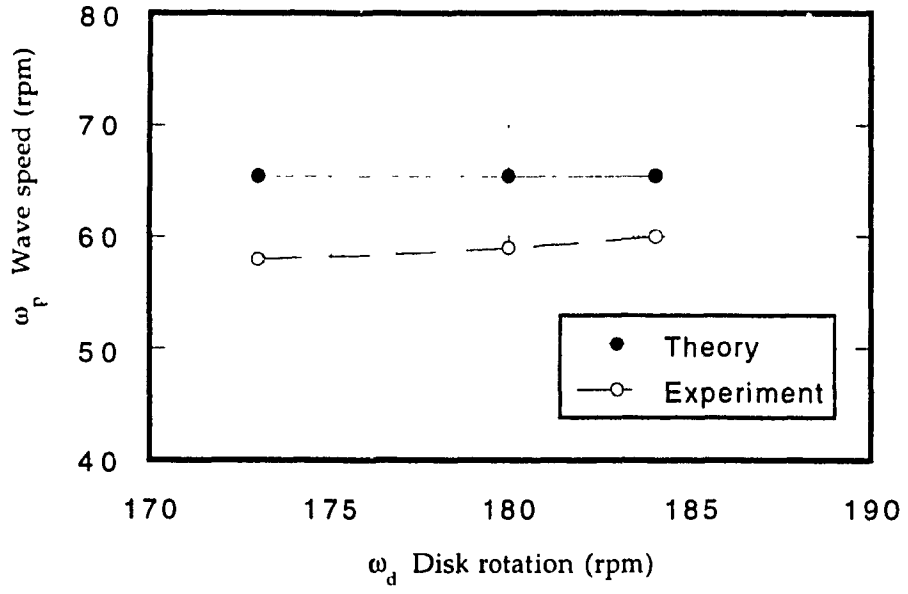

Figure 3-9 Equilibrium wave speed in a free vortex, n = 4, h_O=38 mm

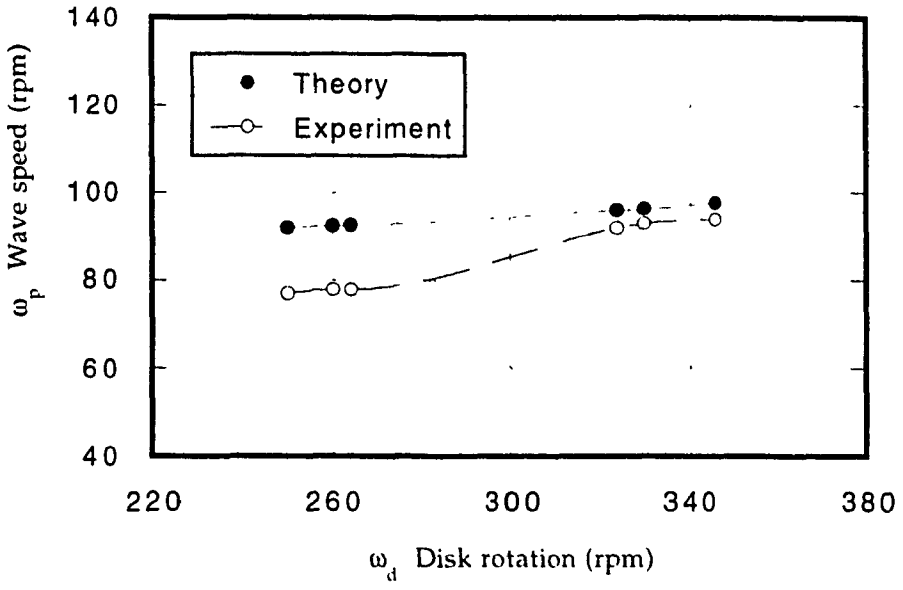

Figure 3-10 Equilibrium wave speed in a free vortex, n = 4, h_O=54 mm

To provide a more complete picture of the equilibria geometry on the free surface, some numerical mapping will follow.

The expression for f '(b) from Equ.(4a) is substituted into Equ. (6a), and together with the equation for the wave speed Equ.(8), one obtains

$$\dot{r}_n (z_e = 0, \theta, t) = 1 - \frac{A_n}{b^{n-1} \kappa} \sqrt{n (1 - \lambda^{4n})}\, e^{i (n\theta - \sigma t)}$$

where

$$\dot{r}_n (z_e = 0, \theta, t) = \frac{r_n (z_e = 0, \theta, t)}{b}$$

An is an integration constant and

$$\lambda = \frac{b}{a}$$

Given c_n, k, a and taking

$$\sigma = 0$$

since what really counts is the relative speed of the wave with respect to the reference frame rotating at a constant angular speed σ, then the core radius at the bottom is

$$\bar{r}_n (z_e = 0, \theta) = 1 - B_n e^{i (n \theta)} \qquad (13)$$

where

$$B_n = \frac{A_n}{b^{n-1} \kappa} \sqrt{n (1 - \lambda^{4n})}$$

For a core in a given equilibrium state, increasing disk rotation speed results in an increase of vortex strength κ while γ decreases. The latter implies that both λ and b become larger. Such an action will produce waves of the same number with smaller amplitudes. Simulation mappings of these characteristics of the core are shown in Figure 3-12 for the case n = 4. The latter is consistent with the observations in chapter 2.

The equilibrium may therefore develop different modal forms as shown in Figure 3-11. As mentioned in previous experimental observations, symmetric equilibrium states emerge within specific disk speed intervals, while in between two such neighboring intervals, mixed states are present.

If two waves are superimposed, the normalized radius of the free surface on the disk can be expressed by

$$\bar{r}_{n,n+1}(z_e = 0, \theta) = 1 - \left\{ D_n e^{\,i\,n(\theta - c_n t)} + D_{n+1} e^{\,i\,[n+1](\theta - c_{n+1} t)} \right\}$$

where

$$D_n = B_n / 2 \qquad \text{and} \quad D_{n+1} = B_{n+1} / 2 \quad \text{respectively,}$$

and

$$\dot{r}_{n,n+1}(z_e = 0, \theta, t) = \frac{r_n(z_e = 0, \theta, t) + r_{n+1}(z_e = 0, \theta, t)}{2b}$$

Simulations based on the above formulae are presented in Figure 3-13 and Figure 3-14. The contribution of neighboring states has been incorporated through the coefficients B_n and B_{n+1}. As an equilibrium going through the evolution of the mixed state region, one of the lobes becomes fatter (smaller amplitude) as the disk rpm increments, splitting into two lobes to approach the higher equilibrium state, see for example Figure 3-13. For a particular mixed state at a constant disk rotation, its geometry deforms continuously as it turns around. This property is graphically demonstrated in Figure 3-15. The main features fit qualitatively well with the experimental revelations.

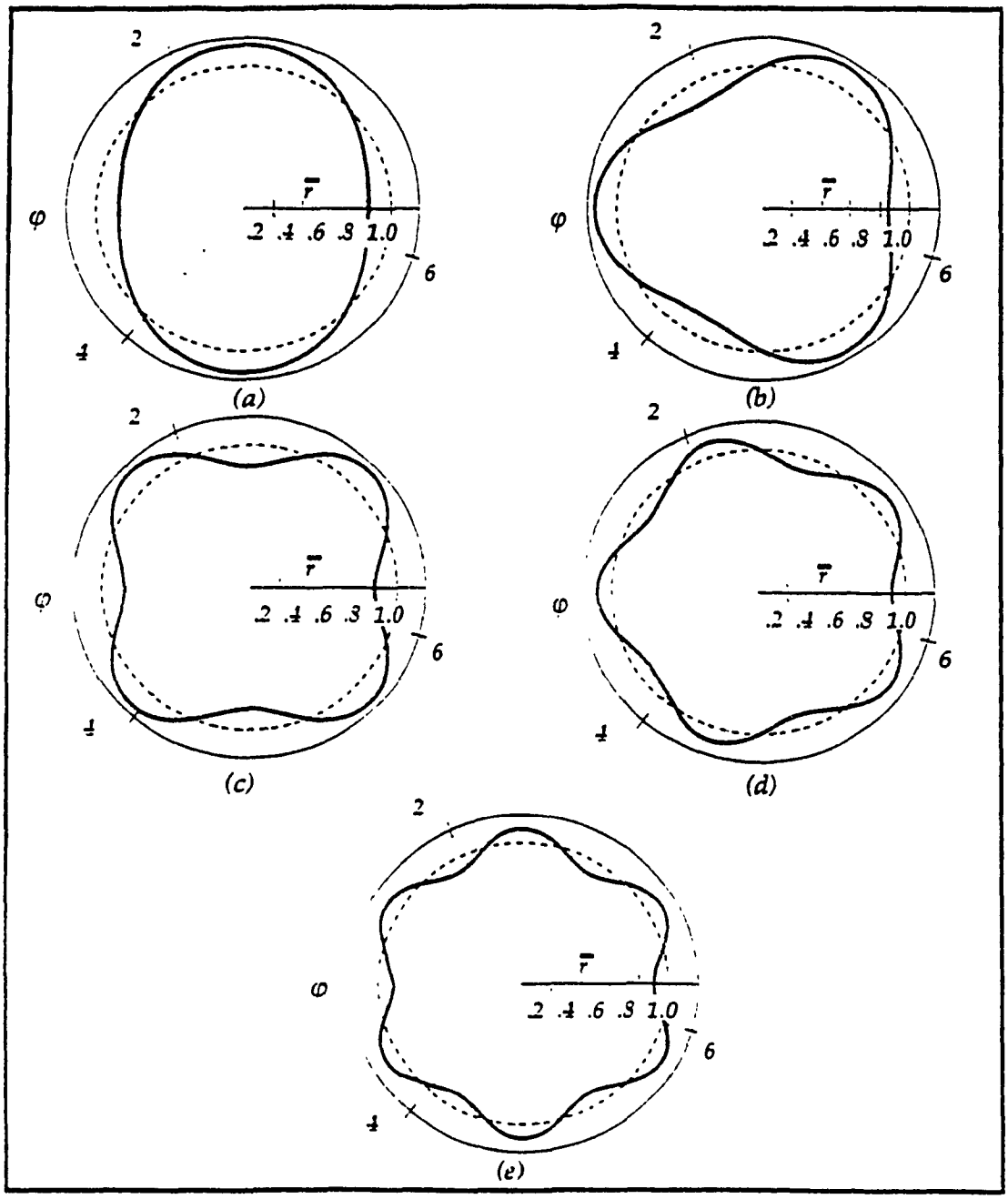

Figure 3-11 Symmetric equilibria of n=2 to 6

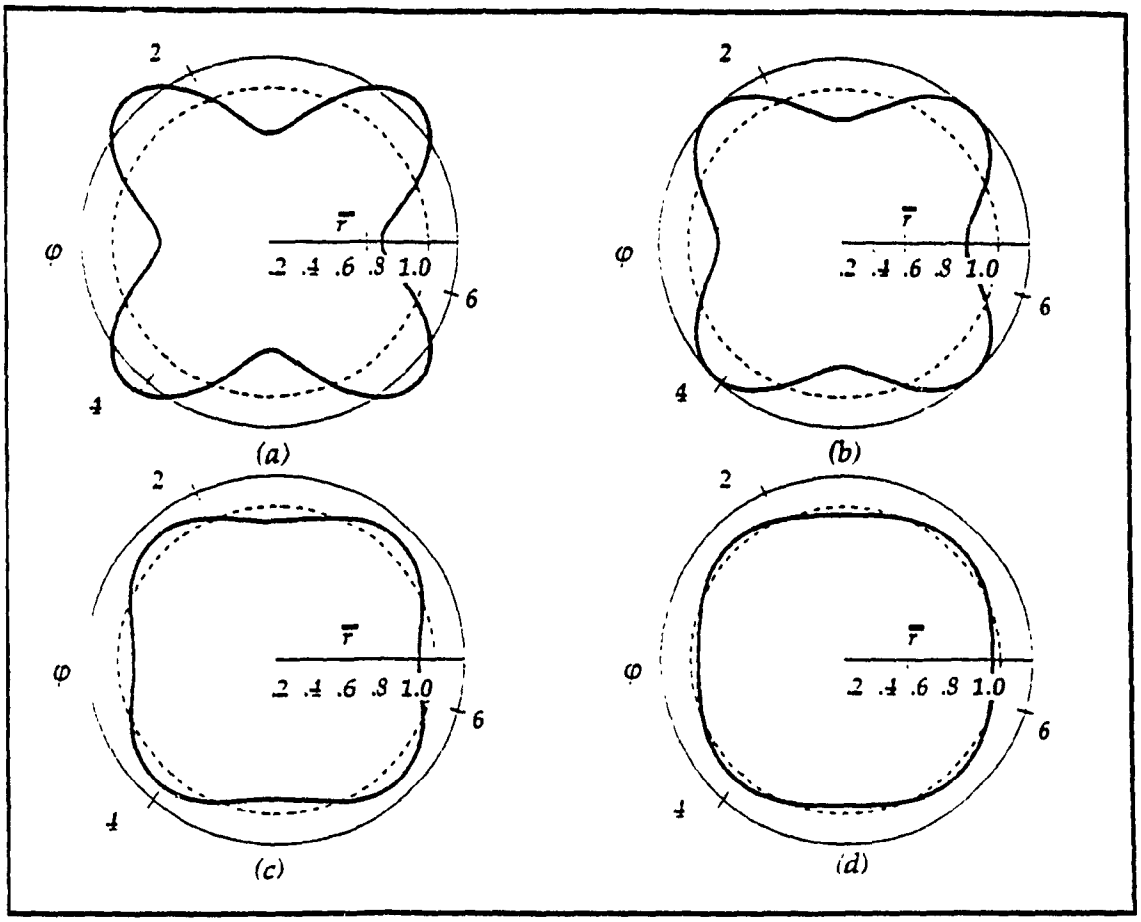

Figure 3-12 Core shape transformations for a symmetric square.

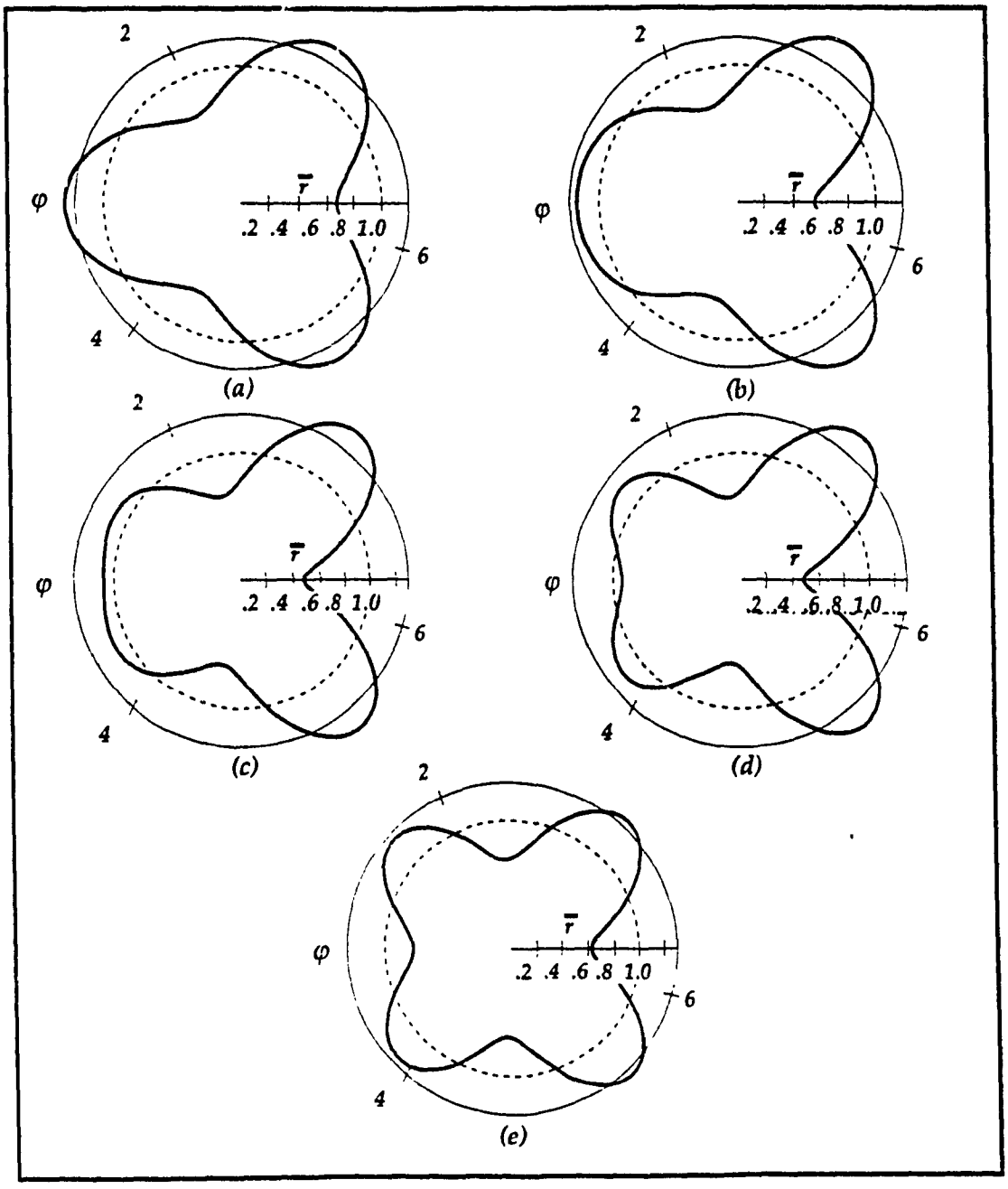

Figure 3-13 Transformations from a lower order of equilibrium to one of higher order through mixed states (n=3 to n=4).

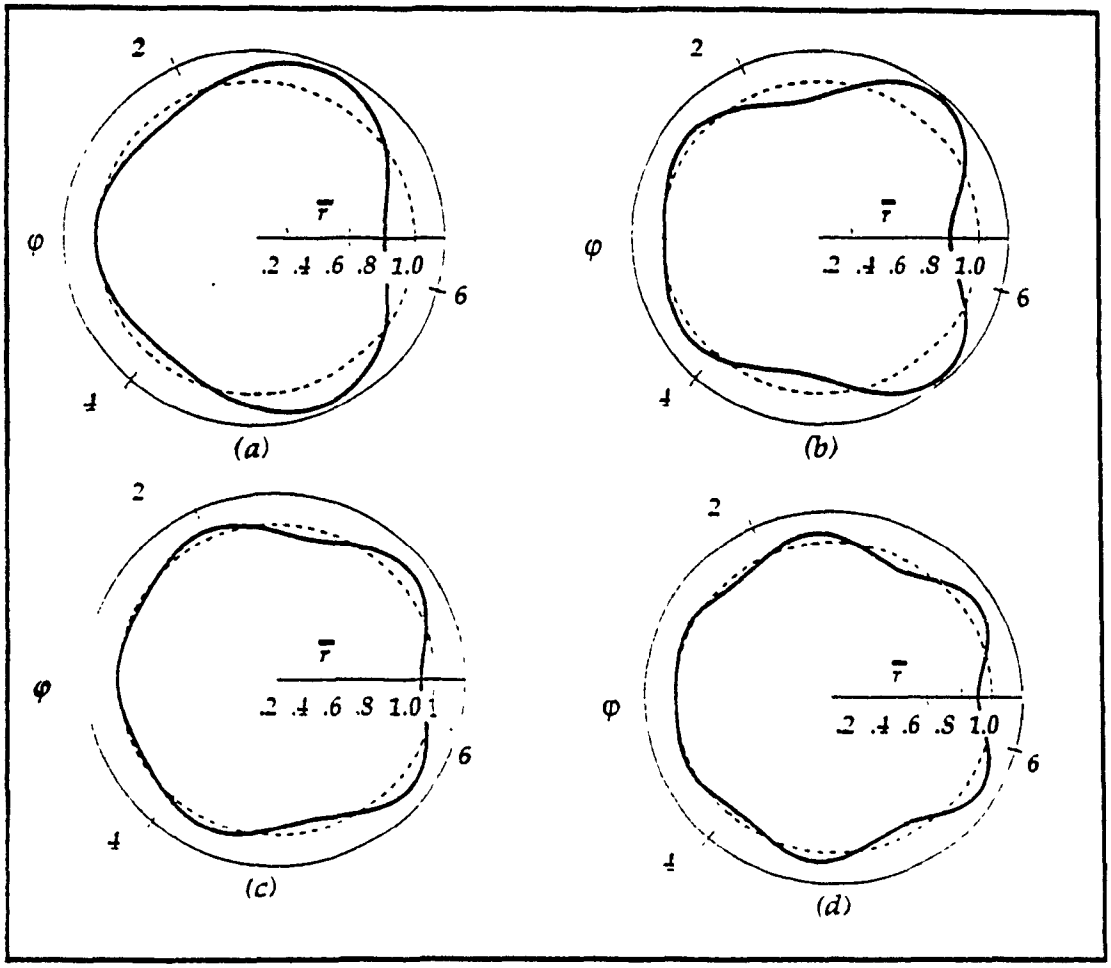

Figure 3-14 Typical mixed states.

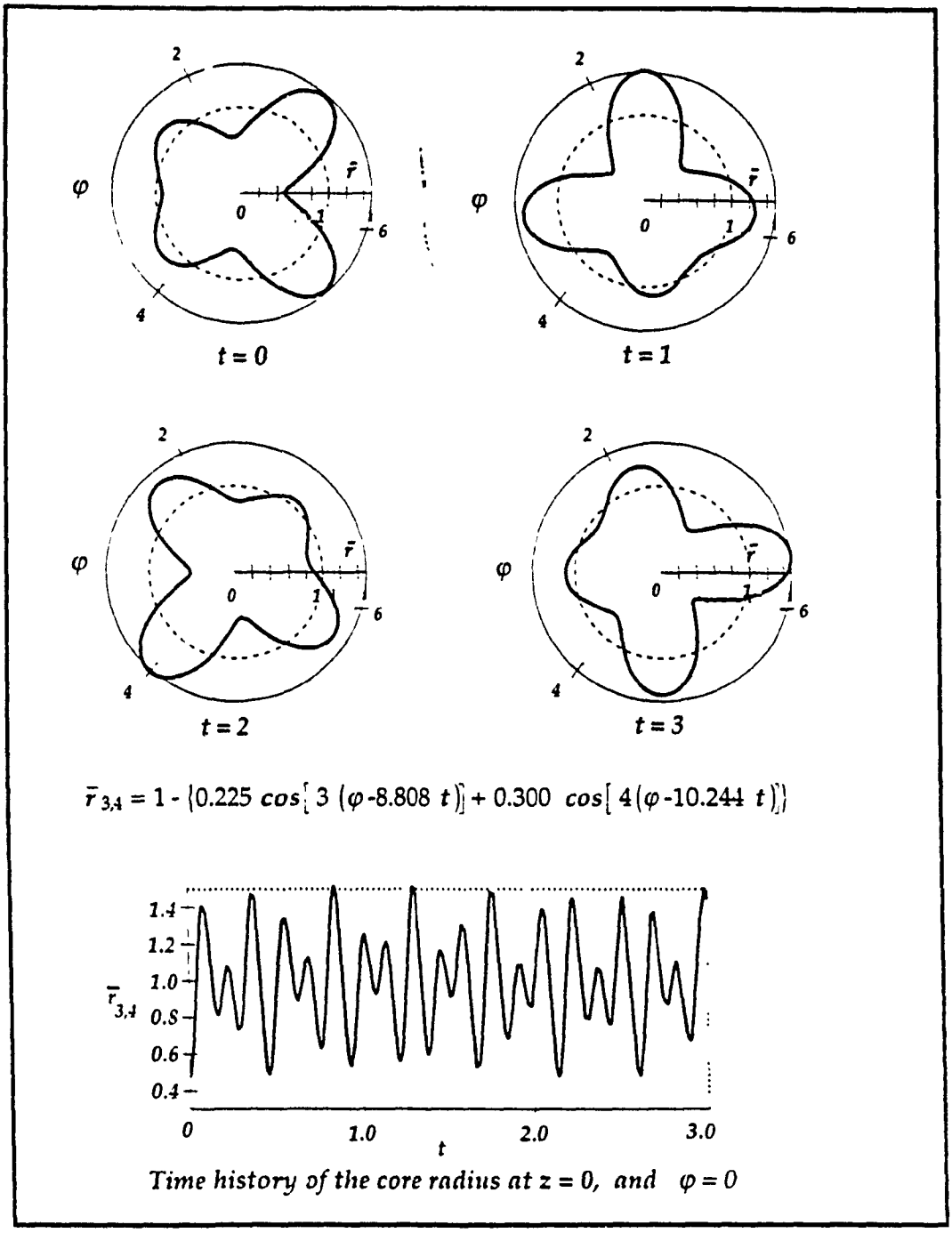

Figure 3-15 Time spectrum of a mixed equilibrium triangle and square, its shape and core radius.

3.2 Base flow is a Rankine vortex

Under certain prevailing conditions (mainly when the initial water level is higher than that of previous free vortices cases and the disk rotation is not reaching high), the core may be flooded with liquid. For this case, due to the fact that the flow is no longer potential, the stream function's formulation is adopted, and the following general flow structure is assumed

$$\psi\ (r,\theta,t\ ) = \Psi\ (r\ ) + \hat{\psi}(r,\theta,t\ ) \tag{15}$$

Where the harmonic disturbance,

$$\hat{\psi}(r,\theta,t\ ) = \xi\ (r\ )\, e^{\ i\ (n\,\theta\ -\ \sigma t\ )}$$

is superimposed onto the main flow:

$$\Psi\ (r\ ) = -\frac{1}{2}\ m\, r^{\,2} \quad for\ r \le r_c \tag{16a}$$

and

$$\Psi\ (r\ ) = -\ \kappa ln\ (\ r\ ) \quad for\ r \ge r_c \tag{16b}$$

Since the vorticity for $0 < r < r_c$ is not zero, the fluid motion in this region is assumed to be inviscid and rotational. According to the vorticity conservation equation for a two dimensional flow, the disturbance satisfies the equation,

$$\frac{\partial}{\partial t}\left(\nabla^2\hat{\psi}\right) + \frac{V\ (r\ )}{r}\ \frac{\partial}{\partial\theta}\left(\nabla^2\hat{\psi}\right) - \frac{1}{r}\frac{d}{dr}\left(\frac{1}{r}\ \frac{d\ (V_r)}{dr}\right)\frac{\partial\hat{\psi}}{\partial\theta} = 0 \tag{17}$$

The derivation of the above equation is at the end of this chapter. The function $\xi(r)$ of the disturbance must fit the above in the core flow region, hence

$$\xi = A_1 r^n + \frac{A_2}{r^n} \qquad (18)$$

Since this yields a singular condition at r=0, therefore A_2 has to be zero.

The velocity components are:

$$u = n A r^{n-1} i e^{i(n\theta - \sigma t)}$$

$$v = m r - n A r^{n-1} e^{i(n\theta - \sigma t)}$$

In the outer free vortex region, the disturbance must obey the irrotationality and the corresponding boundary condition

$$u(r = a) = 0 \qquad (19)$$

We have then

$$\xi = B \left(r^n - \frac{a^{2n}}{r^n} \right)$$

Now the velocity components in this outer flow region become:

$$u = \frac{1}{r}\frac{\partial \psi}{\partial \theta} = n B \left[1 - \frac{r_t^{2n}}{r^{2n}} \right] r^{n-1} i e^{i(n\theta - \sigma t)}$$

$$v = -\frac{\partial \psi}{\partial r} = \frac{\kappa}{r} - n B \left[1 + \frac{r_t^{2n}}{r^{2n}} \right] r^{n-1} i e^{i(n\theta - \sigma t)}$$

The velocity components u and v in the two flow regimes must be continuous at the core boundary $r = r_c$. For u component, we have

$$A = B \left(1 - \frac{a^{2n}}{r_c^{2n}} \right)$$

assuming the core boundary interface is given by

$$r\ (\theta, t\ ) = r_c + \lambda\ e^{i\ (n\theta - \sigma t\ )} \tag{21}$$

Equating the v components in two regimes at this interface and using Newton's binomial expansion,

$$\frac{1}{r_c + \lambda\ e^{\ i\ (n\theta - \sigma t)}} = \frac{1}{r_c}\left(1 + \frac{\lambda\ e^{i\ (n\theta - \sigma t\ )}}{r_c}\right)^{-1}$$

$$= \frac{1}{r_c}\left(1 - \frac{\lambda\ e^{\ i\ (n\theta - \sigma t\ )}}{r_c} + \ldots.\right)$$

By arranging and collecting terms, we have

$$n\,B = -\frac{\lambda\ (m + \frac{\kappa}{2})}{2\ r_c^{n-1}}\ \frac{r_c^{2n}}{a^2}$$

To obtain the perturbation wave phase speed, the following kinetic condition should be matched at the perturbed core boundary (equilvalently to say that the particles on the quasi-vertical core interface Equ. (21) stay there)

$$u \equiv \frac{\partial r}{\partial t} + \frac{v}{r}\ \frac{\partial r}{\partial \theta} \tag{22}$$

This results in

$$\frac{c_n}{\tilde{\omega}} = \frac{n - (1 - x_c^{2n})}{n} \tag{23}$$

where $c_n = \sigma / n$, $\tilde{\omega} = \kappa / r_c^2$ and $x_c = r_c / a$.

Hence, a bounded equilibrium speed depends on only the core size and its wave number.

Lamb presented a case for an unbounded vortex, which is only a subset of the present situation. By taking a to be infinity in the above result, x_c goes to 0 and Equ(23) yields exactly the same dispersion velocity as Lamb's. The graphical representation of Equ(23) demonstrates that the presence of the cylindrical wall enhances the speed of the equilibrium waves.

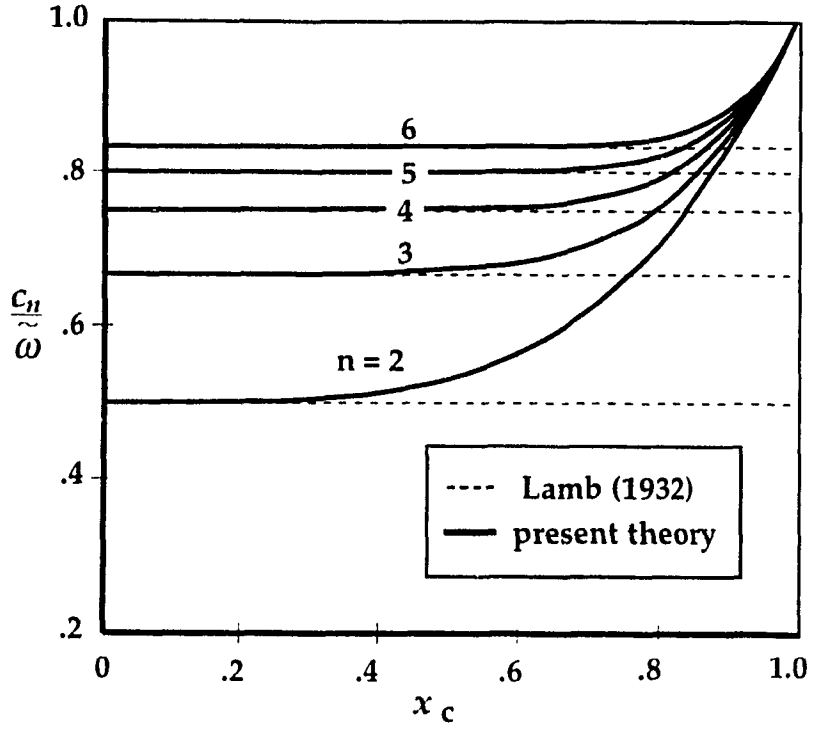

Figure 3-16 Wave speeds, in comparison with Lamb's results

Derivation for Equation (17)

Euler's equations

u- momentum

$$\frac{\partial u}{\partial t} + u\frac{\partial u}{\partial r} + \frac{v}{r}\frac{\partial u}{\partial \theta} - \frac{v^2}{r} = -\frac{1}{\rho}\frac{\partial p}{\partial r} \tag{30a}$$

v- momentum

$$\frac{\partial v}{\partial t} + u\frac{\partial v}{\partial r} + \frac{v}{r}\frac{\partial v}{\partial \theta} + \frac{u\,v}{r} = -\frac{1}{\rho\, r}\frac{\partial p}{\partial \theta} \tag{30b}$$

Continuity equation

$$\frac{\partial u}{\partial r} + \frac{1}{r}\frac{\partial v}{\partial \theta} + \frac{u}{r} = 0 \tag{31}$$

Let

$$u(r,\theta,t) = \hat{u}(r,\theta,t)$$

$$v(r,\theta,t) = V(r) + \hat{v}(r,\theta,t) \tag{32}$$

$$p(r,\theta,t)/\rho = \Pi(r) + \hat{\pi}(r,\theta,t)$$

Inserting the above into Eqn.(30a), (30b) and (31), neglecting the second order terms we get,

$$\frac{\partial \hat{u}}{\partial t} + \frac{V(r)}{r}\frac{\partial \hat{u}}{\partial \theta} - \frac{2V(r)}{r}\hat{v} = -\frac{\partial \hat{\pi}}{\partial r}$$

$$\frac{\partial \hat{v}}{\partial t} + \frac{V(r)}{r}\frac{\partial \hat{v}}{\partial \theta} - \frac{1}{r}\frac{d(rV(r))}{dr}\hat{u} = -\frac{1}{r}\frac{\partial \hat{\pi}}{\partial \theta} \tag{33}$$

$$\frac{\partial \hat{u}}{\partial r} + \frac{1}{r}\frac{\partial \hat{v}}{\partial \theta} + \frac{\hat{u}}{r} = 0$$

To eliminate pressure perturbation, differentiate the two momentum equations with respect to θ and r, then do the subtraction.

Defining

$$\xi = \frac{\partial \hat{u}}{\partial \theta} - \frac{\partial (\hat{v}\, r)}{\partial r} \tag{34}$$

and introducing intermediate variables

$$A = \frac{V(r)}{r}\frac{\partial^2 \hat{u}}{\partial \theta^2} - V(r)\frac{\partial^2 \hat{v}}{\partial \theta \partial r} = \frac{V(r)}{r}\left[\frac{\partial \xi}{\partial \theta} + \frac{\partial \hat{v}}{\partial \theta}\right] \tag{35}$$

and

$$B = -\frac{\partial \hat{v}}{\partial \theta}\frac{1}{r}\frac{d(r\,V(r))}{dr} - \frac{d(rV(r))}{dr}\frac{\partial \hat{u}}{\partial r} - \frac{d^2(V(r)\,r)}{dr^2}\hat{u}$$

from continuity, this turns out to be

$$B = -\frac{d(r\,V(r))}{dr}\left(-\frac{\hat{u}}{r}\right) - \frac{d^2(V(r)\,r)}{dr^2}\hat{u}$$

$$= -r\frac{d}{dr}\left(\frac{1}{r}\frac{d(Vr)}{dr}\right)\hat{u}$$

Then we get

$$\frac{\partial \xi}{\partial t} + \frac{V(r)}{r}\frac{\partial \xi}{\partial \theta} - \frac{d}{dr}\left(\frac{1}{r}\frac{d(Vr)}{dr}\right)\hat{u} = 0 \tag{36}$$

Using a stream function for the perturbed velocity components

$$\hat{u} = \frac{1}{r}\frac{\partial \hat{\psi}}{\partial \theta} \tag{37}$$

$$\hat{v} = -\frac{\partial \hat{\psi}}{\partial r}$$

$$\xi = \nabla^2 \hat{\psi} \tag{38}$$

The final equation is what we set out to derive,

$$\frac{\partial}{\partial t}(\nabla^2 \hat{\psi}) + \frac{V(r)}{r}\frac{\partial}{\partial \theta}(\nabla^2 \hat{\psi}) - \frac{1}{r}\frac{d}{dr}\left(\frac{1}{r}\frac{d(Vr)}{dr}\right)\frac{\partial \hat{\psi}}{\partial \theta} = 0 \tag{39}$$

Calculations of core size and base vortex intensity

Base flow

$$\begin{aligned} V_\theta &= \omega r \qquad && r \le r_c \\ V_\theta &= \frac{\kappa}{r} \qquad && r \ge r_c \end{aligned} \tag{40}$$

To calculating the free surface profile, neglecting the impact of small wave perturbations on the pressure at the bottom, then the pressure is uniform in the 360 degrees circumferential at a fixed radius. From the r momentum equation,

$$-\frac{1}{\rho}\frac{dp}{dr} = -\frac{V_\theta^2}{r} \tag{41}$$

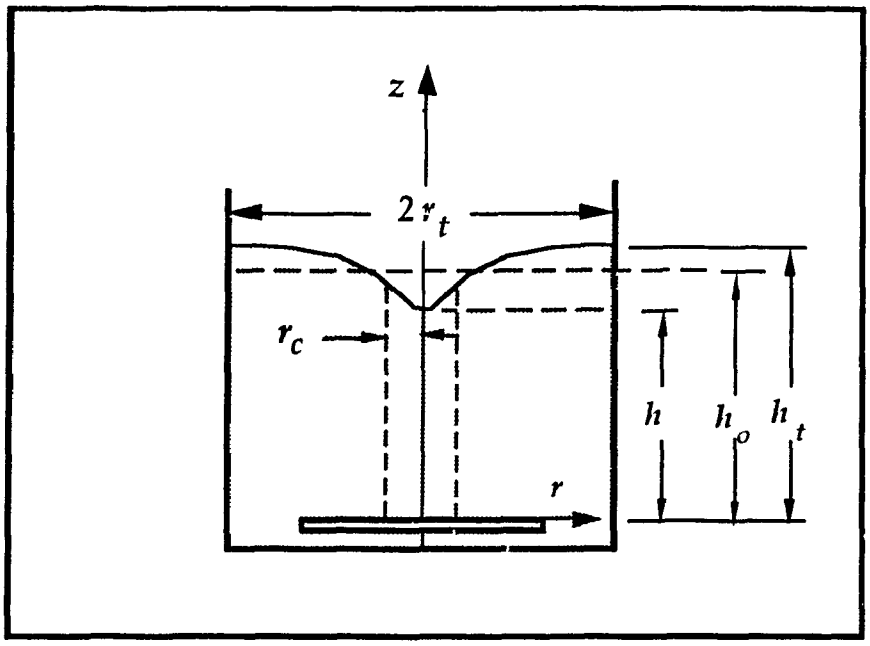

Figure 3-17 Cross-sectional schematic for a Rankine vortex.

Integration of it in the two flow regimes by substituting the tangential velocity with the two respective representations Equ.(40), and dividing the pressure by density gives the vertical elevations of free surface

$$z = h + \frac{\omega^2 r^2}{2g} \tag{42a}$$

and

$$z = z_c + \frac{\kappa^2}{2g}\left(\frac{1}{r_c^2} - \frac{1}{r^2}\right) \tag{42b}$$

where z_c is the free surface vertical elevation at core.

One more condition is the conservation of the liquid volume before and during the steady rotation,

$$\int_0^{r_c} z\ 2\pi r\, dr + \int_{r_c}^{r_t} z\ 2\pi r\, dr = h_0 \pi\, r_t^2 \qquad (43)$$

Setting r equal to the core radius in Equ(42a), then putting the z_c into Equ(42b), setting the r in the resulting expression to tank radius, ends up with,

$$h_t = h + \frac{v_c^2}{2g}\,(2 - x_c^2)$$

Integrating the volume conservation equation Equ.(43), substituting the velocity v_c from above , arranging terms gives,

$$\delta\,(2 - x_c^2) - (2 - \tfrac{3}{2} x_c^2 + 2x_c^2 \ln x_c) = 0 \qquad (44)$$

where

$$\delta = \frac{h_0 - h}{h_t - h}$$

Up to this point all the parameters as to calculating the core size and vorticity have been completed. In turn the wave phase speeds can be evaluated without difficulty.

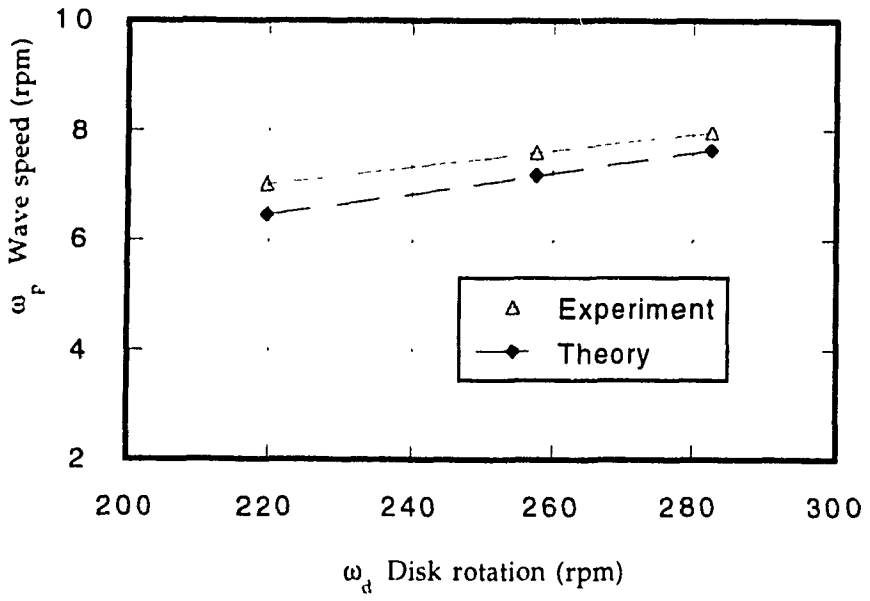

Figure 3-18 Wave speed in a Rankine vortex, h_O = 87.5 mm, n = 2.

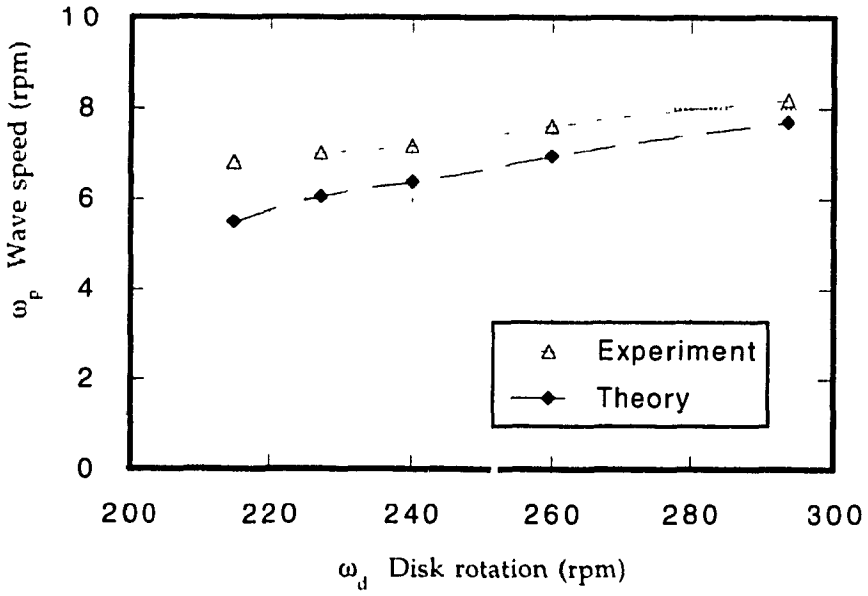

Figure 3-19 Wave speed in a Rankine vortex, h_O=100 mm, n= 2.

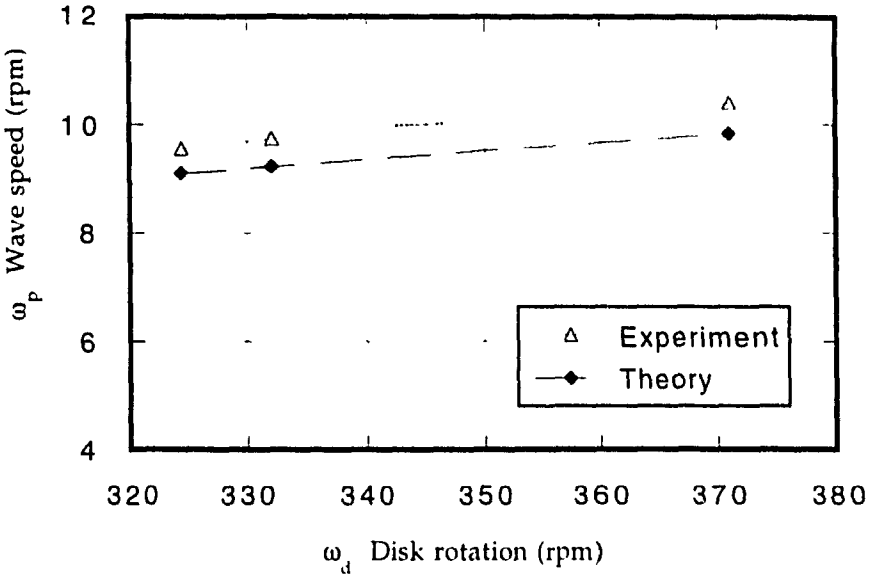

Figure 3-20 Wave speed in a Rankine vortex, h_0 = 87.5 mm, n = 3.

CHAPTER 4

Oil Vortex Equilibria

4.1 General description

To continue the previous exploration of vortex equilibria, we turn to a fluid of higher viscosity. Although liquids with intermediate viscosity (Shell oil 10W $\nu = 5.67 \times 10^{-6}$ m/s) bear many similarities to water, their evolution shows quite different behavior.

The common behavior that, during the quasi-static (very slow) spin-up and spin-down of the driving disk, the hollow vortex core transform into a sequence of symmetric equilibria with varying wave numbers. The waves rotate in the base flow. At the same time, there are a few notable differences which distinguish the oil equilibria properties from water's.

First, there are no fixed rotation speeds at which transformation from one wave pattern into another takes place, as the transitional speed depends on the special circumstance. The transformation is often abrupt without any mixed state region in between two symmetric patterns, as was the case with water.

Second, there are more equilibria attainable in higher viscosity vortices than in water. Core patterns in terms of circumferential wave numbers ranging from n=1 to n=11, shown in the photo plate 2, are observed during the investigations. In contrast to water, low wave number cores appeared mainly at higher disk velocities than those for high wave number equilibria.

The third main difference is that, given the initial liquid level, the final flow pattern for a given disk rotation depends on the time history of the spin up or spin-down process. Detailed descriptions will follow to expose the scenarios and variables which come into play.

Another point is the sensitivity to initial conditions of the present problem. There were times when we started the disk rotation for the same amount of oil from the rest, different equilibria could emerge ! It seems that some very subtle variations of temperature and bubble content may have caused this. Similar circumstances have been reported in the concentric rotating spheres problem, the Taylor vortices and Bernard convection, see Wimmer (1976), Benjamin and Moulin (1982), and Busse (1978), respectively.

An extensive summary of hydrodynamic bifurcation theories is given by D. Joseph (1985). He presented some simplified theoretical base for Hopf bifurcations, isolated solutions, and the Landau conjecture, along with the common features from past experiments involving transitions, bifurcations and hysteresis. Of special interest to the present problem are bifurcations from a steady flow into a time periodic flow (one single frequency, Hopf), and from time periodic to a quasi-periodic flow of two frequencies. A quasi-periodic flow solution of 2 frequencies behaves like this,

$$f(\omega_1 t, \omega_2 t) = f(\omega_1 t + 2m\pi, \omega_2 t + 2n\pi)$$

The two angular speeds are rationally independent, since these are the two types of bifurcations observed in our experiments.

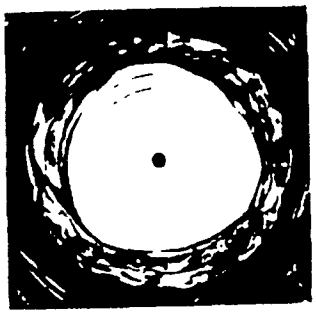

(a)

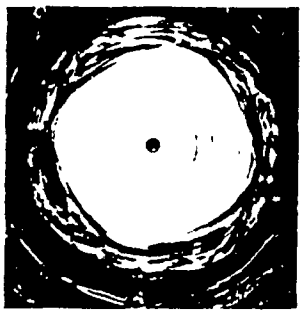

(b)

(c)

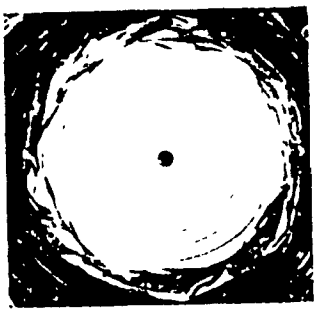

(d)

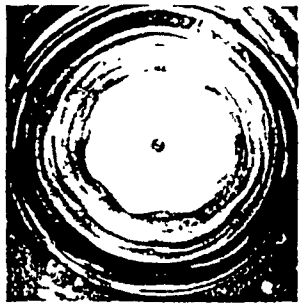

(e)

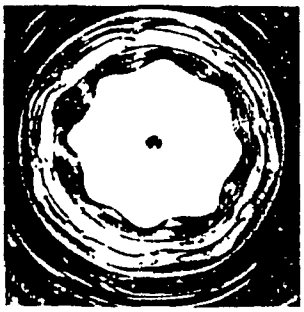

(f)

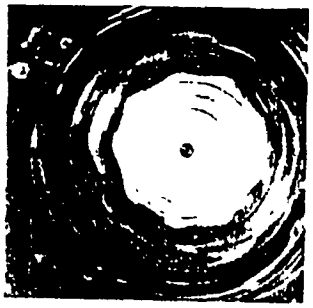

(g)

(h)

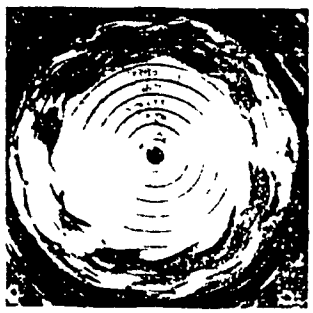

(i)

Photo plate 2 Oil equilibria

4.2 Oil equilibria development for different initial heights

Since the behavior of the oil equilibria may change dramatically for different initial liquid height, even though the difference may be sometimes only a few millimeters, detailed descriptions will be presented for each of the initial oil heights (presented as test cases) conducted. In most cases, two sequences, ascending (spin-up) and descending (spin-down), are included to investigate the issue of hysteresis. The increment and decrement of the disk's angular velocity in the two sequences is kept small (in the order of 2 to 4 rpm per adjustment) for most of the time to approach the static condition.

4. 2. 1 Test case initial level h_0 = 5 mm

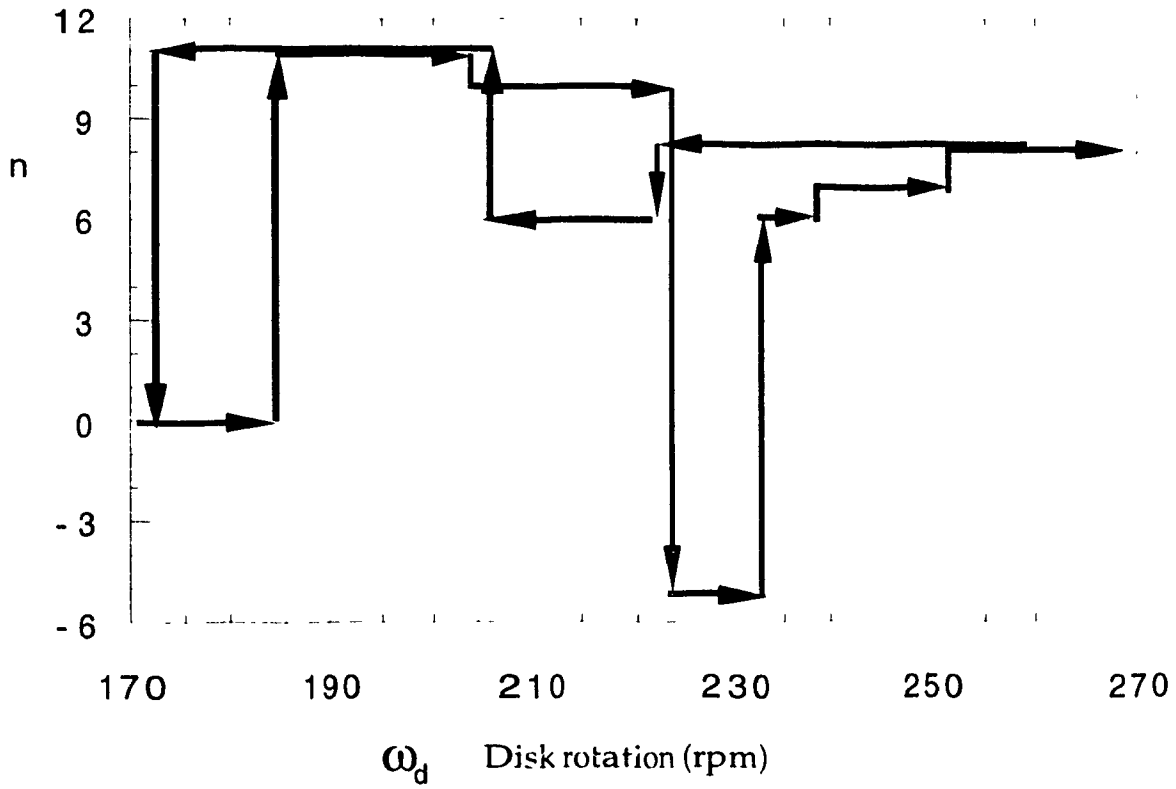

Figure 4-1 Equilibrium sequences during spin-up and spin-down of the disk for oil at h_0 = 5 mm

Ascending sequence

The ascending sequence is represented by the arrowed line segments pointing to the right (disk rotation speeds up) shown in the Figure 4-1. Prior to the experiment, the oil level is horizontal, then the disk is set into rotation by a gradual adjustment of the variac. The central part of the oil level lowers, then it touches the disk, and a circular contact line forms. As the disk speed is increased, the flow starts to lose stability at ω_d=184 rpm, where a wave of n= 11 replaces the circle (n=0), and we denote this core mode as n=11+. The number refers to the equilibrium wave number, and the plus sign indicates that the wave is co-grade (or it rotates in the same direction as the fluid). The equilibrium speed is lower than the angular velocity of the disk, and increases with the disk rotation ω_d (at ω_d=184 , 189 , 199 rpm, ω_{11} = 85.7, 90.0, 91.0 rpm, respectively). The 11+ mode persists until ω_d=204 rpm. At this speed, the wave number reduces suddenly to n=10+. At approximately ω_d=210 rpm, the core is harmonically modulated by a retrograde n=5 wave, superimposed onto the flow. The modulation produces some unequal distribution of wavelength among the 11 wave segments (some are larger than the others). The amplitude of the modulation increases as ω_d goes up. Finally, at ω_d=224 rpm, a pure retrograde n=5- emerges, and this mode lasts up to ω_d=233 rpm. At ω_d=233 rpm, the n=5- flow smoothly changes into n=6, a standing wave pattern (the hexagon crest does not rotate at all). When ω_d increases slightly, the hexagonal core begins to move slowly in the direction of disk. At ω_d=238 rpm, n=6+ transforms into an n=7+. This equilibrium state persisting up to ω_d=252 rpm; where, an n=8+ wave evolves. This core pattern endures until ω_d=270 rpm where in turn a wave of n=9+ emerges. From this point onwards, many small vapor bubbles are produced. The n=9+ flow persists until ω_d=304 rpm, where the multitude of bubbles give rise to a milky appearance of the oil. The ascending sequence is terminated there.

Descending sequence

The descending sequence is depicted in Figure 4-1 by the arrowed line segments pointing to the left, they represent the flow behavior during the spin-down of the driving disk.

In order to eliminate the small vapor bubbles, we stopped the rotation for about 3 hours. Then quickly accelerating the disk to ω_d = 258 rpm, where a pattern of n=8+ appeared that was consistent with what happened in the ascending sequence. Reducing quasi-statically ω_d down to 223.5 rpm, the symmetric octagon remains while the wave phase speed decreases. However, the present speed interval covers those for n=5-, 6+ and 7+ in the ascending sequence. Both hysteresis and bifurcation are evident. At ω_d=223.5 rpm, an n=6+ replaces the n=8+ mode. As ω_d is lowered to 210 rpm, the n=6+ wave starts to be modulated by waves of a smaller wavelength, the macro hexagonal pattern remains until ω_d=206 rpm, where n=11+ presents itself, which has some trace of modulation by a macro 6+ wave at about ω_d=200 rpm. The n=11+ flow disappears when disk speed is quasi-statically reduced to 172 rpm, a circle contact line resumes.

Hysteresis is a general phenomenon in non linear problems. In the case of this equilibrium transition, its cause is the molecular interaction of the water.

Comparing the two flow sequences of increasing and reducing disk speed, several points could be made on the hysteresis and bifurcation in this laminar flow spectrum:

1) Bifurcation between a steady motion and a time periodic one

The lowest hysteresis zone (ω_d=172 to 184 rpm) for n=11+ and the steady circle (n=0) is clearly a Hopf bifurcation. In this speed segment, the ascending flow is a steady one, that is flow properties are constant in time. The flow parameters in the descending flow are time periodic, with a period of one eleventh of the equilibrium phase speed.

2) Bifurcation between two different time periodic flow patterns

Any speed intervals on the diagram where the two sequences trace out different lines indicates such a bifurcation. Hence, there are in total six combinations of bifurcations in one frequency periodic flows. Some of them last for a very narrow disk speed interval (204 to 206 rpm, 223.5 to 224.0 rpm, and 233 to 238 rpm).

3) Potentially non-unique bifurcations

The mode n=8+ in the descending sequence overlaps the three modes n=5-, 6+ and 7+ in the ascending sequence. This reveals the possibility of transformations among four distinctive modes.

Another distinction between the transition of oil and water is that for water, there always exists a speed gap between two consecutive symmetric patterns, while for oil, the transitions generally happen at some specific speed in a catastrophic manner. The origin of this behavior lies in the high viscosity of the fluid.

The observations just described are the result of several trials with this initial height of level. It would be interesting to see how a continuously ascending and descending circle develops, without having to wait a few hours for the small eddies to decay at the end of the ascending sequence. Another test was performed for a lower final disk speed where bubbles are not allowed to be formed, see Figure 4-2.

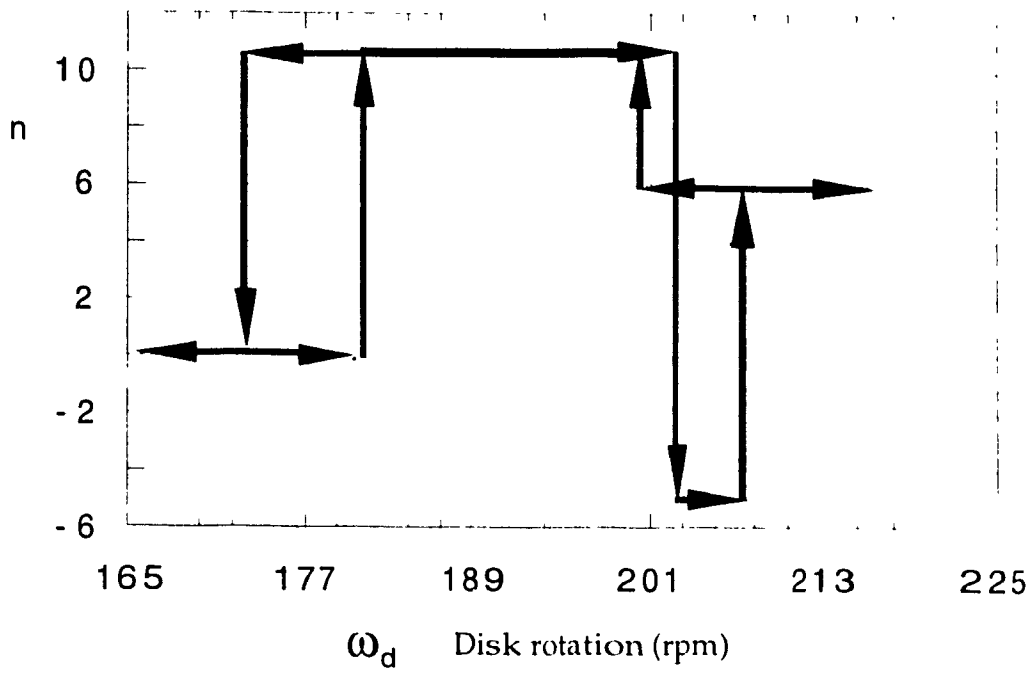

Figure 4-2 Equilibrium sequences of oil at h_0=5 mm in a continuous spin-up and spin-down cycle

Ascending process

The flow loses the circular interface shape to a wave n=11+ at ω_d=181 rpm, this mode continues up to 202 rpm. There, the flow is modulated by a retrograde n = 5- equilibrium, which dominates the flow field as the disk approaches a speed of 207 rpm. This n= 5- equilibrium persists to ω_d=206, where the n=5 wave concedes to a co-grade n = 6+.

Descending sequence

Spinning down the disk from 216 rpm, the hexagon wave changes into n=11+ at ω_d=200 rpm, and this pattern remains upto ω_d=174 rpm, where a circle resumes.

In this second run of the same liquid level, the hysteresis and bifurcation are repeated as in the first cycle, showing that the pause between the two sequences in the first case was not adding side effects on these two characteristics. Two types of bifurcations are also reproduced.

Carefully examining the two flow state diagrams, it is easy to see some discrepancies between them. For example, at disk rpm 216, the flow modes in case one are at 10+ and 6+, while in case two both sequences are at 6+. The causes for the discrepancies are obscure, and attention has been made to resemble all the experimental conditions and procedures. The very small deviations of the disk speed from absolute quasi-static increments may be the source.

4. 2. 2 Test case with initial level h_0=7 mm

A modest increase (2 cm) of the original liquid height, yields dramatic changes in the flow behavior, as compared with previous cases, see Figure 4-3. In this case, the quasi-static ascending sequence was followed by a quasi-static descending one without having to stop the disk.

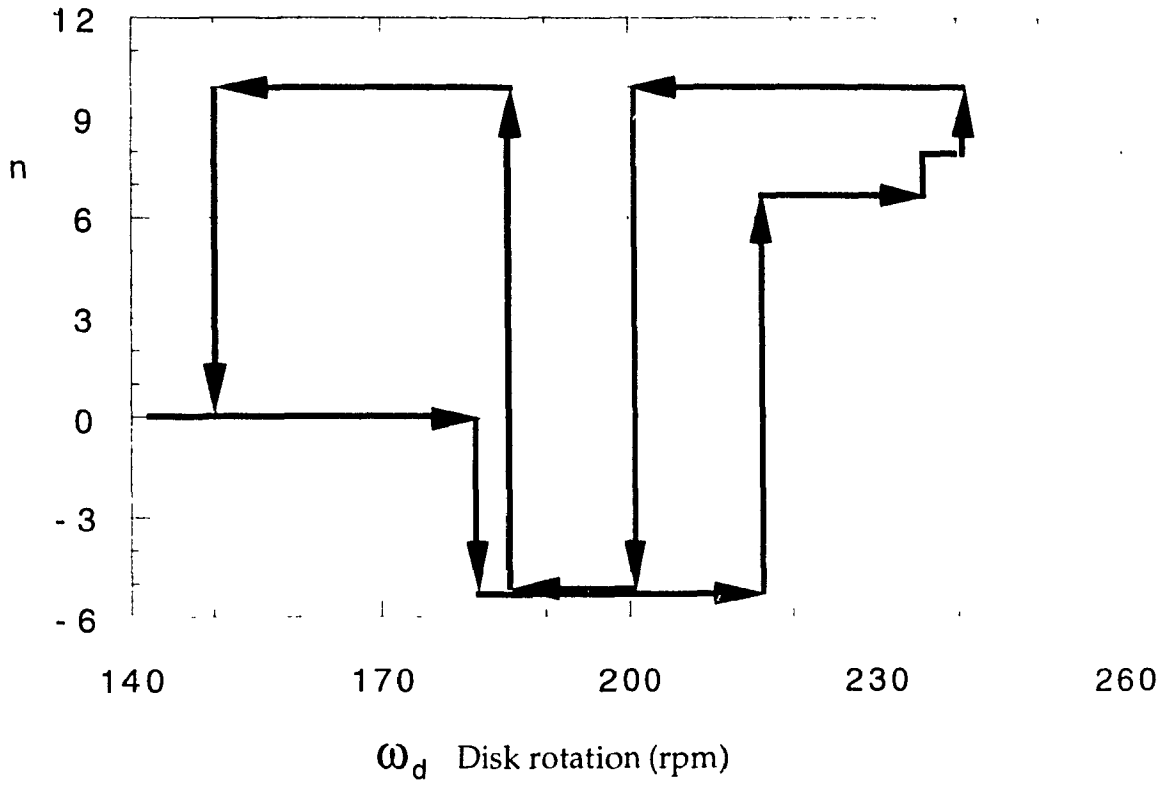

Figure 4-3 Equilibria spectrum in two flow sequences for oil at h_0 = 7 mm

Ascending sequence

After a quasi-static increase of the disk speed from rest to ω_d=183 rpm, the circular interface is first replaced by a retrograde pentagon. The flow is superposed by a weak precession. This flow fashion persists until ω_d=217 rpm, where a pattern of n=7+ emerges through an abrupt transition. This flow state remains up to 236 rpm, giving away to a pattern of n=8+. At ω_d=240 rpm, a core pattern of n=10+ replaces the octagon. This state could have persisted further, but the ascending sequence is stopped at 242 rpm.

Descending sequence

Slowly reducing the disk speed from 242 rpm at the end of the ascending process, the n=10+ pattern stays all the way to a speed of ω_d=200 rpm, thus overlapping the speed spectrum for n=8+, 7+, 5- of the ascending process. At

ω_d=200 rpm, the flow abruptly evolves into n=5- pattern. This retrograde pentagonal core changes into an n=10+ at ω_d=186 rpm. A further gradual speed reduction shows that the latter pattern lasts to ω_d=150 rpm, and disappears at lower rotations, then a circle resumes.

Special features of quasi-static sequences at this height of oil:

1) A profoundly different core behavior, even with a modest variation of the initial oil level, was apparent,

2) The n=10+ was not available at the beginning of the ascending sequence, but it happened at the end of the descending process,

3) Two typical bifurcations are persistent in this case too : between steady and time periodic flows, and between two single frequency time periodic ones.

The initial conditions have been shown to leave a great impact on the particular flow arrangements. Until now, the time history has been limited as quasi-static multi-steps of infinitesimal changes. In order to appreciate the effect of acceleration on the development of the individual equilibria, we forced the disk from rest to reach a specific speed which has been attained in the above quasi-static flow sequences. One fast acceleration from the resting state of the disk to 202 rpm, a co-grade hexagon n=6+ appears, instead of n=5- or n=10+ as was the case for the quasi-static sequences. Clearly, this time dependent, non-linear problem is absolutely dependent on the time varying external force.

4. 2. 3 Test case with initial level $h_0 = 10$ cm

At this liquid level three new phenomena with striking features appeared, these are summarized below.

First, the circular core shape persisted until certain specific rpm was reached, where suddenly a wave of n=4- appeared, see Figure 4-4. The dispersion velocity shown in Figure 4-5 was found to reduce linearly with the disk speed; later on, a core of n=5+ appears (for a detailed description of the evolution process, see case 1 below). At a later ω_d (221 rpm), one additional solitary wave was seen to encircle the core, a state of n=5+1 (the one after the plus sign indicates the presence of the solitary wave). The solitary wave's speed is greater than the dispersion velocity of the basic wave pattern. The influence of the extra solitary wave on the base wave pattern is visually illustrated in photo plate 3. The process leading to the occurrence of the solitary wave is also presented in case 1.

Second, a lowest order of flow state (circle) exists in between two higher orders of equilibria (case 2). This gives evidence that a flow may look very stable, but it could go unstable if some critical parameter assumes values that are slightly higher or even lower.

Third, and most astonishing for this height, the bifurcation can be visualized interactively by introducing an external disturbance. The key evidence is apparent during a test run at 216 rpm, in which three stable symmetric equilibrium states were obtained by disturbing the flow with a rod (e.g. intruding into the flow and withdrawing it). This means that there exist three stable solutions for the exact same boundary conditions. Here, multiple bifurcations are evident. Case 3 gives further details on this.

Case 1 Quasi-periodic flow, linear phase speed

Ascending Sequence

Quasi-static increase of ω_d to 187 rpm, the circular contact line changes into a square, a wave of retrograde n=4- is present, and the wave speed is linearly reducing with ω_d, see Figure 4-5. From ω_d=219 rpm, the square wave evolves into a n=5+ pattern, rotating in the direction of the disk, ω_5=4.7 rpm. The n=5 wave persists for a very short ω_d range (around 2 rpm). At ω_d=221 rpm an extra solitary wave is superimposed on the base n=5+ pattern. This solitary wave rotates in the same direction, but faster than the base wave (ω_5 = 12 rpm, ω_s = 51.4 rpm; while at ω_d = 226 rpm, ω_5 = 15 rpm, ω_s = 52.5 rpm, slightly increasing), see Photo plate 3 for its impact. The 5+1 flow changes into 6+1 at ω_d=229 rpm, which is a faster rotating solitary wave superimposed on a basic hexagonal pattern, (the hexagon being co-grade). When ω_d=234 rpm, the flow changes into n=7+1, which is a septangular pattern combined with a faster tidal solitary wave as before. The solitary wave slows down at a higher disk speed, and finally at ω_d = 246 rpm, a stationary octagon n=8 results with the solitary wave becoming one of the 8 vertices. This flow persists up to ω_d=280 rpm; later on, the flow becomes turbulent.

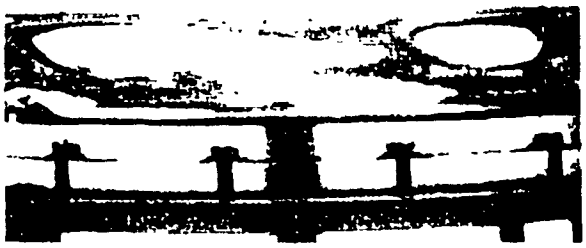

(a)

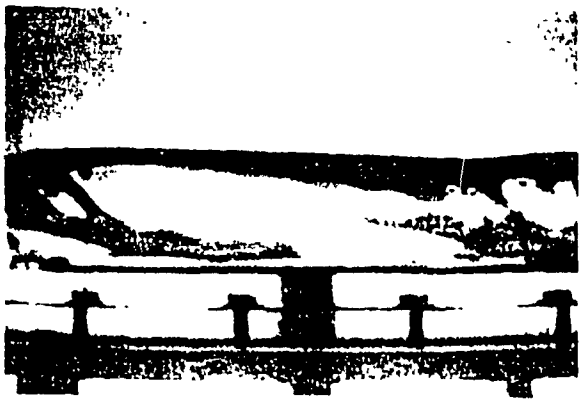

(b)

Photo plate 3 Solitary wave superimposed on an oil equilibrium

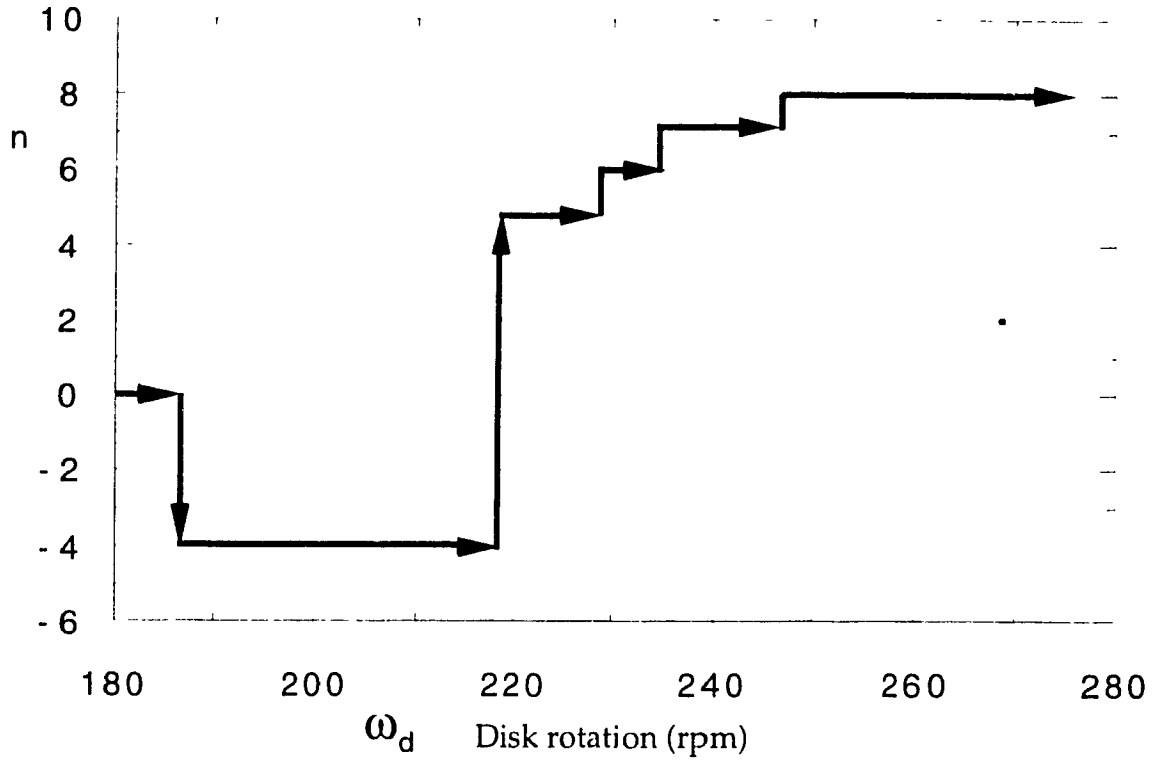

Figure 4-4 Equilibrium states in an ascending sequence of oil at h_0 = 10 mm

An important flow state is present in this case, that is the two frequency quasi-periodic flow. Starting from disk speed 221 rpm, the existence of the solitary wave represents the addition of a second frequency to the equilibrium vortex flow. This quasi-periodic state is one step further towards turbulence in the course of transition from steady laminar flow.

Also worthy of attention is that the quasi-periodic flow itself goes into a more sophisticated structure as the driving disk rotates faster, n=5+1, 6+1 and 7+1, in turn, getting more fragile to disturbances.

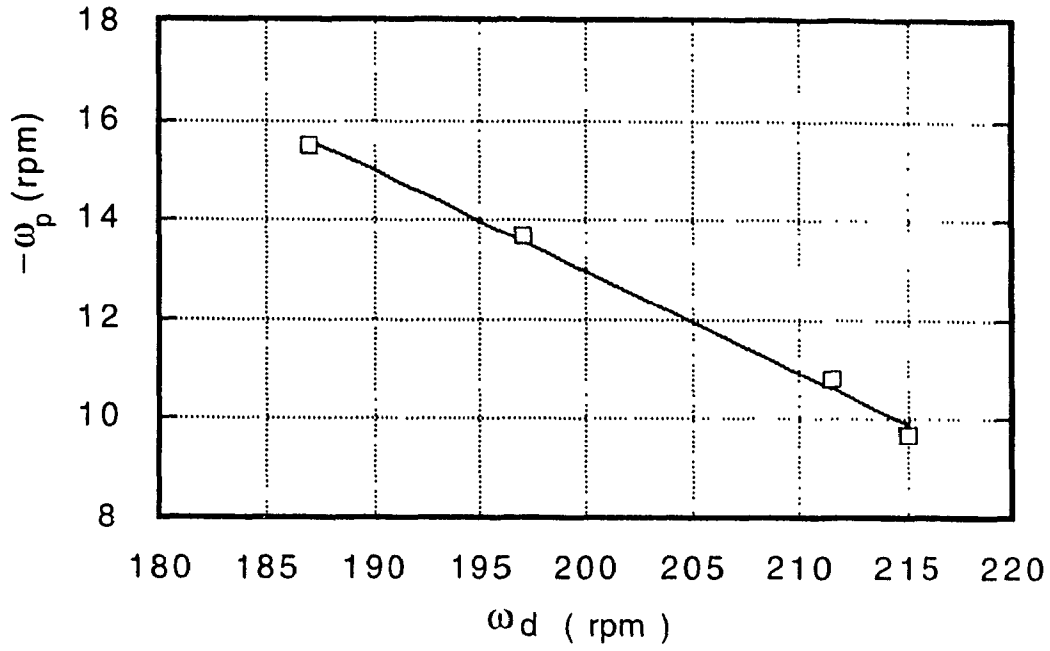

Figure 4-5 The phase speed of an oil n=4 equilibrium wave for h_0=10 mm

Case 2 Test case with an isolated state

A circular state, the simplest structure, is found to exist between two complex ones, n=5- and 10+ during descending sequence. Also another characteristic, multi-edged (more than 6) symmetrical waves are observed in the beginning of a low speed region. This is not always attainable, as sometimes the ω_d is intentionally increased very slowly, the multi-edged waves were not present; instead, flow starts from a square or pentagon equilibrium. It seems that the second characteristic is due to some minor variations of either the property of the oil or the initial height.

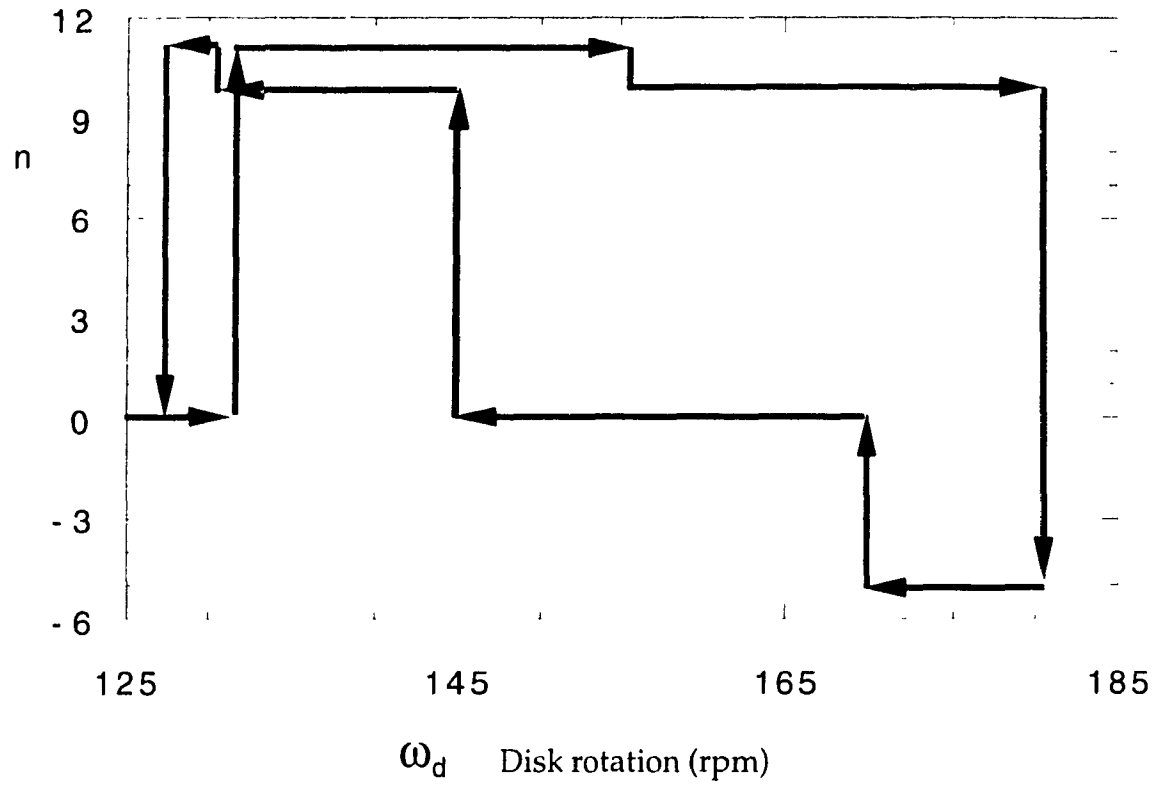

Figure 4-6 Equilibrium states in ascending and descending sequences for oil at an initial height of 10 mm, case 2. (with an **isolated** state).

Ascending sequence

Starting from ω_d=132 rpm, the circular interfacial contact line becomes rough, a pattern of n=11+ appears and persists up to ω_d=156 rpm during the quasi-static speed rising process. At this speed, the flow pattern shrinks to n=10+. Increasing the disk speed close to 180 rpm, a harmonic modulation that intensifies can be observed. Finally at ω_d=181 rpm, a pure retrograde n=5- emerges. In order to explore the hysteresis and multi-solution nature, the spin-up process is stopped and the spin-down starts at this relatively low disk speed in order to avoid the creation of vapor bubbles.

Descending sequence

Reducing slowly ω_d from 181 rpm, a counter rotating pentagon endures until ω_d=170 rpm. The transition results in a circle, as if nothing has happened. The circle continues until the speed is deduced to 145 rpm, an n=10+ re-surges, and it persists to ω_d=131 rpm. Between ω_d=131 and 127.5 rpm, the flow is n=11+. At lower than 127.5 rpm, an undisturbed circular shape of core exists.

Special feature of case 2

Besides the familiar phenomena previously discovered, namely the bifurcations between steady and time periodic states, between the time periodic flows, the most stable structure (a circular one) emerges in between neighbors of periodic solutions. This should be what is known as an isolated solution.

Case 3 Triggering bifurcations by artificial disturbances

This time, the speed of the disk is increased slowly from zero by many increments. Retrograde flow mode n=5- first appears from a circle at ω_d=180.5 rpm instead of n=4-. By intruding a rod for about 4 seconds, then taking it out of the oil, a hexagon n=6+ wave develops. This has been shown that bifurcation can be made by introducing external disturbances in the hysteresis range of speed. The co-grade hexagon can be also changed back by another intrusion of the rod to give into a retrograde pentagon. Hence, the two flow states are both stable solutions. The same process is repeated at a speed of 184 rpm.

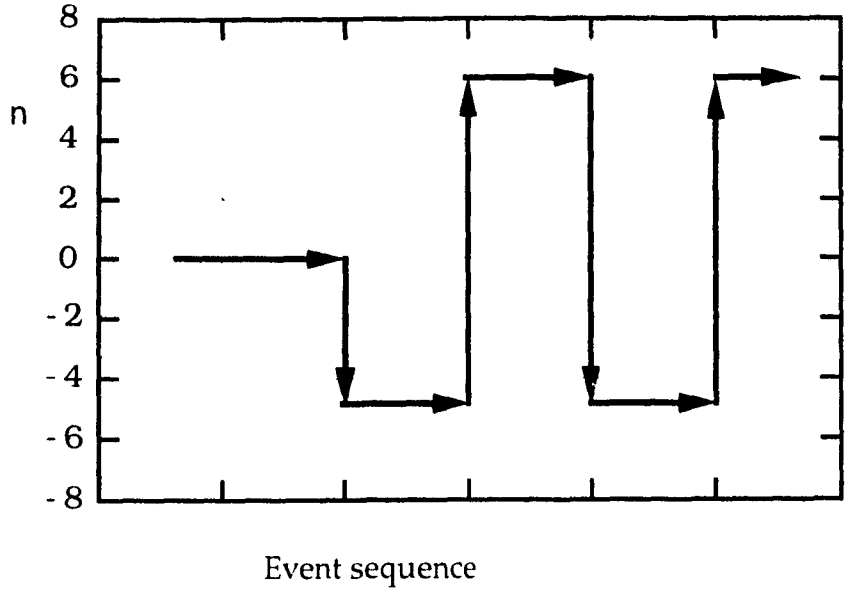

Figure 4-7 Oil equilibrium mutations at h_O=10 mm and disk speed at 180.5 and 184 rpm.

* Special feature :

Modes n= 5- and 6+ are present in the speed range that previously mode n= 4- existed. Hence bifurcations must be present.

Bifurcations between a time periodic flow and a quasi-periodic one

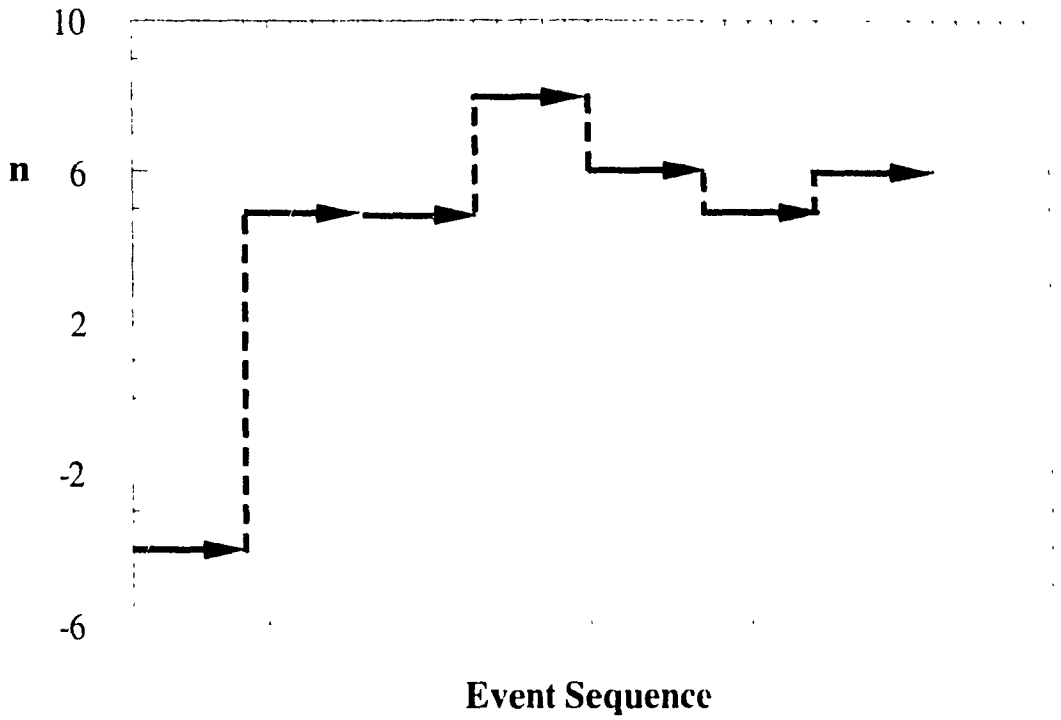

Figure 4-8 Bifurcations between time periodic and quasi-periodic flows. Oil at h_o=10 mm and disk rpm 216.

This is the first time that the bifurcation between a time periodic flow, which is of a single frequency, and a two frequency quasi-periodic flow is visualized interactively ! The latter demonstrates another common characteristic in the development of hydrodynamic instabilities. The manual triggering has vividly brought to life the multiple solutions.

Quasi-statically increasing the disk speed ω_d from zero, at ω_d=184 rpm, the circular contact line gives way to an n=4- wave pattern. By artificial disturbance with the intrusion of a rod in the gap between the outer disk edge and the tank wall, the retrograde square re-surges from a circle after the stick is removed. This indicates that the mode of flow is very stable. The n = 4-

stays up to ω_d = 216 rpm, where the intrusion and taking away of the rod show bifurcations:

(1) First intrusion and pulling away changes the 4- pattern into a 5+ pattern, a pentagon rotating in the direction of the disk,

(2) Second intrusion and pulling away of the stick changes the positive 5 pattern into a transient n=8+, a co-grade octagon equilibrium, which lasts for only about 12 seconds. In turn, a pattern of n=5+1 evolves without artificial interference. The n=5+1 pattern is a state which consists of 5 vertices going in the direction of the disk, but there is a solitary wave present at the same time in the flow that rotates faster than the base hexagon pattern. As a consequence, the base pattern is displaced azimuthally at the crest of the solitary wave, and is not a perfectly symmetric hexagon. The flow is a synthesis of two components each with a different frequency,

(3) Another rod intrusion and pulling out brings the pattern n=5+1 into a pure n=5+ pattern, a symmetric pentagon rotating in the disk's direction; the solitary wave disappears. This is a transition from two frequencies into one frequency flow,

(4) An additional disturbance using the rod changes this pattern back to the 5+1. This type of flow endures up to ω_d=226 rpm.

During the descending sequence from 226 rpm, the n=5+1 pattern persists when ω_d is reduced to 200 rpm. With the rotation of the solitary crest going slower and slower, eventually, at 196 rpm, a pattern of symmetric n=6+ is present. At this time, by one rod operation, an almost standing wave of 5 results. Further reduction of the speed, a retrograde pentagon emerges. At ω_d=183 rpm, another rod disturbance brings the flow from n=5- to n=4-. We were not able to bring the flow back to n=5- by any further rod disturbance, hence the counter rotating square stays until 180 rpm. Following that, a circle resumes at lower speeds.

** Effect of time history via acceleration:

A fast acceleration of the disk from rest to ω_d=201 rpm gives rise to a stable n=5-. But different wave patterns (n=4- in ascending sequence and n=6+ in descending sequence) were seen to manifest when the exact same speed were reached quasi-statically. The latter suggests that the transition from 6+ to 5 in the descending sequence could happen earlier. Therefore, the evolution of the flow depends strongly on the time history of the disk acceleration.

4. 2. 4 Test case with initial levels h_o=15, 22, 31.5 mm

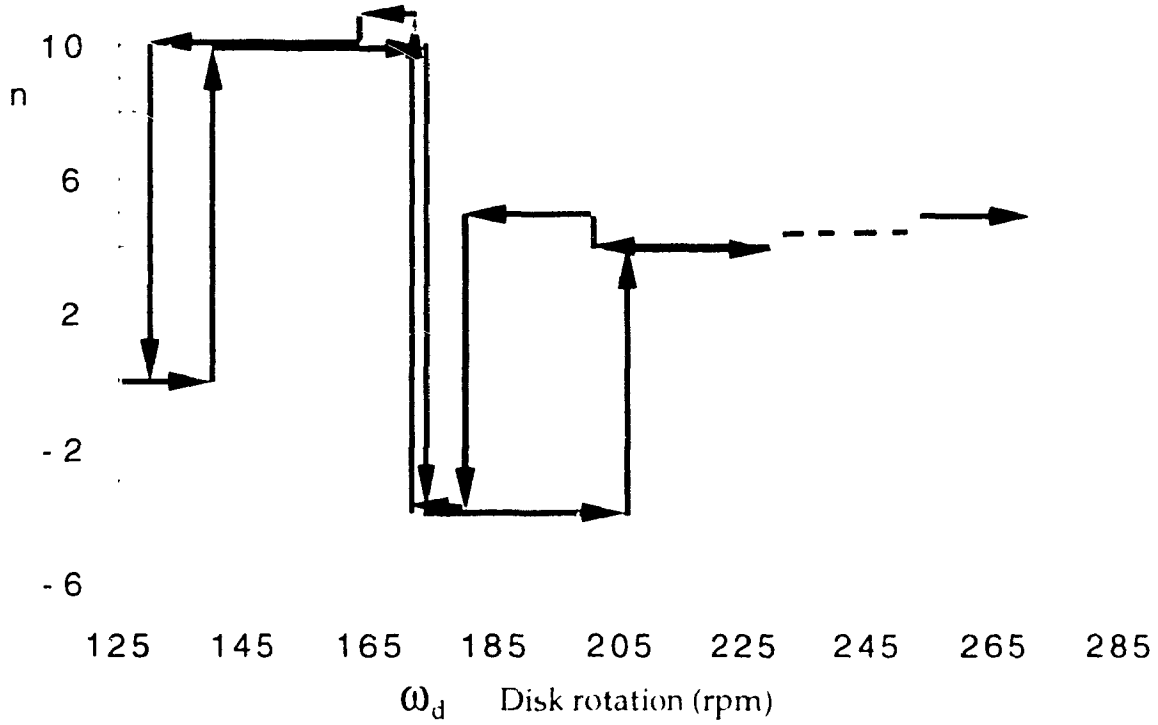

Figure 4-9. Equilibrium states with a speed gap for oil at h_o= 15 mm

Ascending sequence for h_o = 15 mm

By quasi-static increase of the disk speed from zero up to ω_d=140 rpm, the circle outline first breaks into a pattern of n=10+ Some precession is superimposed on it, which attenuates as ω_d is increased. The same flow pattern remains until 175 rpm, and the wave phase speed augments with the disk's rotation. At ω_d=176 rpm, an abrupt transition yields a retrograde square n=4- core shape. Its phase speed becoming slower as ω_d increases. At 207 rpm, an absolute-stationary square core shape is present. When the disk rotation is further gradually increased to 210 rpm, the square starts going in the opposite direction of the disk, and with some tumbling Later on, a faster

revolving solitary wave is observed in the flow, the square is distorted, and there is more shaking Both the phase speeds of the square and the solitary waves are larger with ω_d At 230 rpm, the core pattern is not very clearly defined, however it is close to a pentagon In the speed range of ω_d=234 to 255 rpm, the flow state is not stable, the outline being sometimes n=5, 4 or sometimes 6, 7 This is the first time in our observations that a speed gap on the state diagram occurs with non-unique states. From about ω_d=255 rpm, a pattern of n=5+ appears, and persists up to ω_d=270 rpm Beyond that speed, strong turbulence in the flow makes the outline fuzzy

Descending sequence

At the end of the ascending sequence, since there are many small oil vapor bubbles in the oil, the rotation is halted, leaving the oil to remain at rest for about 3 hours.

A quick disk acceleration to ω_d=230 rpm gives rise to a pattern of n=4+1 is present, which is a faster rotating solitary wave superposed on a positive rotating square, resuming the state in the ascending sequence. The descending sequence starts from there by quasi-statically reducing ω_d all the way to zero. The n=4+1 state remains up to 202 rpm, where the decelerating solitary wave joins the base pattern, and a pure stable n=5+ pattern emerges. The co-grade pentagon lasts until 180 rpm, where a smooth transition leads to a retrograde square n=4- state The negative square wave pattern changes into n=11+ at ω_d=174 rpm, in turn this pattern gives away to n=10+ at ω_d=164 rpm. That flow state is preserved until 132 rpm, after which speed the circular core resumes.

The state diagram also shows that there is bifurcation between n=4- and n=5+ at approximately a speed of 200 rpm. This is convincingly confirmed by quickly accelerating to that speed, intruding a rod in the space between the disk edge and the tank wall for a few seconds and pulling out. A transition from 4- to 5+, or vice versa is observed.

* Special features of the flow:

A speed gap exists in ascending sequence, which has never been possible for any of the previous liquid heights. An n = 11+ emerges before n=10+ in the descending sequence This shows that the two sequences differ not only in time (hysteresis) , but also in flow states

Test case with h_0=22 mm

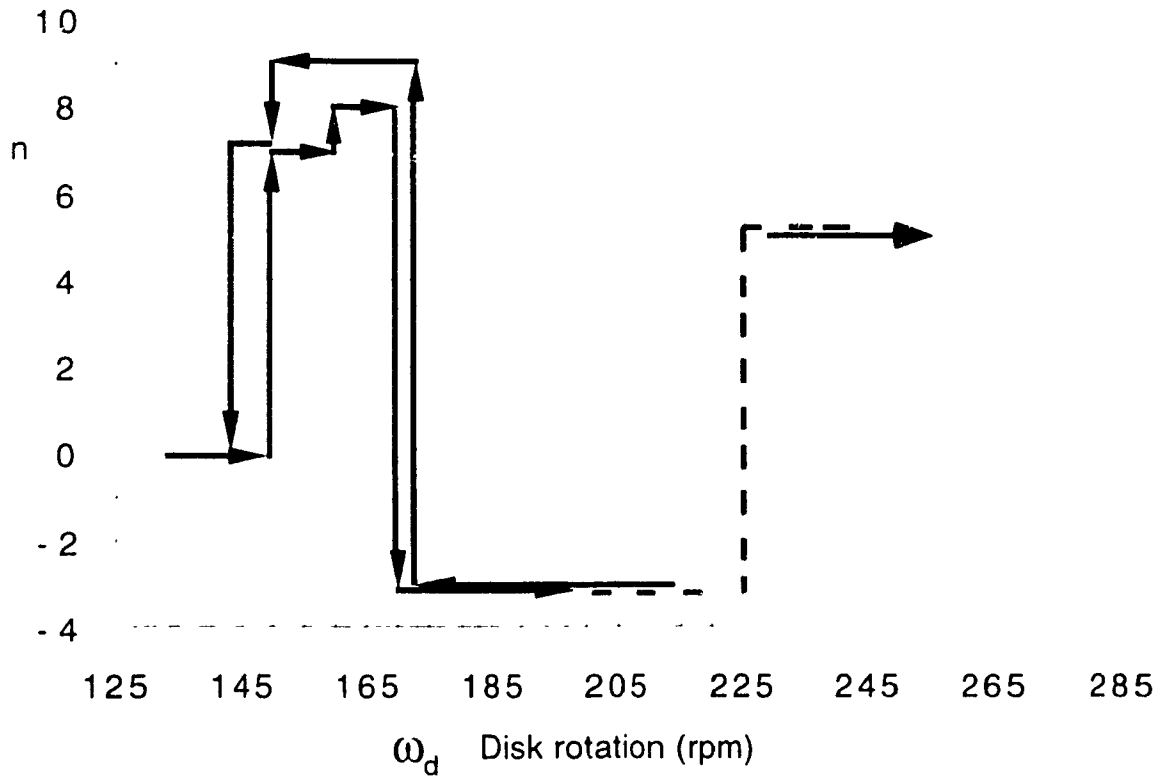

Figure 4-10. Equilibrium states with a speed gap, oil at h_0=22 mm

For a relatively large liquid height (22 mm), some particular features are present. Above 167 until 171 rpm of the disk rotation, the n=8+ core is subharmonically modulated by an n=3- wave, which is another form of the two frequency quasi-periodic flow state. Also, unsteady states appear in speed intervals 212 rpm < ω_d < 232 rpm and ω_d > 254 rpm.

Ascending sequence

At this height, by a quasi-static increase of the disk rotation in the range of ω_d=95 to 130 rpm, strong precession is present in the flow, and the vortex contact line is more or less a circle. The precession weakens as the ω_d tends towards 150 rpm. At 152 rpm, first appears the pattern of n=7+, exhibiting a very small degree of wobbling. When the speed increases to 160 rpm, a positive rotating octagon n=8+ replaces the 7+ pattern. Above ω_d=167 rpm, harmonic modulation of a retrograde triangular wave is present The 8 edges are not equally sized Finally at 171 rpm, transition results in a pattern of a pure n=3-. This flow state is very stable up to 197 rpm. From ω_d=198.5 rpm, due to a solitary wave, a circumferential shaking was observed, that amplifies with increasing ω_d up to 212 rpm. Beyond that speed, unstable flow exists, giving either n=3, or 4 or 5. From 232 rpm, a stable n=5+ shows up, that persists until ω_d=254 rpm, then unstable flow states occur once more. For 254 to 260 rpms, the flow is turbulent and n=5 dominant. For 260 to 270 rpms, the flow is a turbulent n=4

Descending sequence

Letting the oil rest for about 3 hours at the end of the ascending sequence, quickly accelerating the disk to 241 rpm, the descending process starts. At this speed, a pattern of n=5+ exists, consistent with the ascending sequence. The 5+ pattern persists down to 238 rpm. Between this speed and 224 rpm inter-changing modes of n=4, 5 and 6 are observed, the flow being unstable. In the narrow range of 2 to 3 rpm around 223 rpm, the flow is a 4+ state. In the range of 221 to 214 rpms, another unstable speed interval, no unique pattern was possible, with the flow field alternates between n=3 and n=4. When the rotation is between 214 and 172 rpm, the flow is stable, a pure retrograde triangle n=3- is present. Near the lower limit of 172 rpm, modulation starts to appear. From that speed until 150 rpm, the flow state is that of n=9+ . From 150 rpm and lower, the flow is 7+, which disappears at 144 rpm and a circular outline resumes.

Another fast acceleration to 193 rpm from rest brings the flow to a very stable pure square wave 4+, that was the speed for 3- in the two quasi-static approaches. The dependence of flow state on the acceleration course is obvious.

Special features

- A speed gap exists where no stable state is possible,
- Bifurcations and hysteresis at this height are evident, and there is
- Dependence of flow state on acceleration

Test case with h_O=31.5 mm

With this initial oil height, no stable symmetrical wave patterns are ever possible

In this case, during the ascending sequence, the flow starts to wobble (precession) from ω_d=100 rpm. The precession intensifies as ω_d increases and the wobbling core outline is almost circular. This flow state persists until the quasi-statically incremented speed reaches 240 rpm, from where the unstable equilibria n=4 or n=5 emerge occasionally and precession is not significant. The flow develops into a turbulent square-dominant core from ω_d=270 rpm onwards.

Since no laminar distinct stable waves are available in the ascending process, there is no need to explore the relevant properties by performing the descending sequence.

4. 3 Discussions and conclusions on the oil equilibria

During these mainly exploratory studies, the course of flow evolution from a steady state of maximum symmetry enroute to the turbulence was found to be quite complex. A few characteristics can be summarized.

1 Non uniqueness

The flow state is not uniquely determined by macroscopic, measurable parameters like Reynolds or Taylor numbers. For the given geometry of tank and disk, it depends on how the final values of these parameters are reached. As an initial value problem, its solution relies on the time dependent, external forcing function. The boundary conditions are only part of the restrictions imposed on the solution. The physical forms of the employed transient, external forcing functions employed are : quasi-static ascending, quasi-static descending sequences of disk speed, and accelerated approach of a final disk rotation.

2 Common features of hydrodynamic bifurcations

After reviewing the transition processes in Poiseuille flow, Couette flow between concentric rotating cylinders and the flow between rotating spheres, Joseph gave three common features of hydrodynamic bifurcations.

-- a steady spatial symmetric solution is replaced by another steady flow,
-- a single frequency time-periodic flow replaces the steady flow when the Re goes higher , and
-- at higher Re, the single frequency time periodic flow gives up its stability to a multi frequency periodic (quasi-periodic) flow.

Among them, the last two have been observed in the present experiments

Bifurcation between a steady flow and a symmetric rotating flow that is of a single frequency

In the present study, this type of bifurcation happens mainly between the flow at the beginning of the ascending sequence and the flow at the end of the descending sequence. The ascending sequence always starts from a steady, circular core, which is of maximum spatial symmetry On the other hand, the descending sequence near the end always has a symmetric rotating equilibrium before it resumes the circular core at even a lower speed

In one particular case of ho=10 mm with an isolated state, see Figure 4-6, when ω_d (rpm) is in [145, 170], flow bifurcates between the steady, supercritical circle and two periodic states n=11+ and 10+,

Bifurcation to 2 frequency quasi-periodic flow

There are two physical representations, one involving a faster circulating solitary wave in the presence of a base slow symmetric equilibrium, such as the equilibria n=5+1, 6+1, 7+1 at h_0=10 mm and n=4+1 at h_0=15 mm Another involves the harmonic modulation of one equilibrium by another of different wave number, such as in Figure 4-1, ω_d = 210 rpm , h_0=5 mm and in Figure 4-6 ω_d = 180 rpm h_0=10 mm. In both cases, the two wave numbers are both 10 and 5. Bifurcations between one symmetric rotating flow and another are numerous among the two quasi-static sequences This type of bifurcation is not among the common characteristics The first common type of bifurcation between spatial steady flows is not observed in the vortex agitator with oil. Probably, the conditions for two flows of circular core mode at the same Reynolds number are not among those reached

3. Hysteresis

There often exists strong hysteresis in transition from one wave pattern to another in ascending and descending sequences. In these hysteresis speed regimes, two or more persistent solutions are present, which have been convincingly confirmed by introducing external artificial disturbances into the flow for several occasions to trigger the toggling. Three persistent solutions at the exact same determining boundary conditions (except the free surface) and Re or Ta are also experimentally obtained at h_0=10 mm.

4 Difficulty in reproduction

The flow pattern sequences in the descending process could not repeat those in the ascending process for most of the cases. The difference lies in both the order of occurrence and in the patterns themselves. Even for the same sequence (e.g. ascending), the next run is not always the same as the first one though great effort is exerted to reproduce every condition.

This does not look strange in the domain of flow instability. Belyaev (1978) tried to check the results of Munson and Menguturk (1975) on flow between rotating spheres; he found something new instead of reproducing the same sequence of flows.

5 Speed gaps

For low h_0 of oil (5, 7, 10 mm), transitions between consecutive patterns are abrupt and instant at a particular speed. Well-defined, persistent flow states follow one after another along the disk speed axis. For a slightly higher level, like 15 mm and above, there are some speed gaps in which flow state is not persistent, no unique mode exists. This phenomenon is similar to the cases with water, except that there is no persistent mixed modes for oil.

6. Sensitivity of the flow

Small variations of the liquid height can cause a drastic alternation to the flow behavior, like between h_0=5 and h_0=7 mm. The difficulties in reproducing a sequence indicate that slight temperature differences and small variations of the initial residual vorticity levels in the fluid are suspected to influence the evolutions of the equilibrium.

The flow may be also sensitive to small variations of the liquid property (viscosity, surface tension) and to some other as yet unknown effects. For example, in the case of h_0=7 mm, during the ascending sequence, even when very small speed increments were tried, no n=10 pattern showed up, still it exists at the end of the descending sequence. Another example, at h_0 10 mm, only one out of four cases presented starts from a large number vertices wave n=11.

Further studies must address in detail their influences by precise parameter measurement and control.

7. Two possible phases of flow instabilities

The wave numbers in a water equilibrium sequence are 2, 3, 4 upwards. Those for oil in an ascending sequence start from 11, 10, 7, , then drop to considerably smaller numbers 5, 4 ... , upwards hereafter. It seems to suggest that there are two phases of flow patterns for oil: Phase 1, in low speed regime with relatively large azimuthal wave numbers, and Phase 2, in the higher speed regime, with smaller wave numbers.

Phase 2 is closer to the results of water. During investigations with water, no n = 10, 11 or 7 were observed at low speeds. Phase 1 does not exist for water.

The two phases of instability waves in oil suggest that there would be two different courses. One proposition is that phase 1 is due to surface tension, while phase 2 is due to inertial instability. More work needs to be done to either reject or confirm it.

8 Wave number versus liquid height

As a general tendency, in quasi-static sequences, the initial azimuthal wave numbers in phases 1 and 2 diminish with increasing oil level h_0. Since the higher the initial liquid level, the shorter the vortex core circumferential length, the surface tension will reduce the number of vertices. There are exceptions due to the complexity of the intervening parameters.

CHAPTER 5

SLOSHING

The previous chapters have presented, for the most part, well behaved quiet laminar equilibrium wave evolutions, either in very viscous oil or in relatively small viscosity water for lower disk rotation. During the early stages of laminar transitions, the equilibrium waves are present on a permanent basis - one can always see it there as long as the background motion lasts. Also mentioned was the highly turbulent vortex at the end of the laminar transition sequence at higher disk rotation, where the driving force reaches a level that the flow field is dominated by inertia force. The randomly high frequency variations of flow parameters make the flow macroscopically steady, and no orderly waves are possible.

In this chapter, a special form of wave activity that gives rise to violent liquid sloshing is described. The wave has a developing phase, which repeats itself periodically. A typical case follows. The amplitude of the wave starts from zero for a certain period of time, then it develops gradually and rapidly from just visible until it reaches its crescendo. From that point the amplitude is seen to reduce rapidly until it is practically unnoticeable. Then the steady

quiet Rankine vortex resumes as nothing has ever happened. This state lasts for quite some time before the process is repeated again.

One of the characteristics found in sloshing is that the periodically surging wave is possible only within certain limited disk speed limits. These limits depend on the diameter of the disk for a given tank and the initial liquid height. The sloshing wave's amplitude depends on the disk rotation. A general relationship between the initial disk speed at which sloshing starts to emerge and the liquid height is elusive, as sometimes they are locally increasing one with the other.

The mechanism that a sloshing wave is present under some prevailing conditions in a given vortex generator configuration is not pursued here, however, an approximate numerical simulation is performed to suggest that two coexistent harmonic waves of the same number, but of different phase velocities (slow-fast) are the origin.

5.1 Experimental evidence for disk sloshing

Tests have been conducted for disks with diameters, 101, 153, 202 and 268 mm. For each of the disks, the tank is filled at different heights of water to explore its impacts. At each height the disk rotation is the principal variable. The sloshing wave is present only for a certain range of the driving disk rpm.

5.1.1 Typical sloshing wave developing process

Figure 5-1 is a schematic of the time history for a wave sloshing evolution. The vertical axis is the amplitude of the sloshing wave in "snap shots", and the horizontal axis is the time variable.

During the time period 0 to T_q (q stands for quiet), there is visually no oscillation at all on the uppermost free boundary (the intersection between free surface and tank inner wall). The flow field is an elliptical Rankine vortex, and the wave perturbation vanishes at this outer most point. Hence, the sloshing amplitude is unnoticeable. Starting from T_q to T_{max} ($T_q + T_s/2$),

a time span of T_s 2 (s stands for sloshing) the amplitude continuously increases over time The vertical coordinate of the water trace on the transparent wall deviates gradually from the flat horizontal position with each wave passing by There is a moment when the amplitude develops to its maximum From that moment onwards, the violent sloshing reaches its decaying phase Its amplitude diminishes until it is almost invisible at time

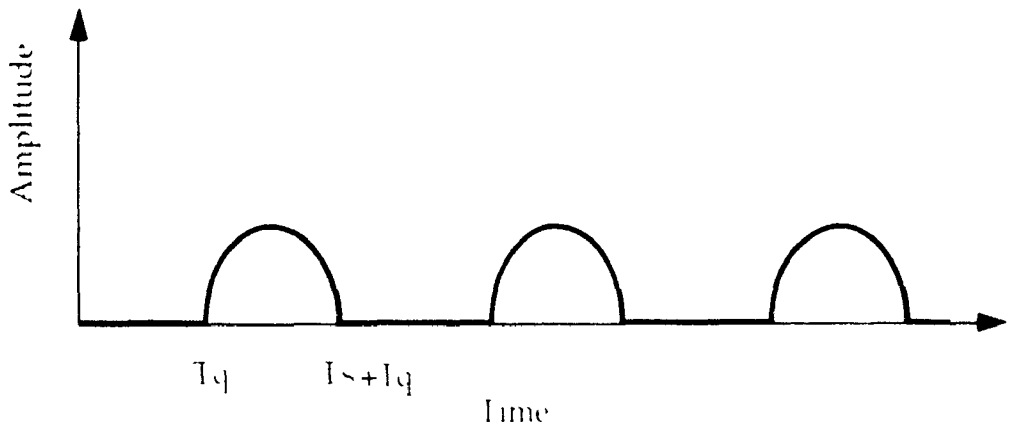

Figure 5-1 The sloshing wave amplitude versus time

$T_q + T_s$ A cycle from 0 to $T_q + T_s$ repeats itself, and after time T_q of non perturbed Rankine flow, another amplitude-increasing and decreasing process begins The whole process repeats itself periodically

If we unfold the cylindrical wall into a two dimensional Cartesian coordinate system, the intersection contact line is a flat one without sloshing, spanning from 0 to 360 degrees During the sloshing period, there are two symmetric concave and convex peaks (see Figure 5-2 for graphical representation), which shows a dominant elliptical wave present in the flow The amplitude in this figure is only for one time frame of the flow, corresponding to one instant during the non-zero region in Figure 5-1

An important aspect of the sloshing process is the variation of the air core shape in the two distinctive time periods, namely the quiet and the sloshing phases. These characteristics are best depicted by the top view visualizations

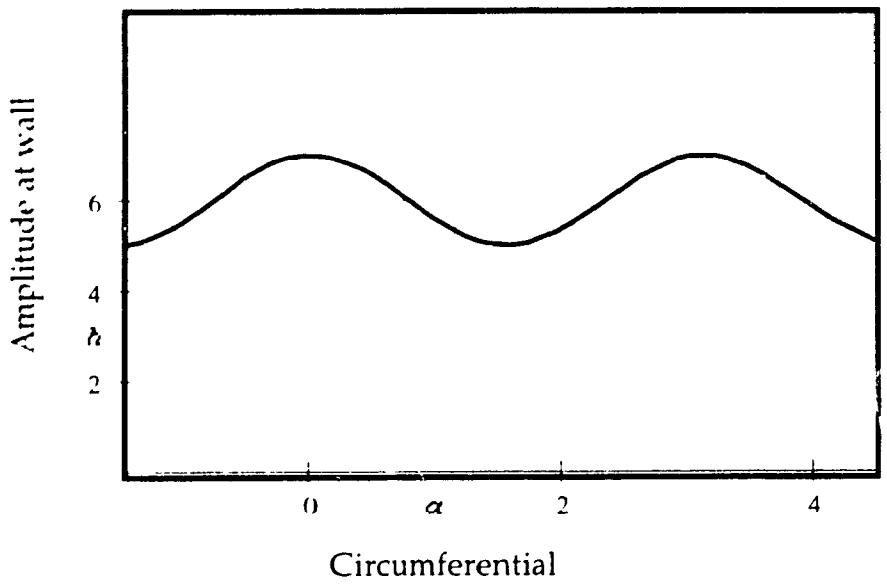

Figure 5-2 A snap shot of the side view of a sloshing wave.

During the quiet non-sloshing period, the core outline is continuously changing. During the initial stages of sloshing the core transformation can be approximated by an ellipse, rotating and changing its aspect ratio. The ratio of the long axis to short axis is nearly one at the start, then the ratio increases until it reaches a maximum, where it is easily viewed from the top that the core is a quite squeezed ellipse. In fact it is so squeezed that it resembles a rectangular ribbon. Following the most squeezed moment, the middle points of the shape begin to rapidly approach one another to join as one point. Further on, separation occurs, and two sides of the joint centre on the long axis turn out to be two vortices. The two newly detached vortices are in a state of self-rotation about their respective centers, at the same time mutually rotating. When the two transient vortices are at full strength, that is the moment when the side-view amplitude is at the peak point. Afterwards, the two separated vortices start to merge, forming a narrow ellipse, and further to a full circle of an aspect ratio one. This state stays throughout the quiet time span before the next wave of sloshing appears again.

For a fixed set of initial conditions of liquid level, disk rotation, disk size, and tank internal diameter, there are at least three parameters essential to the characterization of the sloshing waves, T_q (the quiet duration), T_s (the sloshing duration) and A_{max} (representing the maximum amplitude during a complete cycle).

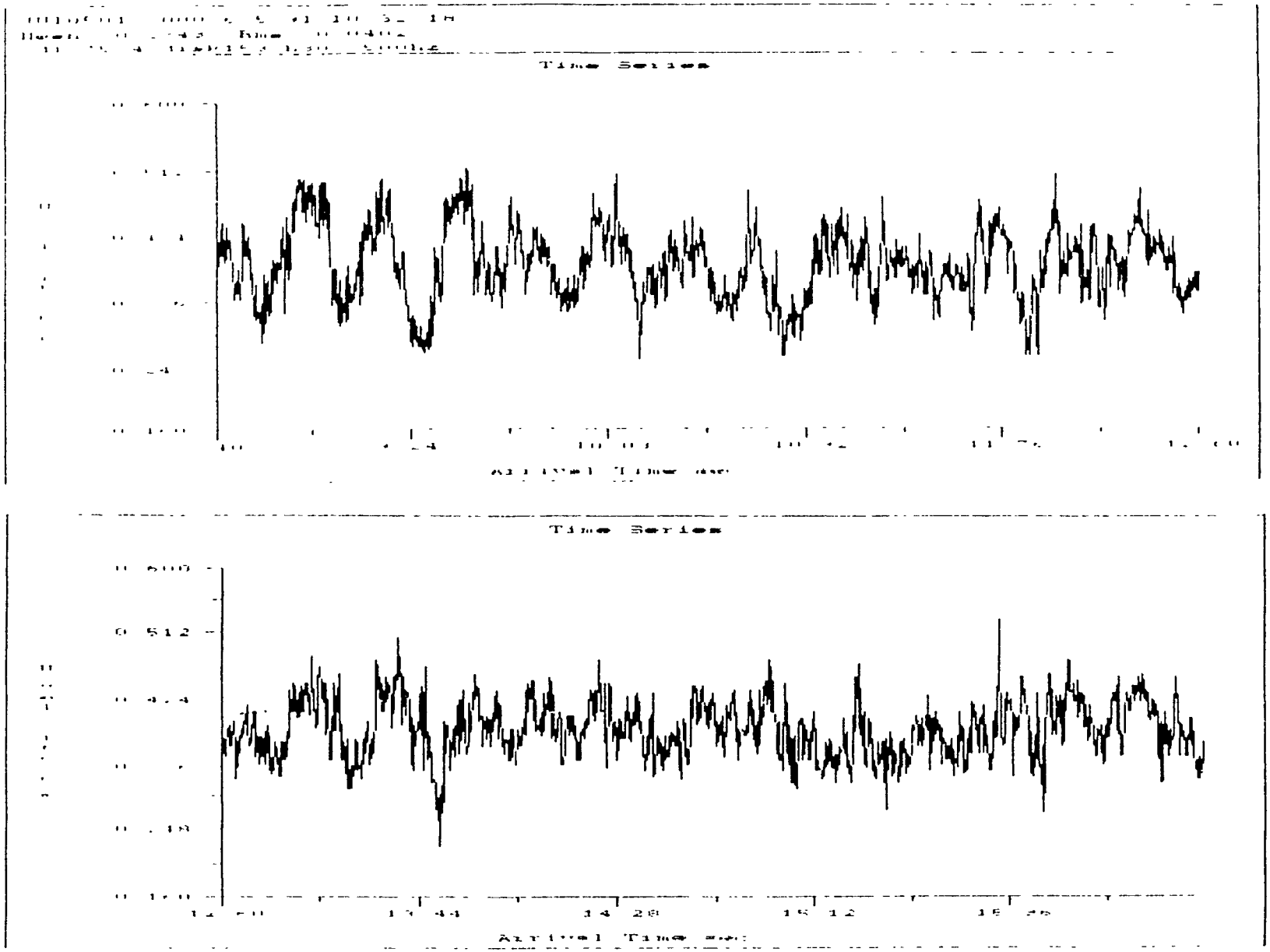

Figure 5-3 Velocity trace by LDA from sloshing to quiet vortex

5.1.2 Visual observations of sloshing for different disk diameters

Case I Disk diameter 101 mm

Tests are conducted at four different levels, h_O=18, 40, 56 and 90 mm.

At a water height of 18 mm, irrespective of the spin-up history, no sloshing was detected. Only transient, unsteady circles and ellipses, were present. Neither stationary equilibria nor sloshing were observed.

At a level of 40 mm, for low speeds, precession and mutual transient patterns were seen between elliptical and triangular waves. When the disk rpm is set at 444, weak sloshing is evident on an otherwise quiet free surface. The base flow is a free vortex at this speed. Beyond that rpm, no wave was observed, this does not mean that there is only one speed suitable for sloshing development; in fact, later cases will show that there exist a relatively small range of disk rpm which permits its presence.

At a water level of 56 mm, through the various steps of increasing the driving disk's rotation, strong sloshing was reached at 760 rpm, where the free surface oscillates vertically. The base flow is a free vortex with the central part of the disk exposed to air during sloshing.

At a level of 90 mm, sloshing is observed at two separate disk rotations When the rpm is 1084, strong sloshing is present with the vertical oscillation amplitude of the free surface at approximately 35 mm (peak to peak, 2A). At a higher rotation (1200 rpm), such oscillation reaches a more significant state with $2A \approx 60$ mm. As the disk speeds up beyond this point, the free surface resumes the relative calm condition, similar to that before the first sloshing was present. For example at disk rpm 1340, there is no sloshing at all.

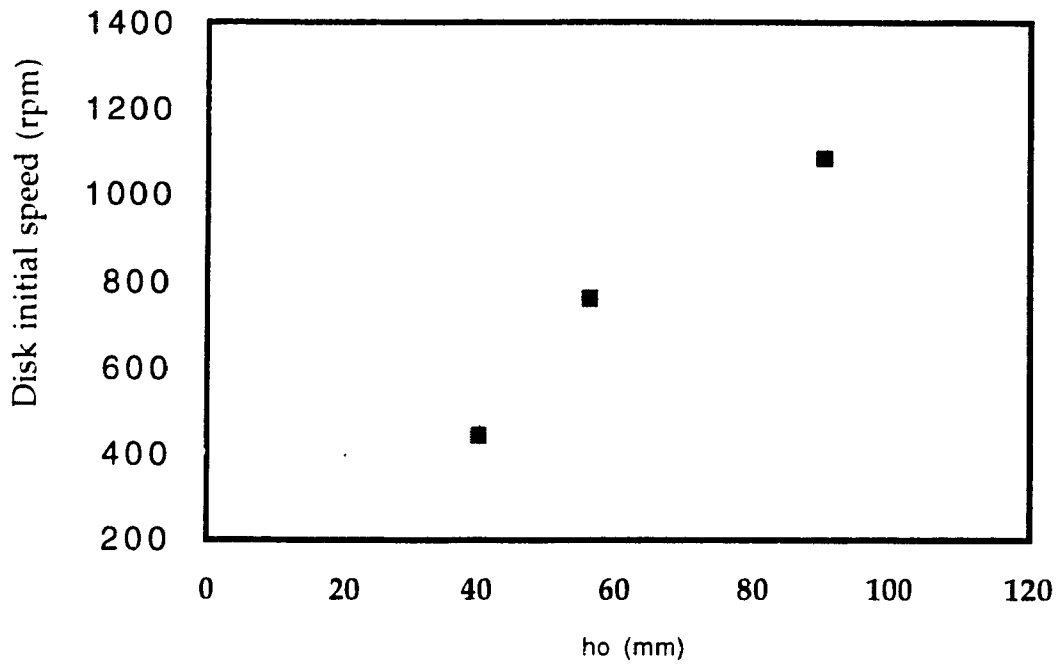

Figure 5-4 Initial disk speed for sloshing versus h_o (mm) for disk 101 mm

Features of the case

From the tests for this size of disk, two behavioral sloshing characteristics are evident:

(1) Speed bounds for sloshing

Given the geometry and the initial water level, sloshing is possible only within certain disk rotation limits if it is ever present for the disk size and water height in question.

(2) Sloshing depends on the liquid level

For the same disk size, the higher the liquid level, the higher the disk rpm for the starting sloshing state.

Case II Disk 153 mm, tank diameter 284 mm

With this disk diameter, for water levels of 41 and 56 mm, during all the rotation speeds, incremented at small steps and waiting for quite some time to see whether sloshing materializes, no traces of the distinct characteristics ever showed up. Instead, only deformed circles, ellipses, transient squares and their mutations were noticed.

At the level of 65 mm, water sloshing is abundantly present for quite a few stable disk speeds. Sloshing waves are evident for 5 different rpm: 182, 196, 216, 235 and 284 . For all five speeds, the core is flooded, suggesting a Rankine base flow.

A sloshing wave goes through a cycle of quiet and manifestation phases. The two time periods are measured and plotted in the figure.

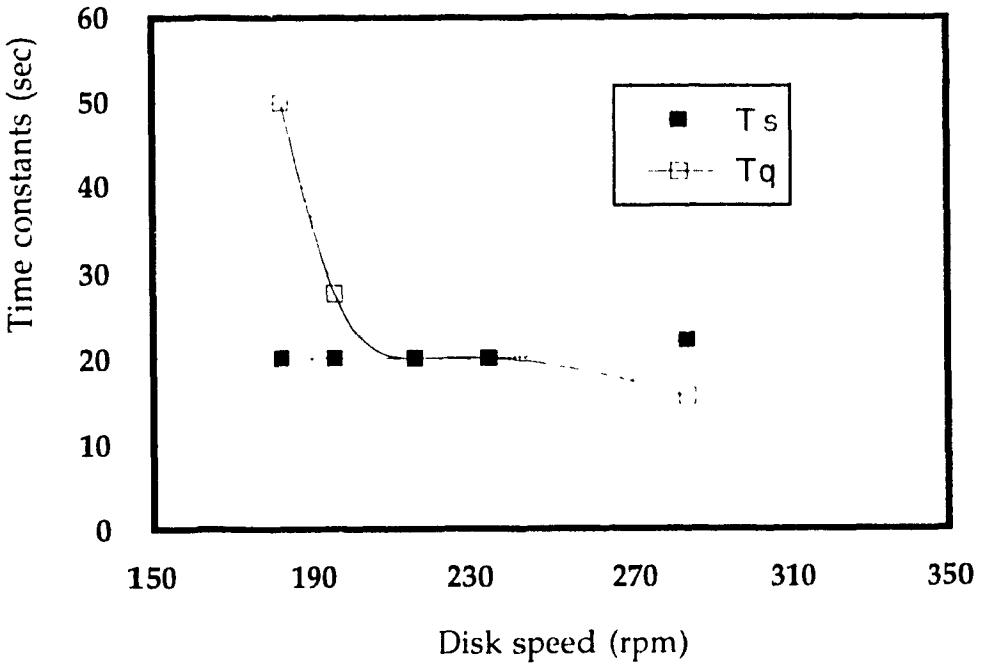

Figure 5-5 T_s and T_q versus disk rotation for h_o=65 mm

The two curves reveal that the sloshing duration is more or less constant, whereas the time duration for the quiet phase reduces with the disk speed.

At this water level, beyond the upper speed limit (slightly higher than 284 rpm), no sloshing is present (e.g. 341, 526 rpm etc.).

Another height examined is 111 mm, and sloshing is present when the disk rpm is at 293 and 392. The sloshing period T_S for these two speeds are 12.0 and 12.5 seconds, and the quiet durations are 11.0 and 8.0 seconds respectively. At higher disk rotations, sloshing is not materialized. For example, when rpm is 543, only a stable twisted, elliptical spiral exists in the Rankine base flow, rotating at a constant angular speed of about 40 rpm.

In order to see the effects of the initial liquid level, more water is added to the tank. Two particular heights are examined, h_0 = 149 mm and 177 mm. In both cases, many small increments of disk rotation are proceeded from rest. No periodically repeating sloshing waves are ever present, except for some unsteady flow patterns, such as mutations between hollow and flooded vortices.

Similar characteristics such as, a higher liquid level needs a higher disk rotation to produce a sloshing, similar to those with a disk of 101 mm are also the case here.

Case III Disk diameter 202 mm

Extensive tests were conducted for this disk size. Many instances of periodic sloshing are found for different water levels. In total, 11 various water heights are examined. The results are reported briefly for several initial liquid heights.

The first three initial heights of 17, 27 and 37.5 mm are shallow compared to this large disk. Free vortex is the prevailing condition in the base flow. No sloshing is present, and observed are non-symmetric, transient equilibria.

They are deformed parallelogram, pentagons, triangles, squares or ellipses. Mutations are frequent among these core shapes.

At h_O = 53 mm, as the disk rotation comes to 206 rpm by small increments, weak sloshing emerges. The free surface oscillates in the vertical direction with an amplitude of about 3 mm only. When the disk is set to higher speeds of 300, 325 ... 900 rpm, no sloshing wave was observed.

The following seven initial water heights of 108.5, 140.0, 174.0, 183.0, 243.0, 267 and 285 mm share some common characteristics when the disk rotation is raised quasi-statically (the case of h_O=267 mm will be given more details later). Generally, there is a lowest starting disk speed at which a weak sloshing is first visualized. The sloshing waves persist at the subsequent speed steps. The oscillation amplitudes and the two time constants (T_s, T_q) depend on the disk's speed and initial height. At a specific speed, the sloshing disappears, and the calm condition remains for any higher rotation. The minimum and maximum disk rpms where sloshing emerges are presented in Figure 5-6.

For h_O = 267 mm, more detailed tests were conducted. With no particular reason, a descending speed sequence is followed instead of an ascending one.

The descending process starts at 677 rpm, where an axially twisted elliptic equilibrium stably rotates. The central part of the disk surface outlined by the elliptic hollow core is exposed to air. It is axially twisted due to the water level being relatively high.

The disk rotation is reduced gradually from 677 rpm in small decrements through 601.75, 588.0, 573.0, 558.0, 537.5, 496.0, 465 25, 424.0, 402.0, 376.5, 350.8 rpm, then finally reaching 325.75 rpm. Starting from 601.75 rpm, due to reduced centrifugal force, the central part of the disk is flooded with water. The liquid free surface is a superposition of a smooth free forced vortex and an elliptical perturbation throughout the flow.

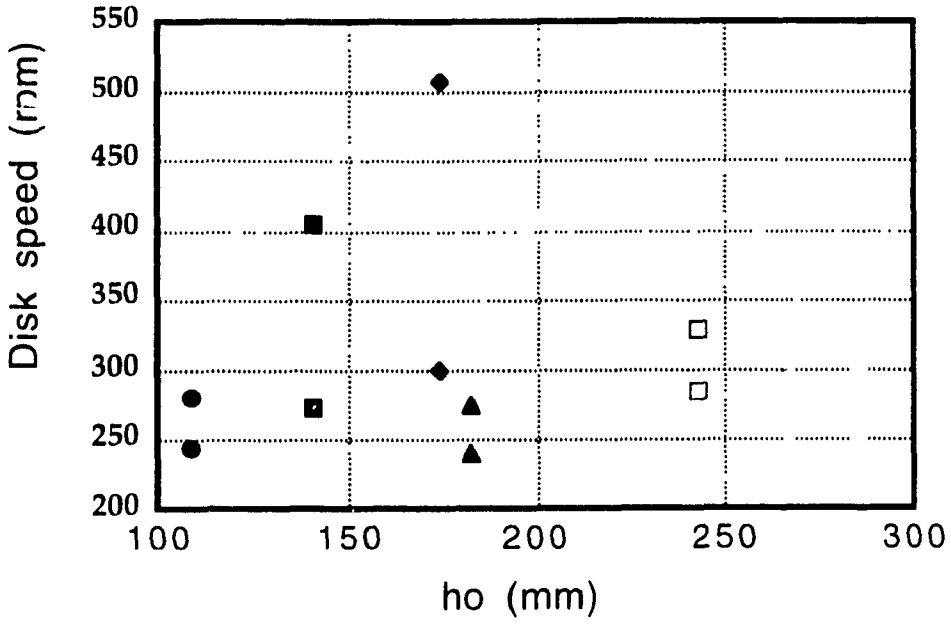

Figure 5-6 The disk rpms where sloshing is taking place at various h_o's

When the driving disk's rpm drops further to 299.75, the free surface periodically manifests weak variations. Such supplemental changes are better visualized from the side view of the contact line formed by the intersection of the water free surface and the tank's interior cylindrical wall.

A reduction of the disk speed intensifies the oscillations. At a disk rpm equal to 275, the maximum amplitude is evidently larger than that for 299.75 rpm; at 247.5 rpm the magnitude is the largest, where sloshing is really strong.

The two time periods at 247.5 rpm are clocked, see Figure 5-7.

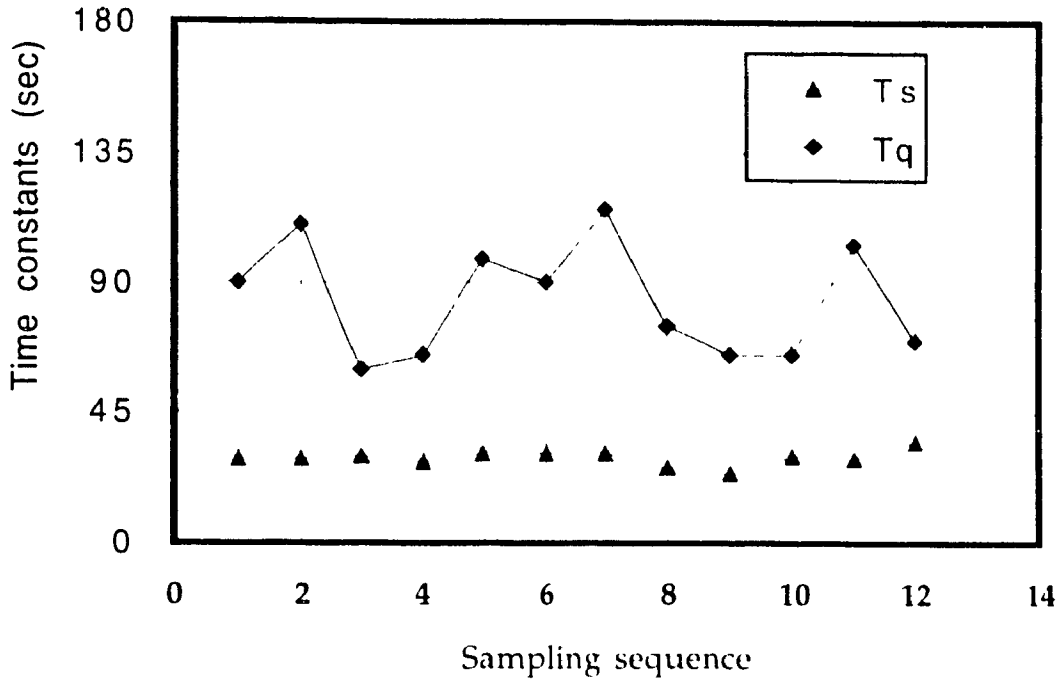

Figure 5-7 Time periods of sloshing for disk 202 mm at 247.5 rpm

In the figure, the vertical axis is time, and the horizontal one is the repetition of measurements. The upper line represents the quiet duration, whereas the lower one is the agitation duration T_S. We can see that T_S is relatively consistent, ranging from -18% to +5.3% about its average, but T_q has a variation from -28% to +37%. Such deviations may come from two sources, one due to the way the data is collected (visual timing), the other probably being the true nature of the phenomenon, which is not yet known. Nevertheless, one point is certain that is the periodicity of its presence.

Once the disk rpm continues to drop to 223.25 and to 201, no more sloshing is present. The field is quiet, elliptically perturbed, showing that 247.5 rpm is the lower bound for sloshing at the height of 267.0 mm.

For a disk diameter of 268 mm, only two initial water levels were performed : 36 and 49 mm. Since the disk is relatively large compared to the tank

(internal diameter is 284 mm), no sign of sloshing was ever present. It seems that the physical geometry of the base flow field makes it difficult for the periodic wave to develop.

5.2 A simulation of the sloshing process

The experimental evidence just presented has demonstrated the unique characteristics of a periodic sloshing wave in this special flow geometry. Visualization and preliminary measurements of periods and amplitudes of the oscillatory interface movements lead to a few general features. But the precise mechanism behind such an interesting and vibrant wave phenomenon is not yet clear. In an attempt to shed some light on this special kind of sloshing phenomenon, a simulation for a sequence of time frames is performed.

The simulation mapping is motivated by the double periodicity of the flow phenomenon, periodical in time (the sloshing emerges within a limited time interval), also periodical in space (symmetric). Superposition of two harmonic functions will yield such features.

From the previous analysis, it has been established that there exist two possible angular phase speeds for a given equilibrium state. This result was based on a few assumptions, including small linear perturbation, the dominance of horizontal flow over vertical motion in the main flow regime and also that the liquid particle trajectory is harmonic in a horizontal flow plane. The harmonic trajectory was the base for both the free hollow vortex and the flooded Rankine vortex in the analysis of Chapter 3.

In this simulation, the time development of the interface pattern of two waves with n=2 but having two different phase speeds, viewed from the top are shown in Fig. 5-8. The equation used for the simulation is,

$$r = 1 - 0.5 \left[\cos \left\{ 2\theta - 2.2\left(1-\frac{1}{\sqrt{2}}\right)t \right\} + \cos \left\{ 2\theta - 2.2\left(1+\frac{1}{\sqrt{2}}\right)t \right\} \right]$$

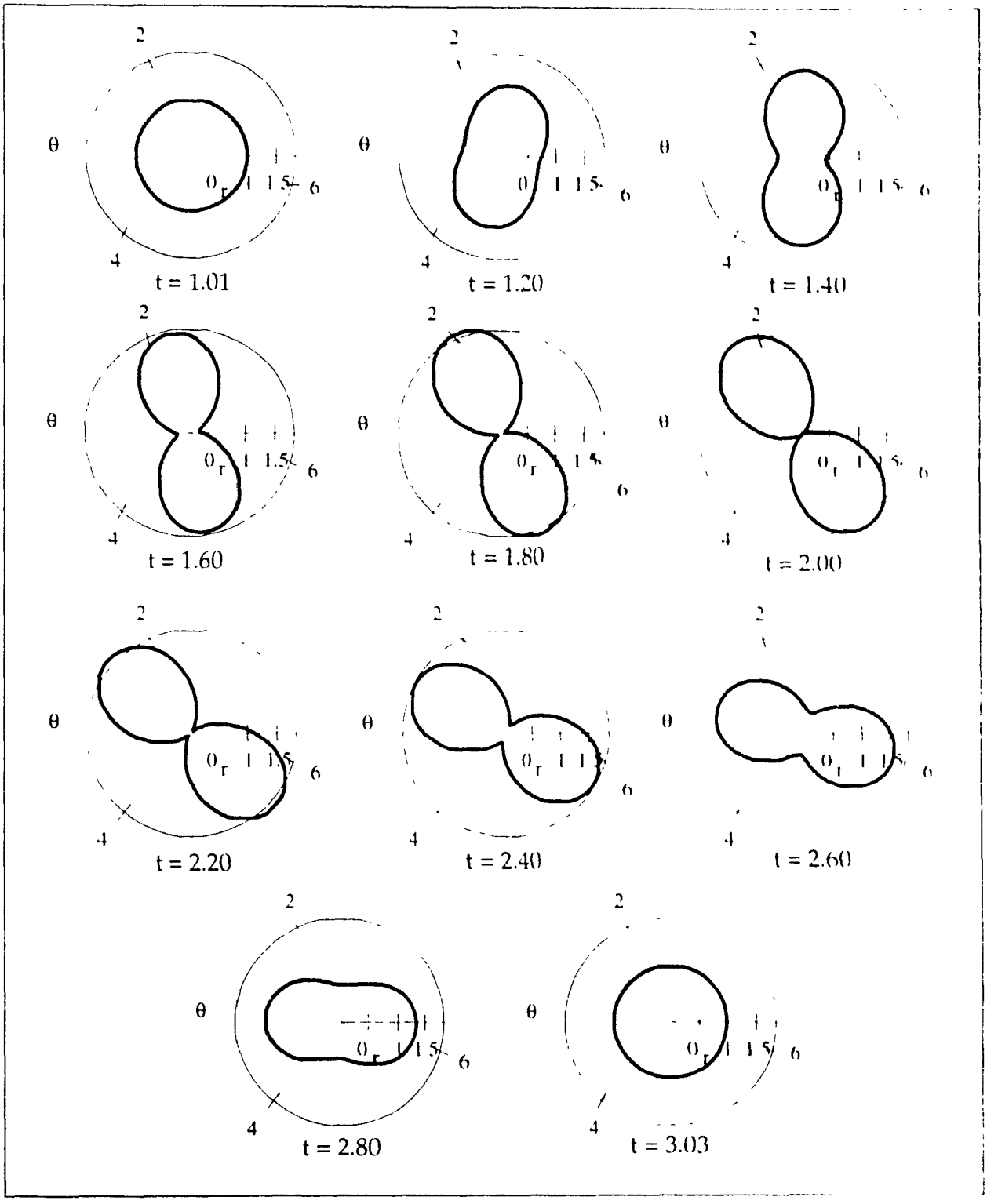

Figure 5-8. Simulation of a sloshing cycle

The results suggest that, under prevailing conditions, the existence of the two waves with the same number but different phase speeds can indeed break a single vortex into two co-rotating vortices. In reality the smaller vortices will not necessarily be equal, nor that the midpoint of their centers will be located at the geometric center of the cylindrical container. Under such conditions, the two vortices will destruct each other thus considerably slowing-down the main vortex and thus can no longer sustain sloshing. Following, the main vortex will again build-up and go through the same cycle. Although the present scenario is based on a simplistic theory it might be a good starting point for one wishing to further explore the origin in the evolution of the phenomenon.

CHAPTER 6

CONCLUSIONS

Recent observations of the liquid motion generated by a rotating disk in a cylindrical container have been reported. For low viscosity liquid (water), gradual core structure transitions from equilibrium patterns of a high degree of order towards chaos have been observed. Between vortex equilibria, gaps of mixed, time dependent states were found to prevail. Within a mixed state gap, the core is continuously changing due to the co-existence of two waves having circumferential wave numbers equal to the two neighboring equilibria. In the equilibrium states, the wave phase velocity and the disk rotational speed exhibit a linear relationship. The disk speed intervals for both vortex equilibria and mixed states were found to decrease as the speed of the disk increased. Increasing the liquid level results in the spectrum shifting towards higher disk speed regime.

The linearized stability analysis has been applied to predict fairly the speed of waves developed in both hollow potential and Rankine's vortices. For the latter case, the presence of a confined cylindrical wall was shown to augment the wave speed compared to a Rankine vortex in an infinite field. Based on

this theory, the hypothesis that a core pattern constructed from the superposition of waves in the two neighboring equilibrium states has been demonstrated to forecast quite well the main features of the observations for mixed states. Numerical mapping has also presented the transformation processes for various equilibria, which emulates well the experimental evidence.

The diameter of the driving disk is shown to have impact on the occurrence of the equilibrium waves. Among the four disks examined, with the exception of the largest one, which is almost the size of the tank's inner wall, the larger the disk, the lower the disk rpm for an equilibrium wave to be present. The discrepancy for the largest disk may be attributed to the change of the base flow structure, since the flow is more like a solid rotation.

Hysteresis is found in the transition between the water equilibria, and it is quantitatively small as compared with liquid of higher viscosity.

Quite different behavior of the hollow core was observed for cases where an intermediate viscosity liquid (oil) was used. Transformations from one core wave pattern to another was abrupt with no apparent intermediate structures. Stationary states with wave numbers ranging from one to eleven were observed. Also peculiar is that there exist retrograde equilibria, that never occurred in water. The speed of equilibria in oil is also found to be linear to the driving disk's rotation in one case.

Bifurcations are abundant in the process of transition from laminar state to turbulence in oil vortices. Two common characteristic bifurcations are repeatedly visualized :

- between a steady flow and a single frequency periodic flow,
- between a single frequency periodic flow and a two-frequency quasi-periodic flow.

The mutual transformations between bifurcating flow states can be brought about by introducing external artificial disturbances when all the other conditions are left unchanged, often the transformations are reversible. If a correlation between the energy of flow field and its corresponding

equilibrium can be established, one will be able to evaluate the relative degree of stability of these waves.

The two frequency quasi-periodic flow is present in two structures, one being that a basic wave pattern is sub-harmonically modulated by another wave of different number, and another form is a flow where a solitary wave encircles a background equilibrium.

Acceleration affects the viscous equilibrium development. This shows that the flow is an initial value problem, depending on an external, time-varying driving function, in addition to the boundary conditions. Different development history (spin-up and spin-down) may well result in different flow states. The detailed mapping between the accelerating course and the oil equilibria variations will give more precision.

Hysteresis is very evident between the two quasi-static sequences of the driving disk, spin-down and spin-up.

Periodic sloshing in the water vortex was observed under certain prevailing parameter combinations (size of the disk, initial water height and disk rotation). Considerable fluctuations of flow parameters are evident between the quiet phase and the sloshing phase. The simulation to emulate the violent process was based on the superposition of two concurrent waves.

References

Abrahamson, S. D., Eaton, J. K. and Koga, D. J. : The flow between shrouded corotating disks. Physics of Fluids, part A, vol. 1, No. 2, 1989.

Aref, A. : Integral, chaotic and turbulent vortex motions in 2D flows. Ann. Rev. of fluid mechanics. vol. 15, 1983.

Benjamin, T.B. and Mullin T. : Notes on the multiplicity. JFM. 1982, vol 121, pp.219-230.

Busse, F.H. : Non linear properties of thermal convection. Report prog. phys. vol.41 (1978), 1929-1969.

Cambell, L.J. and Ziff, R.M. : A catalogue of two dimensional vortex patterns. Los Alamos Sc. Lab. Rep. No. LA-7384-MS. 40pp. 1978.

Chandrasekhar, S. : Hydrodynamic and Hydromagnetic Stability. Clarendon Press, Oxford, 1961.

Chomaz, J.M., Rabaud M. & Couder Y. : Experimental and numerical investigations of a forced circular shear layer. JFM vol.187, 1988.

Drazin, P. G. and Reid, W. H. : Hydrodynamic Stability. Cambridge University Press, N. Y., 1981.

Dritschel, D.G. : The stability and energetics of corotating uniform vortices. JFM, vol. 157,1985.

Dritschel, D.G. : The nonlinear evolution of rotating configurations of uniform vortices. 1985, JFM, vol.172.

Dritschel, D.G. : On the stabilization of a 2 D vortex strip by adverse shear. 1989, JFM, vol 206.

Escudier, M. : Confined vortices in flow machinery. Ann. Rev. Fluid Mech. vol.19 , 77, 1987.

Greenspan, H. P. : The theory of rotating fluids. Cambridge University Press, London, 1969.

Geogory, N., Stuart, J.T. and Walker, W.S. : On the stability of three-dimensional boundary layers with application to the flow due to a rotating disk. Phil. Trans. Roy. soc London A vol.248, 155, 1955.

Griffiths, R.W. and Linden, P.F. : The stability of vortices in a rotating, stratified fluid. J. Fluid Mech. vol.105, 283, 1981.

Hide, R. : Detached shear layers in a rotating fluid. JFM. vol.29, 1966.

Holter, N.J. and Glasscock, W.R. : Vibrations of evaporating drops. The journal of acoustical society of America. vol. 24, (6) , 683-685, 1952.

Joseph, D. : Hydrodynamic stability and bifurcation, in Hydrodynamic instabilites and the Transition to Turbulence, Swinney and Gollub (editors), Springer Verlag, Berlin, N. Y., 1985.

Knauss, J. (editor) : Swirling flow problems at intakes. A. A. Balkema, Roterdam, 165 pp.

Kou, H. : Dynamics of quasi-geostropic flows and instability. Advances in applied mechanics, vol.13, 1973.

Lauer, Tod R., etc. : Planetary camera observations of the double nucleus of M31, The Astronomical Journal, vol. 106, No. 4, Oct. 1993.

Lin, C. C. : The theory of hydrodynamic stability. Cambridge University Press, Cambridge 1955.

Lord Kelvin : Vibrations of a columnar vortex, Proc. of the Royal society, Edinburgh, 1880.

Lugt, H., J. : Vortex flow in nature and technology. John Wiley & Sons, New York 1993.

Markus, S. : The mechanics of vibrations of cylindrical shells. Studies in applied mechanics, vol.17, Elsevier, New York, 159pp, 1988.

Mason, B. J. : Global atmospheric research programme. Nature vol. 233, 382-388 (1971).

Munson, B. R. and Menguturk, M. : Viscous incompressible flow between concentric rotating spheres. Part 3. JFM. vol. 69, p705, 1975.

Pai, S. I. : Turbulent flows between rotating cylinders. NACA, technical note 892, 1943.

Rabaud, M. and Couder, Y. : A shear flow instability in a circular geometry. JFM. vol.136.

Rayleigh, Lord : On the dynamics of revolving fluids. Proc. R. Soc. London A vol. 93, pp148-154, 1916.

Stockert, R. : Beitrag zur optimalen auslegung von tiefbohrwerkzeugen. Doctor-Ingenieur genehmigte Dissertation, Universitat Dortmund, 199p, 1978.

Swinney, H. L. and Gollub J. P. : Hydrodynamic instabilities and the Transition to Turbulence. 2nd edition, Springer Verlag, Berlin, N.Y., 1985.

Taylor, G. I. : Stability of a viscous liquid contained between two rotating cylinders. Philoso. Trans. R. Soc. London A vol. 223, 289-343, 1923.

Vatistas, G. H. : A note on liquid vortex sloshing and Kelvin's equilibria. 1990 JFM. vol. 217.

Vatistas, G. H. : Letter to the editor, New Scientist, No. 1904, page 50, Dec. 1993.

Vatistas, G. H., Wang J. and Lin S. : Experiments on waves induced in the hollow core of vortices. Experiments in Fluids vol.13, page 377-385 (1992).

Vatistas, G. H., Wang J. and Lin S. : On the Waves Produced in Vortex Cores. Tenth Canadian Symposium on Fluid Dynamics, St-Jean, NB. 1992.

Vatistas, G. H., Wang J. and Lin S. : Kelvin's Equilibria. ASME Intl. Joint Power Generation Conference, Atlanta, Oct. 1992.

Vatistas, G. H., Wang J. and Lin S. : Recent Findings on Kelvin's Equilibria. Acta Mecanica, 103, 89-102 (1994).

Weske, J. R. and Rankine T. M. : Physics of fluids, vol. 3, Generation of secondary motions in a field of vortex. 1963.

Wimmer, M. : Experiments on a viscous fluid flow between concentric rotating spheres. JFM. 1976, vol. 78, pp317-335.

Wimmer, M. : Laminar to turbulent transition in a spherical annulus. (editors, Eppler & Fraser) Laminar to turbulence transitions. 1980.

Wygnanski, I. J., Champagne, F.H. : On transition in a pipe. The origin of puffs and slugs and the flow in a turbulent slug. JFM. vol. 21, pp385, 1973.

Zierep, J. and Sawatzki, O. : Three dimensional instabilities and vortices between two rotating spheres. 8th Symp. Naval Hydrodyn. 1970.